Journal of Medicinal Chemistry

Open Access
This article is licensed under CC-BY 4.0

pubs.acs.org/jmc
Article

Structure-Based Design of Potent Pan-YTHDF Ligands

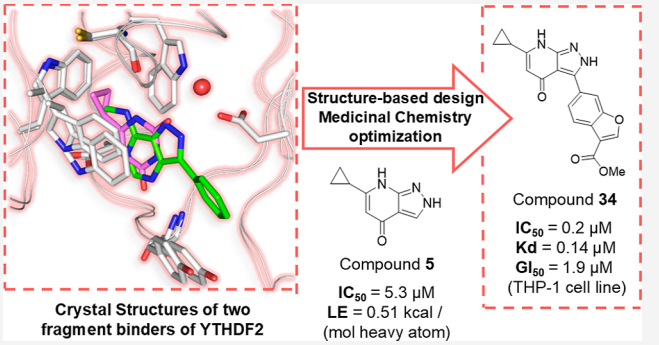
Francesco Errani,[†] Francesco Nai,[†] Elena Bochenkova, Marcin Herok, Annalisa Invernizzi, Rajiv Kumar Bedi, Yaozong Li, František Zálešák,* and Amedeo Caflisch*

Cite This: https://doi.org/10.1021/acs.jmedchem.6c02977

Read Online

ACCESS | Metrics & More | Article Recommendations | Supporting Information

ABSTRACT: The reader proteins YTHDF1-3 recognize m^{6}A-RNA in the cytosol. Here, we present a structure-based medicinal chemistry campaign that culminated in the pan-YTHDF inhibitor **34** (K_d = 0.14 μM for YTHDF2 by calorimetry), which is selective against YTHDC1 and YTHDC2. The high-resolution crystal structures of the complex of YTHDF2 with six members of the series validate the structure-based design. Using the structural information, we designed compound **31** (IC_{50} = 0.22 μM for YTHDF2) and a negative control, i.e., its methylated analogue **31b**. The cellular thermal shift assay provides evidence of YTHDF2 target engagement in cells for inhibitors **34** and **31**, while the negative control **31b** is inactive. Compounds **34** and **31** inhibit the proliferation of the AML cell lines MOLM-13 and THP-1. The inhibition of the YTHDF readers by **31** increases the level and stability of the transcript of *TNFRSF1B*. This renders THP-1 cells more sensitive to TNF-α-induced toxicity.



KEYWORDS: *epitranscriptomics, m^{6}A-RNA readers, protein crystallography, calorimetry*

INTRODUCTION

In humans, N^6-methyladenosine (m^{6}A) is recognized by five YTH domain-containing reader proteins (YTHDC1, YTHDC2 and YTHDF1−3), which share a structurally conserved YTH domain responsible for RNA binding and m^{6}A recognition.[1,2] YTHDC1 is nuclear and acts on splicing and transcript export,[3] YTHDC2 is a putative RNA helicase whose YTH domain shows only a weak preference for m^{6}A,[2,4] whereas YTHDF1, YTHDF2, and YTHDF3 are cytoplasmic. The three YTHDF paralogs play a pivotal role in epitranscriptomic gene regulation by selectively recognizing m^{6}A marks and recruiting effector complexes to the modified transcripts.[5−9] This mechanism has broad biological significance: dysregulation of the YTHDF readers has been implicated in multiple cancers. Aberrant YTHDF1 activity has been reported in esophageal, gastric, colorectal, and liver cancer,[10] YTHDF2 in prostate carcinoma, MYC-driven breast cancer and acute myeloid leukemia (AML),[11−13] and YTHDF3 in breast cancer brain metastasis[14] as well as in ocular melanoma.[15] These connections highlight the YTHDF readers as a promising target family for chemical biology and therapeutic intervention. There is an ongoing debate in the field over whether YTHDF proteins exert specific functions or act redundantly. In terms of function, an earlier model assumed that YTHDF1 promotes ribosome recruitment and enhances mRNA translation efficiency, while YTHDF2 recruits deadenylase complexes and RNA decay machinery to mediate rapid mRNA degradation. In this model, YTHDF3 functions as a coordinator, assisting both YTHDF1 and YTHDF2.[5,16,17] More recent studies indicate that all DF proteins share the same function of promoting mRNA degradation.[6−8,18] Additionally, there are no specific m^{6}A sites recognized by only one YTHDF protein, and they all bind the modified nucleoside in the same way.[1,6,19] A more integrative perspective would suggest that YTHDF proteins have overlapping binding profiles and potential redundancy at the molecular level, but that their divergent low-complexity N-terminal regions, together with their spatial expression patterns, interaction partners, and cellular contexts, collectively determine their functional specificity.[4,7]

Structurally, the YTHDF readers recognize the m^{6}A modification through a conserved YT521-B homology (YTH) domain that provides a specialized binding pocket for N^6-methyladenosine (Figure 1). In YTHDF2, the m^{6}A-binding site consists of a hydrophobic "aromatic cage" formed by three tryptophan residues (W432, W486, and W491), which snugly accommodate the methylated adenine base. The adenine ring is further anchored by hydrogen bonds formed between the backbone carbonyl group of C433 and the N6 of the adenine ring and between the backbone NH group of Y418 and the N3 of the adenine ring.[1,20] The same five residues are present in the

Received: September 16, 2026
Revised: October 15, 2026
Accepted: October 20, 2026

ACS Publications
© XXXX The Authors. Published by American Chemical Society

Downloaded from pubs.acs.org/jmcmar/article-pdf/doi/10.1021/acs.jmedchem.6c02977/6905752/jm6c02977.pdf by guest on 06 November 2026

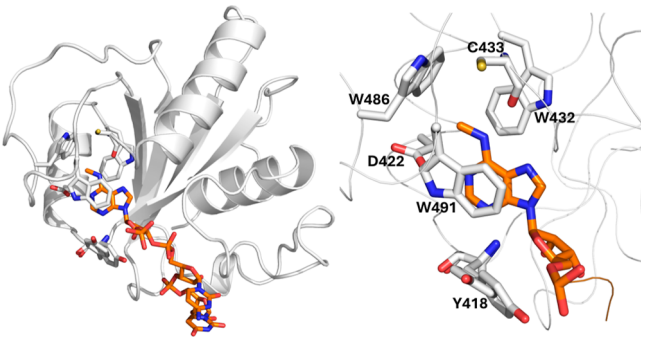


Figure 1. YTHDF2 reader domain (gray) in complex with GGm^{6}ACU-RNA (carbon atoms in orange) and details of the m^{6}A binding site (PDB: 7Z26).

other two paralogs, at W411, W465, W470, C412, and Y397 in YTHDF1 and at W438, W492, W497, C439, and Y424 in YTHDF3, and the superposition of the three reader domains in complex with GG(m^{6}A)CU-RNA (PDB 4RCJ, 7Z26 and 6ZOT for YTHDF1, YTHDF2, and YTHDF3) shows nearly identical binding-site and recognition-loop conformations.[1] Across the three paralogs, the YTH domains share more than 90% sequence similarity, while their N-terminal regions share only 51−62%.[4] The m^{6}A-binding site is therefore essentially the same in YTHDF1, YTHDF2, and YTHDF3, and a ligand that occupies it is expected to bind all three.[2,19] Notably, the binding groove is relatively shallow and partially solvent-exposed, and it is flanked by a flexible loop that can adopt open or closed conformations, modulating the pocket volume.[1] These features present a considerable challenge for ligand design. Despite their biological importance, few small-molecule inhibitors of the YTHDF readers have been reported to date; those described so far act through different modes of action but with modest affinity and limited selectivity among the YTHDF readers.[4] For instance, the organoselenium compound Ebselen was identified as a covalent inhibitor that binds within the YTHDF binding site and blocks m^{6}A recognition by forming a seleno-sulfide bond to a cysteine residue.[21] Other examples include known drugs and natural products such as the Irritable Bowel Syndrome therapeutic Tegaserod and salvianolic acid C (with IC_{50} values for YTHDF2 of 75 and 30 μM, respectively).[22,23] A screening of modified nucleosides yielded a broad-spectrum YTH domain binder dubbed "*N*-7," which inhibits YTHDF1-3 and YTHDC1-2 proteins in vitro (IC_{50} ≈ 30−50 μM).[24] Wang et al. (2023)[25] reported DC-Y13-27 that binds YTHDF2 with an IC_{50} of 22 μM and showed partial selectivity over YTHDF1 (IC_{50} of 165 μM). More recently, a series of substituted pyrazoles were identified as selective YTHDF2 binders, exemplified by compound CK-75. This molecule exhibited an IC_{50} of 13.2 μM against YTHDF2, inducing cell-cycle arrest and apoptosis in the chronic myeloid leukemia cell line K562, while showing no detectable binding to other YTH family members.[26] A YTHDF1-preferring inhibitor, SKLB-Y13, was subsequently reported, with a five-to eight-fold preference for YTHDF1 over the other two YTHDF paralogs.[27] Our group's prior work provided the first evidence that the YTHDF2 pocket is druggable: in 2022 we reported a set of fragment-like ligands that compete with m^{6}A for binding to the YTHDF2 YTH domain.[1] These initial hits showed mediocre affinity (with IC_{50} ≈ 100−200 μM) but exhibited favorable ligand efficiency and established a structural foundation for subsequent optimization. Recently, we have disclosed a new series of binders for the YTH readers, with the best compound being selective for YTHDF2, showing a biochemical affinity of 11 μM.[28] In the same publication, we presented two small molecules with a YTH-pan inhibitory profile featuring low micromolar IC_{50} values. Collectively, these studies highlight both the therapeutic potential and the current limitations for the development of potent ligands for YTHDF1−3 proteins. Thus, there is a clear need for more potent inhibitors and a deeper exploration of structure−activity relationships (SAR). Because a robust crystallization system for YTHDF2 was available from our earlier work,[1] we performed the structure-based design on YTHDF2 and treated it as the representative member of the YTHDF family. As anticipated from the conservation of the pocket, the optimized compounds bind all three YTHDF paralogs with comparable affinity, i.e., they are pan-YTHDF ligands while remaining selective against the more diverse YTHDC1 and YTHDC2. YTHDF2 thus served as the experimental system that guided the campaign rather than as its exclusive target. In the present study, we report a new series of pan-YTHDF binders with substantially enhanced affinity (nanomolar potency) compared to those of earlier fragments. Our medicinal chemistry campaign has resulted in the most advanced small-molecule inhibitors of the YTHDF proteins to date, whose availability will enable more refined investigation of m^{6}A-RNA reader biology.

RESULTS AND DISCUSSION

First, we present the structure-based design of the DiHydroPyrazoloPyridinone (DHPP) head group, followed by its structural growth and the biochemical and cellular validation of the most potent derivatives.

Headgroup Design

Our previous work on YTHDF2 fragment identification served as the starting point for this medicinal chemistry campaign. Two of the most promising compounds were selected for further optimization.[1] As shown in Figure 2A,B, these fragments display distinct structural features. Compound **1** is an uracil derivative bearing a cyclopropyl substituent at position 6 of the ring, whereas compound **2** is a m^{6}A analogue characterized by the replacement of the imidazole ring with a pyrazole and by the presence of a phenyl substituent at position 3. The binding potencies of compounds **1** and **2** were evaluated using a time-resolved fluorescence resonance energy transfer (TR-FRET) assay,[29] yielding IC_{50} values of 174 μM and 161 μM, respectively. We were able to obtain crystallographic structures of YTHDF2 in complex with both ligands **1** and **2**, enabling a detailed binding modes analysis within the m^{6}A recognition pocket.

The uracil core of compound **1** engages in three key hydrogen-bonding interactions, involving C433, Y418, and a structural water molecule that mediates a hydrogen bond to the side chain of W432 (Figure 2A). Notably, the cyclopropyl substituent plays a critical role in the binding affinity. In our previous study, replacing it at position 6 of the uracil ring with an ethyl group markedly weakened binding: the ethyl analogue gave a residual signal of 62% at 1 mM versus 12% for compound **1** (IC_{50} = 174 μM), and did not reach a measurable IC_{50}.[1] This observation likely reflects the highly conserved and spatially constrained nature of the YTHDF2 binding pocket, and in particular the aromatic cage formed by W432, W486, and W491, which presents a challenging environment for ligand design. Compound **2** forms four hydrogen bonds within the binding site, three of which are shared with compound **1**, while the additional interaction involves the side

Downloaded from pubs.acs.org/jmcmar/article-pdf/doi/10.1021/acs.jmedchem.6c02977/6905752/jm6c02977.pdf by guest on 06 November 2026

https://doi.org/10.1021/acs.jmedchem.6c02977
J. Med. Chem. XXXX, XXX, XXX−XXX

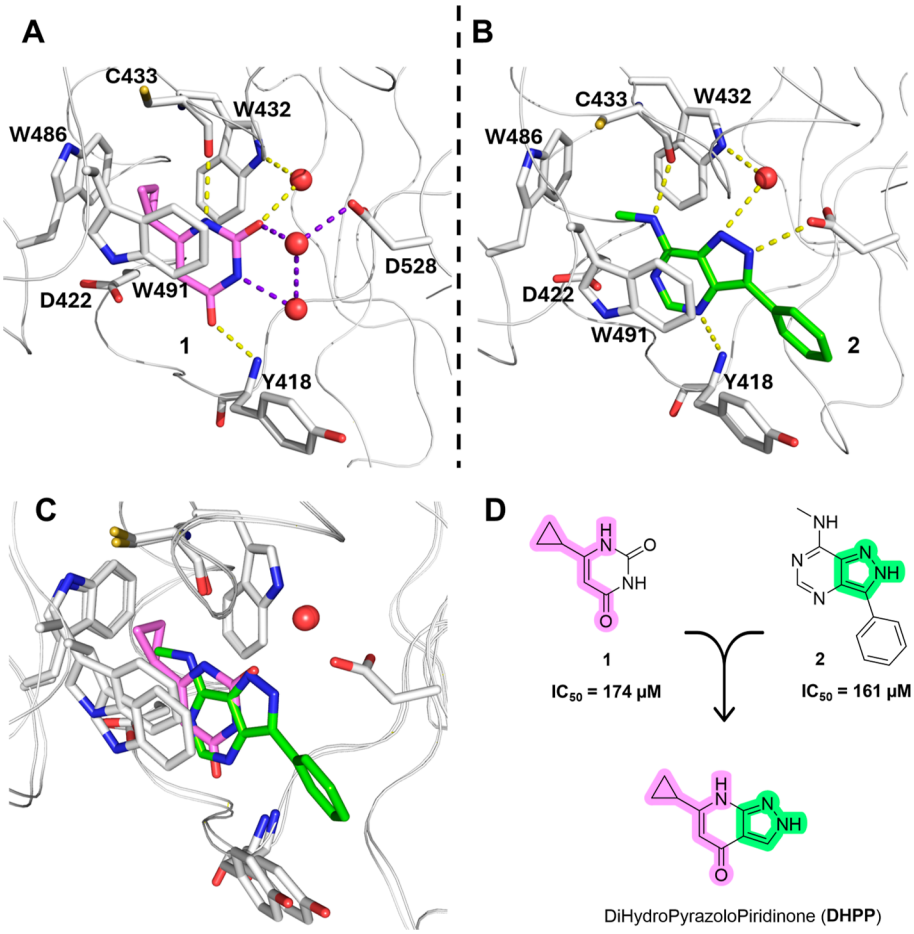


Figure 2. Structure-based design of the DHPP headgroup. Crystal structures of compounds **1** (A, PDB: 7R5W) and **2** (B, PDB: 7YXE) (carbon atoms in pink and green, respectively) in complex with YTHDF2 (gray). The conserved water molecules (red spheres) and the hydrogen bonds (yellow dashed lines for ligand−protein conserved interactions and violet dashed lines for the water network) are emphasized. (C) Superimposition of **1** (pink) and **2** (green). (D) 2D schematic of the head-group merger.

chain carboxyl of D528 (Figure 2B). Two structural features distinguish this ligand: the pyrazole ring and the phenyl substituent. In contrast to m^6A, the pyrazole moiety enables the formation of an additional hydrogen bond with D528, an interaction not accessible to the imidazole ring. Furthermore, the phenyl substituent is oriented toward Y418, allowing a $\pi-\pi$ stacking interaction. This interaction was suggested by the study of the crystal structure of the natural ligand in complex with YTHDF2. As it is shown in Figure 1, Y418 could adopt two different orientations, one of which seems to engage the O4 of the adenosine ribose in a lone pair−π interaction.[1] Despite these favorable interactions, compounds **1** and **2** display comparable binding potencies, which may be attributed to suboptimal accommodation of the methylamino group of compound **2** within the aromatic cage. This observation further underscores the importance of appropriately sized and shaped substituents in the aromatic cage region of the binding pocket. The structural overlap of compounds **1** (PDB: 7R5W) and **2** (PDB: 7YXE), as shown in Figure 2C, suggested fusing them into a single scaffold, leading to a DHPP, as illustrated in Figure 2D. To investigate the influence of the aliphatic substituent on binding, three different DHPP analogues were evaluated, bearing cyclopropyl, methyl, and ethyl groups, as shown in Figure 3. All three compounds were evaluated by the TR-FRET assay and displayed improved binding affinities toward YTHDF2 (Figure 3) relative to the parent fragments,

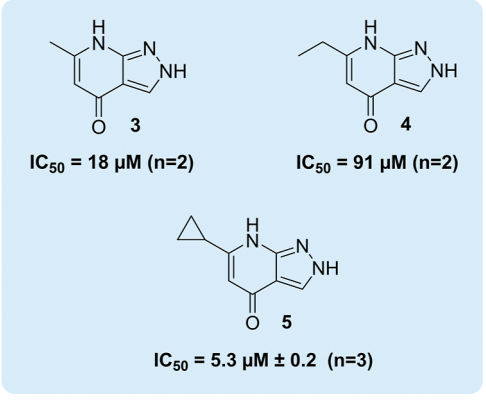


Figure 3. 2D structures and IC_{50} values of the methyl-, ethyl-, and cyclopropyl-substituted DHPP derivatives. IC_{50} values were determined as described in Table 1; the number of biological replicates is given as (n), and values are reported as mean ± SD where $n \geq 3$.

molecules **1** and **2**. The methyl derivative **3** exhibited an IC_{50} of 18 μM and the ethyl analogue **4** an IC_{50} of 91 μM. Compound **3** was also tested for selectivity against YTHDC1, for which the IC_{50} value is close to 200 μM (not shown). Given the conservation of the binding sites in YTHDC1 and YTHDF2, the key interactions

Downloaded from pubs.acs.org/jmcmar/article-pdf/doi/10.1021/acs.jmedchem.6c02977/6905752/jm6c02977.pdf by guest on 06 November 2026

https://doi.org/10.1021/acs.jmedchem.6c02977
J. Med. Chem. XXXX, XXX, XXX−XXX

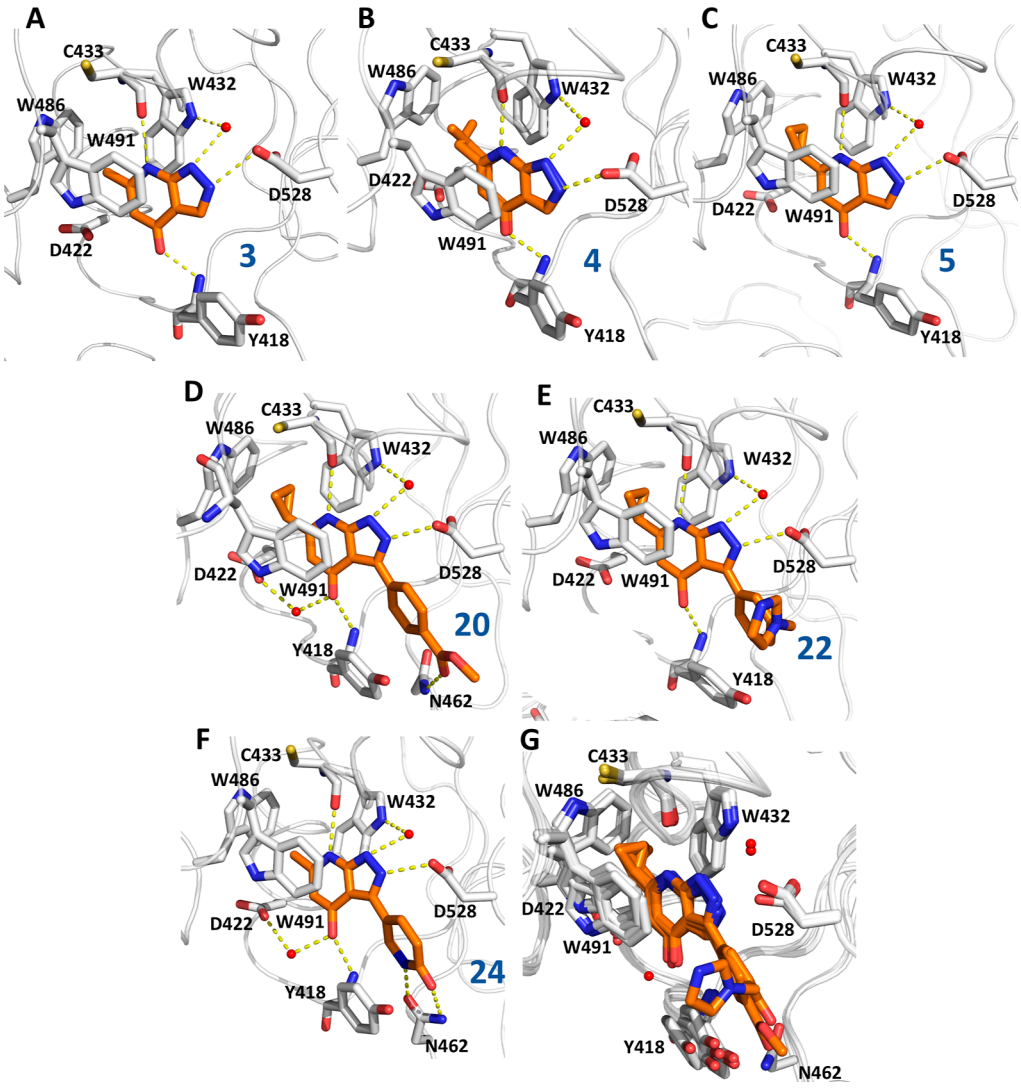


Figure 4. Crystal structures of compounds **3** (resolution 1.55 Å; PDB: 32RD), **4** (1.61 Å; PDB: 32SH), **5** (1.52 Å; PDB: 32SA), **20** (1.68 Å; PDB: 32TH), **22** (2.2 Å; PDB: 32SJ), and **24** (1.84 Å; PDB: 32QY) in the complex with YTHDF2 (A−F) and their superimposition (G). The carbon atoms of the ligands are shown in orange, and those of the protein in gray. The conserved water molecules (red spheres) and hydrogen bonds (yellow dashed lines) are emphasized. Data collection and refinement statistics are reported in Table S1.

observed in YTHDF2 are expected to be maintained in YTHDC1 as well.

One notable difference between the two binding pockets is a non-conserved residue: D422 in YTHDF2 corresponds to N367 in YTHDC1 (Asp→Asn substitution). Therefore, a potential explanation for the observed selectivity is that the C−H at position 5 of the DHPP scaffold can form a favorable polar interaction with the carboxylate of D422 in YTHDF2, whereas in YTHDC1, it is involved in an unfavorable polar contact with the amide (NH_2) group of N367. Consistent with the trend observed in our previous work,[1] the cyclopropyl moiety in compound **5** resulted in the most potent derivative with an IC_{50} of 5.3 μM. Crystal structures of all three DHPP derivatives were obtained (Figure 4A−C), confirming that the key interactions observed from compounds **1** and **2** were successfully retained and combined within the merged scaffold. Through X-ray crystallography, we observed that the ethyl substituent can adopt two different orientations within the aromatic pocket (Figure 4B). The methyl group (Figure 4A) forms less favorable nonpolar interactions with W432, W486, and W491 compared to the cyclopropyl substituent (Figure 4C), which likely accounts for the approximately threefold difference in potency between these two analogues. Inspection of the crystal structures of compounds **3**, **4**, and **5** revealed an additional opportunity for optimization. In particular, the binding poses suggested the possibility of introducing an aromatic substituent to get a $\pi-\pi$ stacking interaction with Y418, analogous to that observed for compound **2** (Figure 2B). Guided by these structural insights, we therefore proceeded with the design and synthesis of further substituted derivatives.

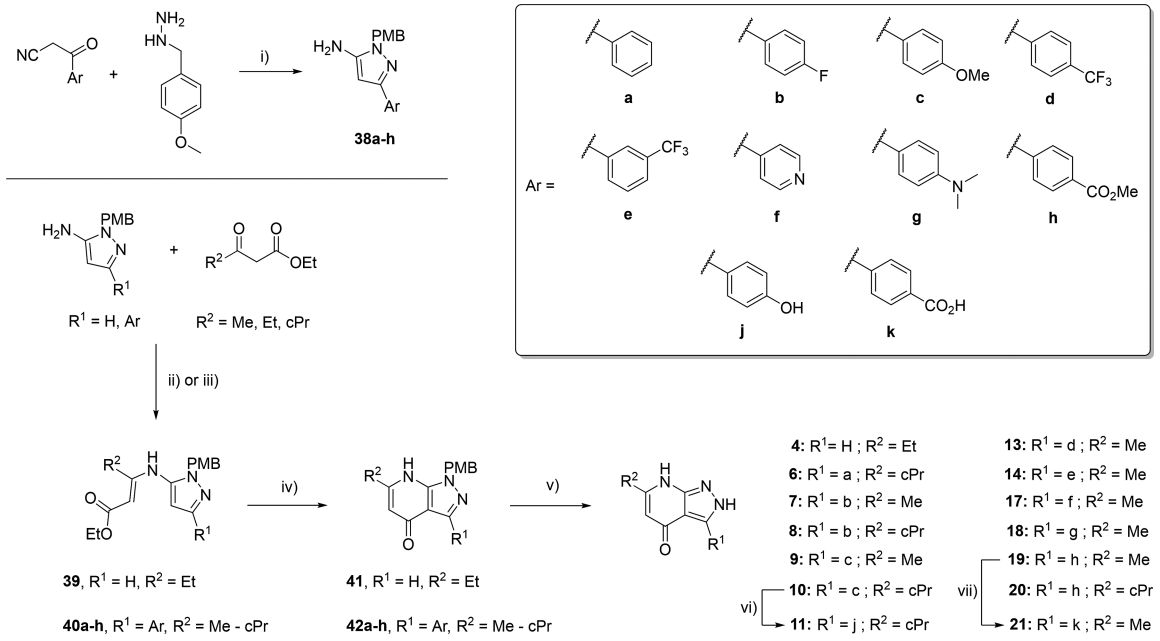
DHPP Ligand Growth—Phenyl Substituents

As mentioned above, the DHPP scaffold is able to satisfy all the main interactions within the inner part of the binding pocket. At this point, we needed to grow larger molecules from this scaffold, aiming to engage with other residues at the rim of the recognition pocket. To enable the introduction of an aryl substituent at position 3 of the DHPP scaffold, the synthetic strategy was modified accordingly (Scheme 1). The first analogue prepared using this approach was compound **6**, bearing an

Downloaded from pubs.acs.org/jmcmar/article-pdf/doi/10.1021/acs.jmedchem.6c02977/6905752/jm6c02977.pdf by guest on 06 November 2026

https://doi.org/10.1021/acs.jmedchem.6c02977
J. Med. Chem. XXXX, XXX, XXX−XXX

Scheme 1. Synthesis Route for Compounds 4, 6−11, 13, 14, 17−21[a]



[a]Reagent and conditions: (i) AcOH, EtOH, 85 °C; (ii) for R^1 = H, R^2 = Et, pTSA, DCE, rt; (iii) for R^1 = Ar, R^2 = Me−cPr, AcOH, 70 °C; (iv) neat, 200 °C; (v) TFA, reflux; (vi) EtSNa, dry DMF, 150 °C; (vii) HCl 6 M, dioxane, 120 °C.

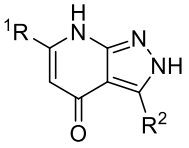
unsubstituted phenyl ring. As reported in Table 1, this modification resulted in an IC_{50} value of 2.5 μM, improving by twofold the binding potency of compound **5**. This result was consistent with the anticipated contribution of a $\pi-\pi$ stacking interaction with Y418. We therefore proceeded with a SAR study on the phenyl ring, with the dual aim of identifying optimal substituents and obtaining crystallographic data to further guide our structure-based design. In total, 18 analogues featuring different substitution patterns were synthesized and evaluated (Table 1). As shown in Table 1, *para*-fluoro substitution in compounds **7** and **8** did not lead to a significant improvement in binding potency compared to **6**, with IC_{50} values of 6 μM and 2 μM, respectively. The *ortho*, *meta*, and *para* descriptors are relative to the connection between the DHPP scaffold and the phenyl substituents. In contrast, the introduction of a *para*-methoxy group resulted in a fivefold enhancement in potency relative to that of **6**, yielding compound **10**, the first sub-micromolar YTHDF2 ligand (IC_{50} = 0.5 μM).

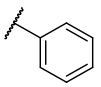
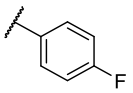
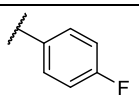
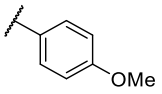
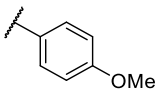
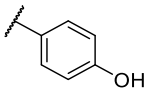
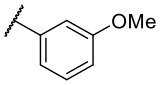
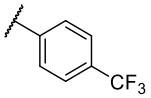
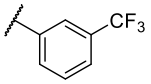
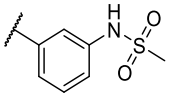
Across multiple matched pairs, a consistent three- to fourfold improvement in potency was observed when switching from methyl- to cyclopropyl-substituted analogues, e.g., compounds **7**, **8**, and compounds **9**, **10** (6 μM to 2 μM for the first couple and 2 μM to 0.5 μM for the second). This trend was particularly noteworthy because, at this stage of the project, the synthetic strategy proved to be highly inefficient for the preparation of cyclopropyl derivatives, resulting in very low overall yields. Consequently, we decided to prioritize methyl-substituted compounds to have a more rapid SAR exploration, with the intention of transferring the most promising substitution patterns onto the superior cyclopropyl scaffold.[30] This strategy explains why most compounds in Table 1 feature a methyl group rather than a cyclopropyl group at R^1. The conversion of the methyl ether of **10** to the corresponding hydroxy group resulted in compound **11**, with an IC_{50} of 1.8 μM, showing a fourfold reduction in potency, as the parent compound had an IC_{50} of 0.5 μM. To evaluate positional effects on the aromatic ring, the *meta*-substituted analogue of **9** was synthesized, yielding compound **12**. Transferring the methoxy group from the *para* to the *meta* position of the phenyl ring resulted in a loss in potency, with **12** showing an IC_{50} value of 11 μM. A preference for *para*-substitution was further supported by the comparison of compounds **13** (IC_{50} = 2 μM) and **14** (IC_{50} = 10 μM), where a fivefold difference in potency was observed between the *para*- and *meta*-trifluoromethyl analogues. To assess whether alternative functionalities at the *meta*-position could improve binding, an additional derivative bearing a sulfonamide group, compound **15**, was synthesized. This analogue showed an inhibition potency of 6 μM, further confirming a clear preference for *para* substitutions over *meta* substitutions. The importance of an aromatic moiety at position 3 of the DHPP headgroup was further validated by compound **16**, in which the phenyl ring was replaced by a morpholine ring. As expected, this modification led to a pronounced decrease in binding affinity compared to **6**, with an IC_{50} value of 23 μM, reinforcing the role of aromatic $\pi-\pi$ stacking interactions with Y418. Replacement of the phenyl ring with a heteroaromatic system, specifically a pyridine, resulted in compound **17**, with an IC_{50} value of 8.5 μM. The introduction of a *para*-dimethylamino substituent yielded a potent analogue, compound **18**, (IC_{50} = 4.5 μM). However, particularly notable were the matched-pair compounds **19** and **20**, with IC_{50} values of 2 μM and 0.3 μM, respectively. In this case as well, a significant improvement in potency was observed upon the replacement of the methyl group (compound **19**) with the cyclopropyl group (compound **20**). Importantly, a crystal structure of **20** in complex with YTHDF2 was obtained. As shown in Figure 4D, in addition to the anticipated $\pi-\pi$ stacking interaction with Y418, the carbonyl of the methyl ester substituent engages in an additional hydrogen bond with the side chain $-NH_2$ group of N462. This interaction provides a structural rationale for the marked increase in potency relative to the unsubstituted phenyl analogue **6**. As expected for the reasons listed in the introduction, the two sub-micromolar

Downloaded from pubs.acs.org/jmcmar/article-pdf/doi/10.1021/acs.jmedchem.6c02977/6905752/jm6c02977.pdf by guest on 06 November 2026

https://doi.org/10.1021/acs.jmedchem.6c02977
J. Med. Chem. XXXX, XXX, XXX−XXX

Table 1. 2D Structures and Potency of a Series of Aryl-Substituted Binders of the YTHDF2 Reader Domain[a,b,c]

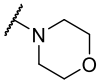
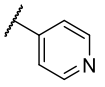
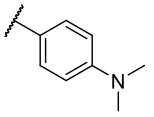
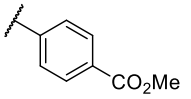
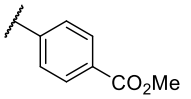
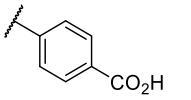
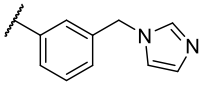
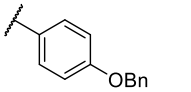


Code	R^1	R^2	IC_{50} (μM)[a]	LE[b]	GI_{50} (μM) MOLM-13/ THP-1[c]
6			2.5 (n=2)	0.40	
7			6	0.40	
8			2	0.39	
9			2 (n=2)	0.41	
10			0.5 ± 0.2 (n=3)	0.41	3.2 ± 0.22 (n=5)/ >50
11			1.8	0.33	
12			11	0.36	
13			2 (n=2)	0.37	
14			10	0.33	
15			6 (n=2)	0.33	

Downloaded from pubs.acs.org/jmcmar/article-pdf/doi/10.1021/acs.jmedchem.6c02977/6905752/jm6c02977.pdf by guest on 06 November 2026

https://doi.org/10.1021/acs.jmedchem.6c02977
J. Med. Chem. XXXX, XXX, XXX–XXX

Table 1. continued

Code	R^1	R^2	IC_{50} (μM)[a]	LE[b]	GI_{50} (μM) MOLM-13/ THP-1[c]
16			23 (n=2)	0.38	
17			8.5 (n=2)	0.41	
18			4.5 (n=2)	0.38	
19			2 (n=2)	0.37	
20			0.3 ± 0.2 (n=4)	0.39	3.9 ± 0.26 (n=4)/ 2.6 ± 0.24 (n=5)
21			3.5 (n=2)	0.38	
22			7.5 (n=2)	0.28	
23			0.9 ± 0.2 (n=3)	0.33	19 ± 2.46 (n=3)/ >50

[a]The IC_{50} value for the YTHDF2 reader domain is measured using a TR-FRET-based binding assay as previously reported. The signal decreases (with respect to the buffer-only measurement) when the binder competes with the binding of the natural ligand, i.e., m^6A-oligoRNA. Thus, the lower the signal, the higher the affinity of the fragment. Each reported value is the average of the IC_{50} values obtained from the individual biological-replicate curves, each of which is itself the average of two technical replicates (Figure S1); the number of biological replicates is indicated as $(n = X)$. Values reported as mean ± SD were measured in biological triplicate or quadruplicate ($n = 3$ or $n = 4$), whereas values shown without an (n) correspond to a single biological replicate. [b]Ligand efficiency calculated according to $LE = \frac{\Delta G}{n_{HA}} \approx -RT\frac{\ln(IC_{50})}{n_{HA}}$. [c]Growth inhibition 50 (GI_{50}) values after 72 h of treatment. The reported values are expressed with their standard deviations (SD) and with the number of replicates given as $(n = X)$.

inhibitors, compounds **10** and **20**, feature similar IC_{50} values among the three YTHDFs (Figure S5). **10** and **20** show selectivity over YTHDC1, and while **10** is only moderately selective (Figure S5), **20** shows a substantially higher potency on the YTHDFs with respect to YTHDC1 (Figure S5). To confirm the selectivity observed through the TR-FRET assay, we conducted a differential scanning fluorimetry (DSF) assay. The results corroborated the previous findings: YTHDF1, YTHDF2, and YTHDF3 show increased stability with both compounds **10** and **20** (Figure S4). In contrast, YTHDC1 and YTHDC2 do not exhibit a significant increase in melting temperature (Figure S4). It is important to consider that YTHDC1 has a substantially lower melting temperature compared to that of YTHDFs, which implies a higher expected stabilization. This is further supported by the results obtained with the 17mer GGm^{6}ACU-containing oligonucleotide control, which shows the expected effect (Figure S4). Compound **20** was further characterized by isothermal titration calorimetry (ITC), which showed a K_d of 0.4 μM for YTHDF2 (Figure 5D). The carboxylic acid **21** showed an IC_{50} of 3.5 μM, and thus no improvement in potency compared to compound **19**. Guided by the structural insights gained from the complex of **20** and YTHDF2 (Figure 4D), we next explored the introduction of larger substituents. The latter was designed to catch more distal interactions, pointing toward the solvent-exposed area, which is part of the RNA-binding groove. To this end, compounds **22** and **23** were synthesized. Compound **23** was particularly noteworthy, as it represented the first submicromolar ligand with a methyl substituent at R^1 (IC_{50} = 0.9 μM, Table 1). Despite its favorable binding affinity, further optimization of this scaffold was not pursued due to its poor solubility, which prevented a reliable evaluation. A crystal structure was obtained for compound **22**, providing additional structural information for this class of analogues (Figure 4E).

Downloaded from pubs.acs.org/jmcmar/article-pdf/doi/10.1021/acs.jmedchem.6c02977/6905752/jm6c02977.pdf by guest on 06 November 2026

https://doi.org/10.1021/acs.jmedchem.6c02977
J. Med. Chem. XXXX, XXX, XXX–XXX

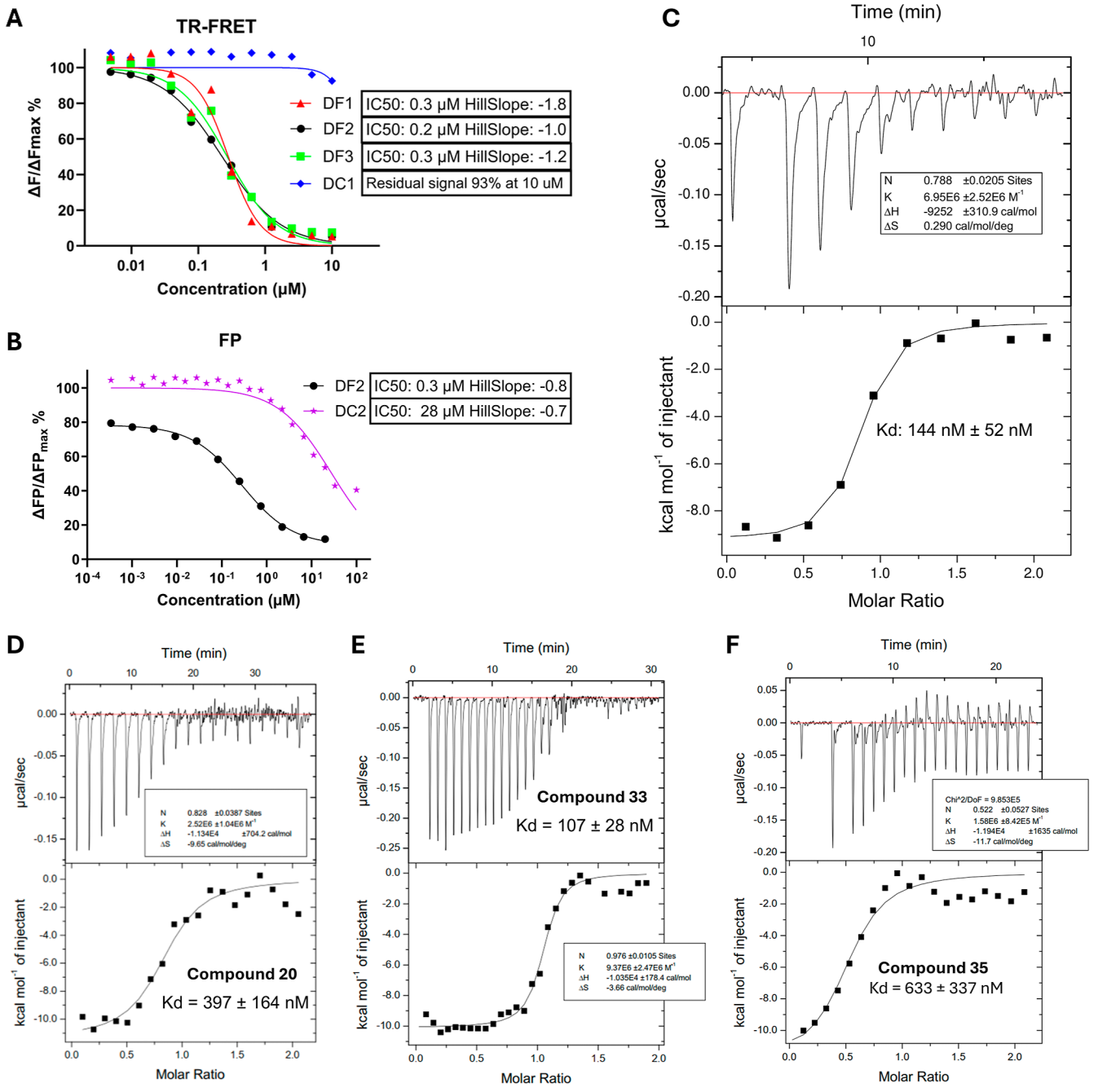


Figure 5. Biochemical characterization of compound **34** and ITC data on four members of the series. (A) TR-FRET and (B) FP dose−response curves for compound **34** against the indicated YTH proteins. In (A), one representative biological replicate is shown for each protein. (C) ITC of compound **34** binding to YTHDF2: raw thermogram (top) and integrated heats fitted to a single-site model (bottom). In this titration, the initial injection was excluded from the fit, and the first fitted point corresponds to a half-volume injection (2 μL vs 4 μL for the following injections), so that its peak and integrated heat are proportionally smaller; the lag time between the first and second injections (~3 min) was longer than the ~1.5 min cadence used thereafter, which accounts for the small offset of the initial integrated points. (D−F) ITC titration curves and thermograms as in (C) for compounds **20**, **33**, and **35**, each acquired with its own injection scheme (see Material and Methods); the larger uncertainty for **35** reflects its limited aqueous solubility.

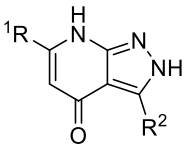
DHPP Ligand Optimization—Heteroaromatic Substituents

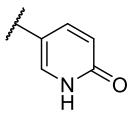
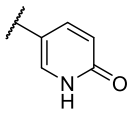
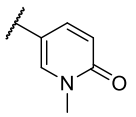
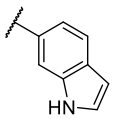
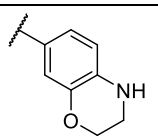
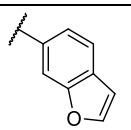
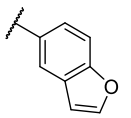
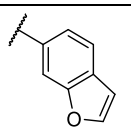
After the completion of the first set of derivatives bearing differently substituted phenyl rings, we decided to further refine the design strategy. Inspection of the crystal structure of **20** highlighted the importance of the additional hydrogen bond formed with N462. We therefore moved toward the identification of aromatic substituents capable of simultaneously enhancing the $\pi-\pi$ stacking interaction with Y418 and engaging the side-chain amide of N462 through one or two hydrogen bonds. With this objective, we shifted our focus from substituted phenyl rings to condensed heteroaromatic substituents, as shown in Table 2. In compound **20**, the hydrogen bond with N462 is mediated by the methyl ester substituent. In contrast, heteroaromatic rings inherently contain nitrogen and/or oxygen atoms that can directly participate in hydrogen bonds. This can

Downloaded from pubs.acs.org/jmcmar/article-pdf/doi/10.1021/acs.jmedchem.6c02977/6905752/jm6c02977.pdf by guest on 06 November 2026

https://doi.org/10.1021/acs.jmedchem.6c02977
J. Med. Chem. XXXX, XXX, XXX−XXX

Table 2. 2D Structures and Potency of Heteroaromatic-Substituted Binders of the YTHDF2 Reader Domain[a,b,c]

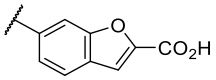
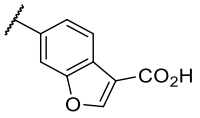
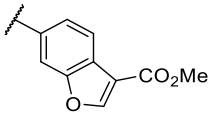
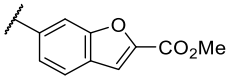
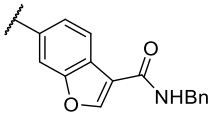
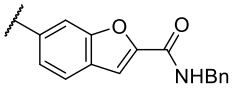


Code	R^1	R^2	IC_{50} (μM)	LE	GI_{50} (μM) MOLM-13/ THP-1
24			3.5 (n=2)	0.42	
25			0.55 (n=2)	0.44	>50 / >50
26			8 (n=2)	0.33	- / >50
27			1.5 (n=2)	0.39	
28			0.85 (n=2)	0.37	16 ± 0.52 (n=3) / >50
29			0.9 ± 0.2 (n=3)	0.41	7.4 ± 0.36 (n=3)/ 10 ± 0.29 (n=3)
30			3 (n=2)	0.38	
31			0.22 (n=2)	0.42	5.6 ± 0.23 (n=3)/ 19 ± 0.74 (n=3)

Downloaded from pubs.acs.org/jmcmar/article-pdf/doi/10.1021/acs.jmedchem.6c02977/6905752/jm6c02977.pdf by guest on 06 November 2026

https://doi.org/10.1021/acs.jmedchem.6c02977
J. Med. Chem. XXXX, XXX, XXX–XXX

Table 2. continued

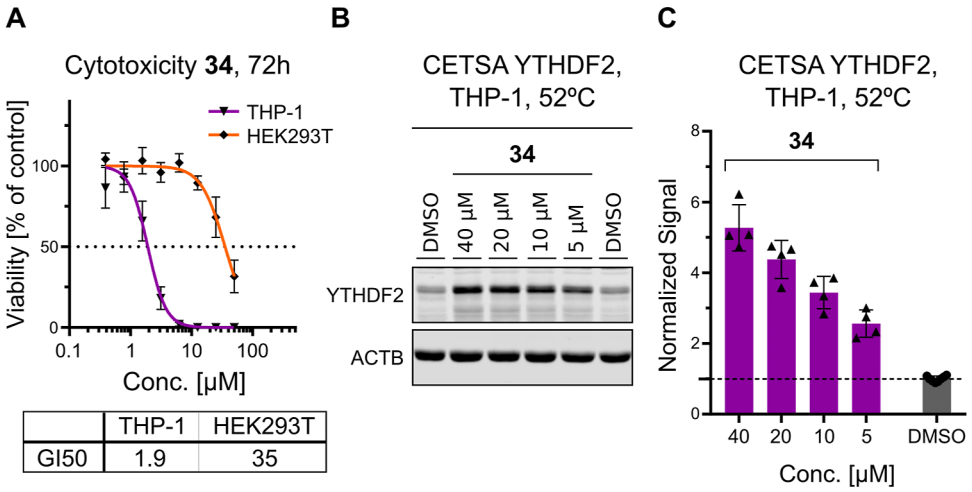
Code	R^1	R^2	IC_{50} (μM)	LE	GI_{50} (μM) MOLM-13/ THP-1
32			0.18 (n=2)	0.36	>50 / >50
33			0.08 (95% CI: 0.078–0.086) (n=3)	0.39	>50 / >50
34			0.2 ± 0.1 (n=3)	0.35	8.9 ± 0.08 (n=2)/ 1.9 ± 0.12 (n=4)
35			0.3	0.34	3.0 ± 0.05 (n=3)/ 1.7 ± 0.03 (n=3)
36			0.5 (n=2)	0.26	7.6 ± 0.16 (n=3)/ 20 ± 1.11 (n=3)
37			1.5 (n=2)	0.25	13 ± 0.48 (n=3)/ 28 ± 1.43 (n=3)

[a]The IC_{50} value for the YTHDF2 reader domain is measured using a TR-FRET-based binding assay as previously reported. The signal decreases (with respect to the buffer-only measurement) when the binder competes with the binding of the natural ligand, i.e., m^6A-oligoRNA. Thus, the lower the signal, the higher the affinity of the fragment. Each reported value is the average of the IC_{50} values obtained from the individual biological-replicate curves, each of which is itself the average of two technical replicates; the number of biological replicates is indicated as $(n = X)$. Values reported as mean ± SD were measured in biological triplicate or quadruplicate ($n = 3$ or $n = 4$), whereas values shown without an (n) correspond to a single biological replicate. For compound **33**, one biological-replicate curve was incomplete, so its IC_{50} was obtained from a single average fit of the pooled complete replicate data and is reported with its 95% confidence interval (95% CI). [b]Ligand efficiency calculated according to $\mathrm{LE} = \frac{\Delta G}{n_{HA}} \approx -RT\frac{\ln(IC_{50})}{n_{HA}}$. [c]Growth inhibition 50 (GI_{50}) values after 72 h of treatment. The reported values are expressed as mean ± SD, with the number of replicates given as $(n = X)$.

potentially lead to more efficient molecules, engaging all the important interactions with the binding pocket while preserving the possibility of further ring modifications. Initially, we focused on nitrogen-containing heteroaromatic rings. The first compound synthesized within this series was compound **24**, bearing a pyridinone ring. The design rationale behind this choice was to form two H bonds with the side chain of N462. This analogue displayed a binding potency of 3.5 μM. Analysis of its crystal structure in the complex with YTHDF2 confirmed that the pyridinone forms two hydrogen bonds with the side chain of N462 (Figure 4F). The oxygen of the pyridinone forms an interaction with the $-NH_2$ of N462, the same observed for compound **20**, while the nitrogen participates in an additional H bond with the carbonyl of the same asparagine. As expected, compound **25**, the corresponding cyclopropyl derivative of **24**, exhibited enhanced potency, with an IC_{50} value of 0.55 μM. To assess whether both pyridinone interactions with N462 were fundamental to the binding affinity, we decided to methylate the nitrogen of the ring. The implementation of this modification yielded compound **26**, which showed a pronounced loss in binding affinity in comparison to **25**, displaying an IC_{50} of 8 μM, confirming the essential role of both H-bonds for the binding. We subsequently explored indole (compound **27**) and benzoxazine (compound **28**). These two compounds showed high binding affinity, with IC_{50} values of 1.5 μM and 0.85 μM, respectively. It is important to note that the difference in potency between these two is probably connected to the different aliphatic group at position 6, methyl for **27**, and cyclopropyl for **28**. However, compound **29**, featuring a benzofuran ring connected to the DHPP headgroup, was found to be the most promising analogue in the series. This compound exhibited sub-micromolar potency ($IC_{50} = 0.9$ μM), similar to that of **28** ($IC_{50} = 0.85$ μM), despite the methyl group at position 6 of the DHPP headgroup instead of a cyclopropyl group. On this basis, we selected the benzofuran ring for further SAR exploration and ligand growth. We first evaluated an alternative connection point between the benzofuran ring and the

Downloaded from pubs.acs.org/jmcmar/article-pdf/doi/10.1021/acs.jmedchem.6c02977/6905752/jm6c02977.pdf by guest on 06 November 2026

https://doi.org/10.1021/acs.jmedchem.6c02977
J. Med. Chem. XXXX, XXX, XXX–XXX



	THP-1	HEK293T
GI50	1.9	35

Figure 6. Biological characterization of compound **34**. (A) Growth inhibition of THP-1 (AML cell line) and HEK293T (non-cancerous cell line control) after 72 h of treatment with compound **34**. Cell viability is expressed as a percentage relative to the DMSO control, $N = 4$. (B) Representative western blot for CETSA of compound **34** in THP-1. (C) Dose-dependent thermal stabilization of YTHDF2 protein upon compound **34** treatment in the dose range of 5 to 40 μM for 1 h, followed by heat shock at 52 °C (CETSA). The data are presented as fold change normalized to ACTB and DMSO control (dotted line at 1.0). The bars show the mean ± SD, and $N = 4$.

DHPP headgroup by synthesizing compound **30**. This compound showed an IC_{50} value of 3 μM, resulting in an approximately threefold decrease in binding affinity compared to **29**. We then synthesized the corresponding cyclopropyl analogue of **29**, compound **31**. Consistent with our previous observations, replacing the methyl group with a cyclopropyl substituent improved the potency, yielding a compound with an IC_{50} of 0.22 μM. Compound **31**, similarly, inhibits YTHDF1 and YTHDF3. In contrast, up to 100 μM, it shows no binding to YTHDC1 in the TR-FRET assay. Additionally, we performed DSF on YTHDF2 and YTHDC1: consistently, **31** stabilizes YTHDF2 but not YTHDC1 (Figure S4).

We next proceeded with the functionalization of the benzofuran ring, following an approach analogous to that employed for the phenyl series. We initially introduced a carboxylic acid group at the 2 and 3 positions of the benzofuran ring, synthesizing compounds **32** and **33**, respectively. Besides probing the tolerance for a negatively charged group in this region of the pocket, the carboxylic acid provides a versatile synthetic handle for further potential optimization by esterification or amide coupling. Compound **32** displayed a potency comparable to that of **31** with an IC_{50} value of 0.18 μM. In contrast, installation of the carboxylic acid at position 3 resulted in a threefold improvement in potency compared to that of **31**, yielding compound **33** with an IC_{50} value of 0.08 μM and a K_d of 0.1 μM, measured by TR-FRET and ITC, respectively.

The carboxylic acid moieties were then further derivatized to the corresponding methyl esters and amides. Methyl esters **34** and **35** showed IC_{50} values of 0.2 μM and 0.3 μM, respectively, therefore displaying slightly reduced potency in the biochemical assay compared to their parent carboxylic acids **33** and **32**. Benzyl amides **36** and **37** were also prepared, with IC_{50} values of 0.5 μM and 1.5 μM, respectively. Although amide formation reduced the binding affinity relative to the parent carboxylic acids, the amide at position 3 of the benzofuran ring (compound **36**) exhibited a higher binding affinity than the one at position 2 (compound **37**), consistent with the trend observed for the methyl esters and parent acids. Compounds **32**, **33**, and **36** were also tested against YTHDF1 and YTHDF3 and, unsurprisingly, showed potencies comparable to those measured for YTHDF2 (Figure S5). Compound **34** was then screened across the full YTH family by TR-FRET, binding YTHDF1, YTHDF2, and YTHDF3 with equal potency (IC_{50} = 0.2–0.3 μM) and showing no detectable binding to YTHDC1 up to 10 μM (Figure 5A). Fluorescence polarization (FP) confirmed binding to YTHDF2 (IC_{50} = 0.3 μM) and revealed a nearly 100-fold selectivity over YTHDC2 (IC_{50} = 28 μM; Figure 5B, S2 and S3), and ITC yielded a K_d of 144 ± 52 nM for YTHDF2 (Figure 5C). Notably, when **34** and **35** were tested in cell viability assays, both compounds inhibited THP-1 proliferation with GI_{50} values of 1.9 μM and 1.7 μM, respectively (Table 2). In contrast, their parent compounds **32** and **33** did not show any biological activity (GI_{50} > 50 μM) when tested under the same conditions. The calculated physicochemical descriptors for **31** (*c*log *P*/tPSA: 3.65/74.7 Å^2), **32** (*c*log *P*/tPSA: 3.30/112.0 Å^2), **33** (*c*log *P*/tPSA: 3.22/112.0 Å^2), **34** (*c*log *P*/tPSA: 3.51/101.0 Å^2), and **35** (*c*log *P*/tPSA: 3.60/101.0 Å^2) are similar in lipophilicity across the series and generally compatible with cell permeability.[31−33] The main distinction is the carboxylic acid group of **32** and **33**, which increases the polar surface area to 112 Å^2 and is deprotonated at physiological pH, consistent with the reduced passive permeability and greater efflux liability expected for the free acids. In the methyl esters **34** and **35**, this carboxylate is masked as a neutral ester,[34,35] consistent with the markedly higher cellular potency of **34** and **35** in the THP-1 cell line (GI_{50} of 1.9 μM and 1.7 μM, respectively) relative to the parent acids **32** and **33** (GI_{50} > 50 μM). By contrast, the descriptors for **31** are fully compatible with cell permeability, so its lower cellular potency (GI_{50} = 19 μM in THP-1) cannot be rationalized based on these physicochemical properties. Compounds **31** and **34** were chosen for a more in-depth biological evaluation, which will be described in the next section.

Biological Characterization

For our biological assays, we selected the THP-1 and MOLM-13 AML cell lines. Multiple studies have demonstrated that the cytosolic m^{6}A-RNA reader proteins YTHDF play an oncogenic role in AML. These proteins are overexpressed in samples

Downloaded from pubs.acs.org/jmcmar/article-pdf/doi/10.1021/acs.jmedchem.6c02977/6905752/jm6c02977.pdf by guest on 06 November 2026

https://doi.org/10.1021/acs.jmedchem.6c02977
J. Med. Chem. XXXX, XXX, XXX–XXX

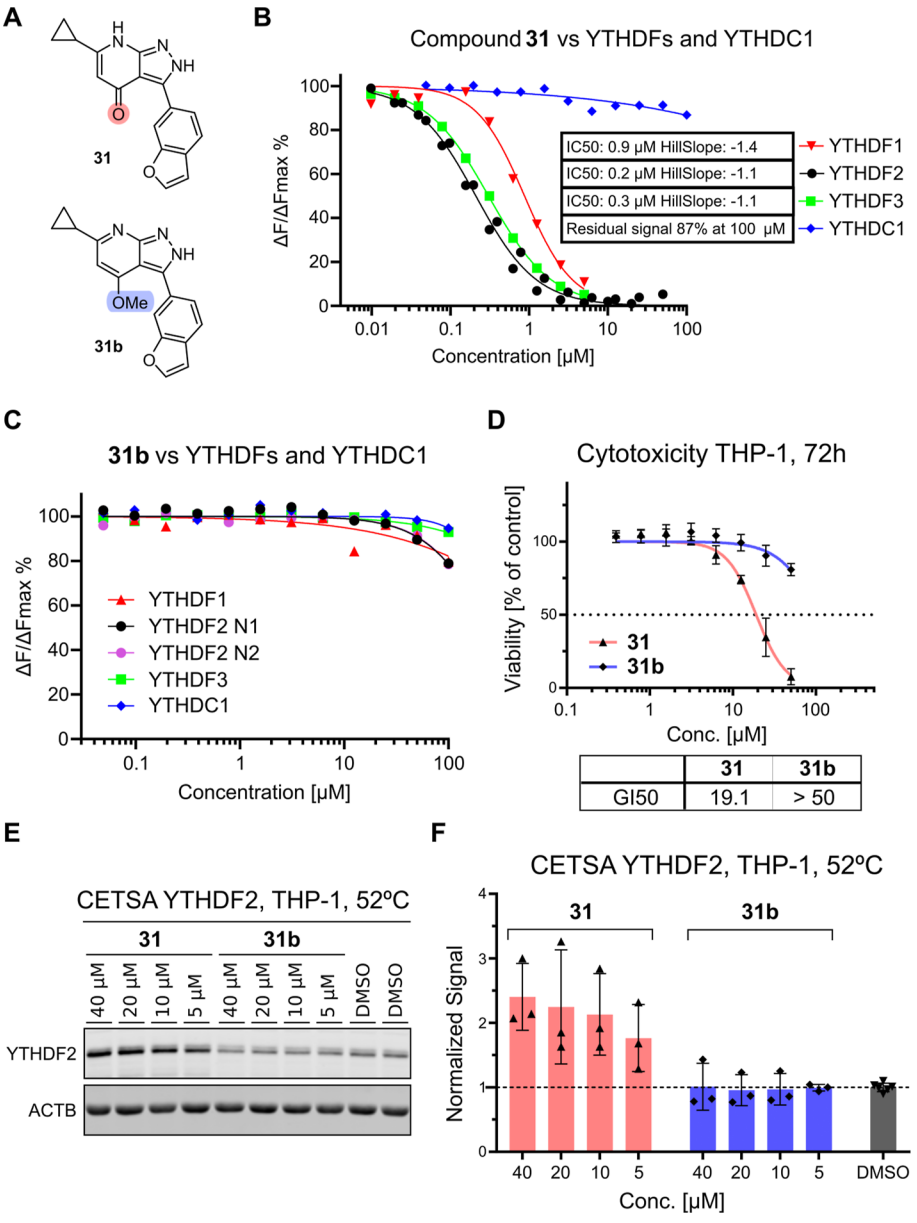


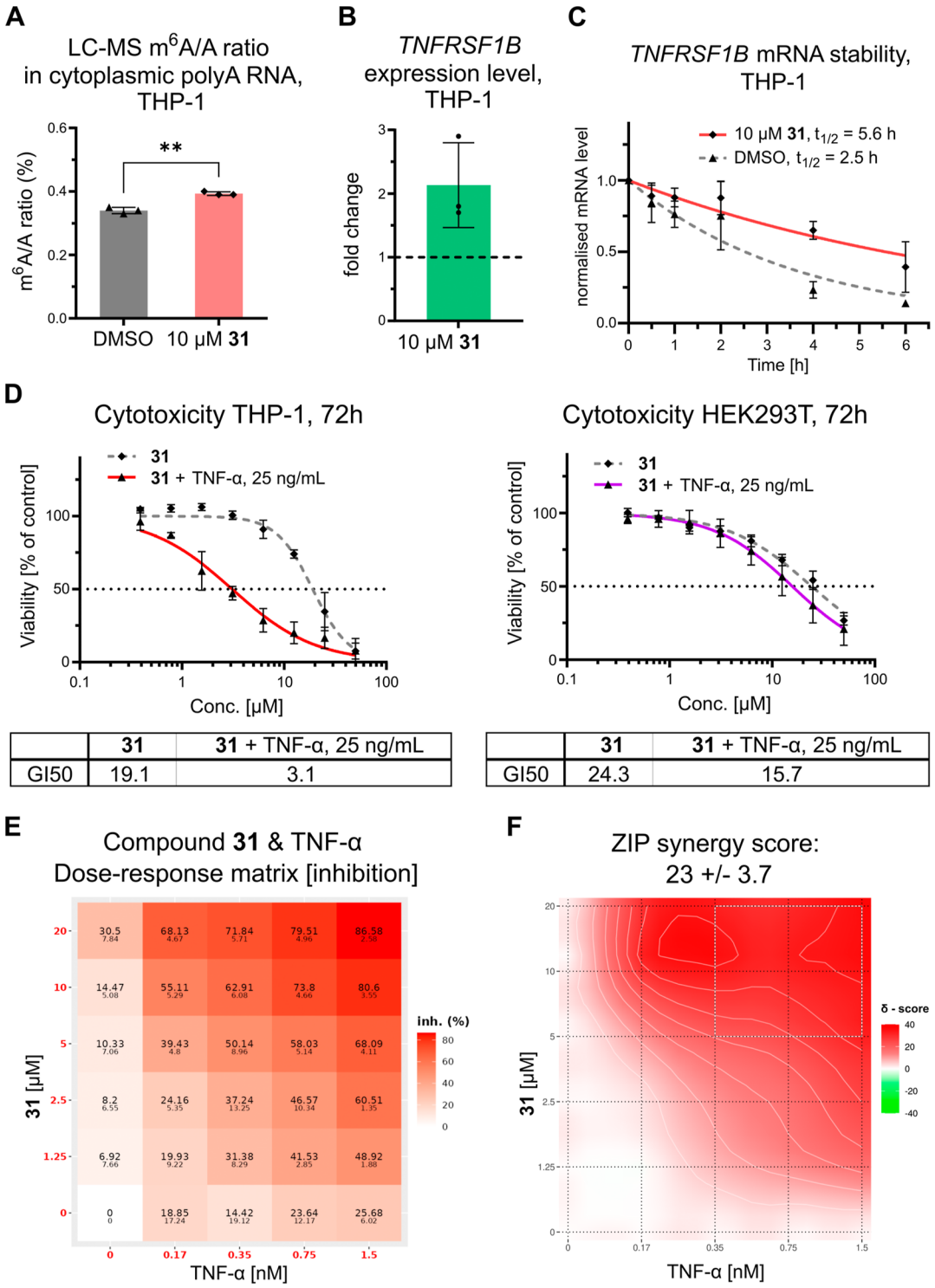
Figure 7. Biological evaluation of compound **31** and its negative control **31b**. (A) Chemical structure of compounds **31** and **31b**. TR-FRET dose–response curves of 31 (B) and 31b (C) against YTHDF1, YTHDF2, YTHDF3, and YTHDC1. (D) Growth inhibition of THP-1 by **31** and **31b** after 72 h of treatment. Cell viability is expressed as a percentage relative to the DMSO control. $N = 3$. (E) Representative western blot for CETSA of **31** and **31b** in THP-1. (F) Dose-dependent thermal stabilization of YTHDF2 protein upon **31** and **31b** treatment at a dose range of 5 to 40 μM for 1 h, followed by heat shock at 52 °C. The data are presented as fold change normalized to ACTB and DMSO control (dotted line at 1.0). The bars show the mean ± SD, and $N = 3$.

collected from AML patients and are essential for the development and maintenance of leukemia.[11,22,36−38] Compound **34**, one of the most potent binders in biochemical assays, was selected for further biological characterization. As shown in Figure 6A, this compound inhibits THP-1 cell proliferation with a GI_{50} value of 1.9 μM after three days. Moreover, compound **34** has a GI_{50} value of 8.9 μM for MOLM-13 (Table 2) and a lower level of toxicity in the HEK293T non-cancerous cell line (GI_{50} = 35 μM), which was used as a control. To provide evidence of binding of compound **34** to YTHDF2 in the cell, we performed a cellular thermal shift assay (CETSA).[39] As shown in Figure 6B,C, inhibitor **34** induces pronounced thermal stabilization of YTHDF2 across the entire concentration range tested (5−40 μM), confirming the interaction between the binder and the target protein inside the THP-1 cells.

Compound **31** shows submicromolar affinity for the three paralogs and is selective against the nuclear reader YTHDC1 (Figure 7B). It was selected for biological evaluation and further cellular experiments as the corresponding O-methylated analogue **31b** had been synthesized as a negative control (Figure 7A). The synthesis of **31b** proved considerably faster and more straightforward than that of the negative control corresponding to the more potent ester **34**. Since an equally well-validated negative control was not readily accessible for **34** and given that **31** is itself among our most potent compounds, the **31**/**31b** pair was chosen for the subsequent mechanistic studies. In **31b**, the 4-oxo group of the DHPP headgroup is replaced by a 4-methoxy

Downloaded from pubs.acs.org/jmcmar/article-pdf/doi/10.1021/acs.jmedchem.6c02977/6905752/jm6c02977.pdf by guest on 06 November 2026

https://doi.org/10.1021/acs.jmedchem.6c02977
J. Med. Chem. XXXX, XXX, XXX−XXX



	31	31 + TNF-α, 25 ng/mL
GI50	19.1	3.1

	31	31 + TNF-α, 25 ng/mL
GI50	24.3	15.7

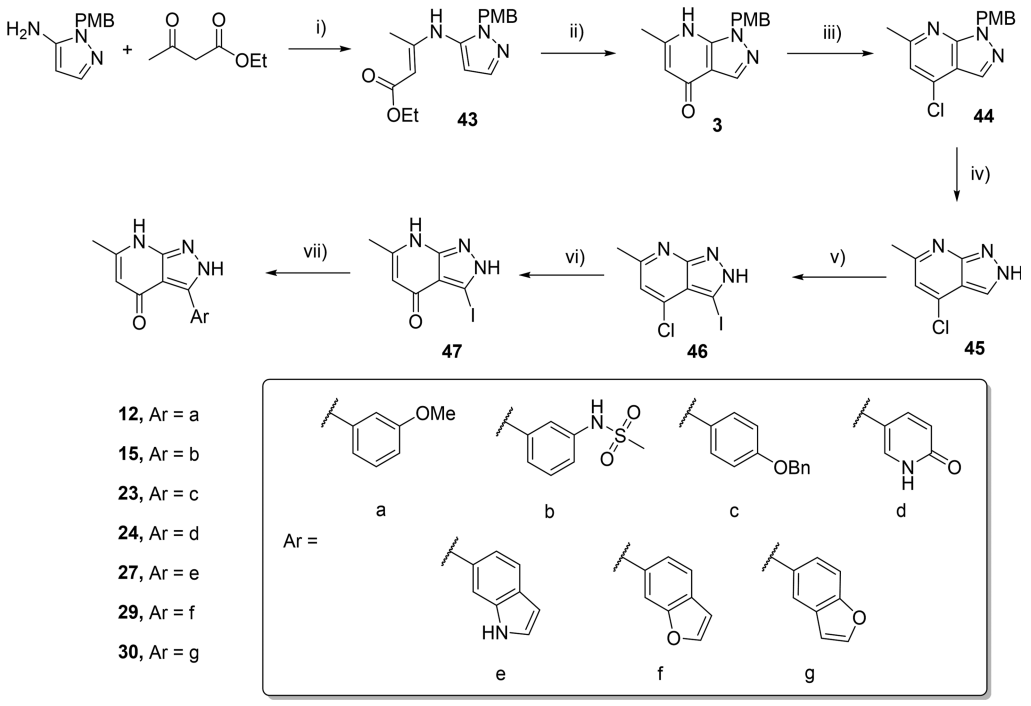
Figure 8. Synergistic effect of YTHDF inhibition with **31** and TNF-α treatment. (A) m^6A/A ratio (%) in the cytoplasmic polyA RNA fraction after 72 h of treatment with 10 μM of compound **31**, measured with LC−MS, $N = 3$. (B) RT-qPCR analysis of *TNFRSF1B* mRNA expression, shown as fold change normalized to 18S rRNA and DMSO control (dotted line at 1.0), $N = 3$. (C) *TNFRSF1B* mRNA stability assessed by the actinomycin D chase. Relative mRNA levels are normalized to 18S rRNA and time 0, $N = 3$. Half-life: in the presence of **31** at 10 μM, $t_{1/2} = 5.6$ h; DMSO control, $t_{1/2} = 2.5$ h. (D) Growth inhibition effects of **31** alone and in combination with TNF-α (25 ng/mL) after 72 h of treatment. Cell viability is expressed as a percentage relative to DMSO control for **31** alone and relative to DMSO + TNF-α (25 ng/mL) for the combination, $N = 3$. (E) Dose−response inhibition matrix for the combined treatment of **31** (0−20 μM) and TNF-α (0−1.5 nM) in THP-1 cells. Inhibition percentages are normalized to untreated controls (**31** 0 μM, TNF-α 0 nM), and $N = 3$. (F) ZIP synergy score analysis (23 ± 3.7) derived from the dose−response matrix data.

group, which results in unfavorable contacts with the binding site. Accordingly, **31b** shows no detectable binding to the three YTHDF paralogs or to YTHDC1 by TR-FRET (Figure 7C), and does not stabilize YTHDF2 in DSF (Figure S4). This makes compound **31b** a useful negative probe. Compound **31** inhibited the proliferation of MOLM-13 with a GI_{50} of 5.6 μM,

Downloaded from pubs.acs.org/jmcmar/article-pdf/doi/10.1021/acs.jmedchem.6c02977/6905752/jm6c02977.pdf by guest on 06 November 2026

https://doi.org/10.1021/acs.jmedchem.6c02977
J. Med. Chem. XXXX, XXX, XXX−XXX

Scheme 2. Synthesis Route for Compounds 12, 15, 23, 24, 27, 29, 30[a]



[a]Reagent and conditions: (i) pTSA, DCE, rt; (ii) neat, 200 °C; (iii) $POCl_3$, *N,N*-dimethyl aniline, reflux; (iv) TFA, reflux; (v) NIS, DMF, 50 °C; (vi) TFA/H_2O, reflux; (vii) $B(OR)_2Ar$ with R = H or Pin, Na_2CO_3, $Pd(dppf)Cl_2$, dioxane, 120 °C.

and the proliferation of THP-1 with a GI_{50} of 19 μM (Figure S7), whereas the negative control **31b** showed negligible cytotoxic activity up to 50 μM (Figure 7D). In the case of MOLM-13, both compounds had a similar effect on proliferation (GI_{50} of around 5 μM, Figure S8). As **31b** showed no measurable binding to the three YTHDF paralogs and YTHDC1 (Figure 7C), this nonspecific activity appears to be restricted to the MOLM-13 cell line. In addition to growth inhibition, treatment with **31** induced morphological changes consistent with myeloid differentiation. Quantitative real-time PCR (RT-qPCR) analysis confirmed that 10 μM of compound **31** significantly upregulated the mRNA levels of myeloid differentiation markers CD11b and CD14 relative to the DMSO control (Figure S6). These results indicate that inhibition of the YTHDF readers by **31** suppresses leukemia cell proliferation and promotes differentiation, suggesting a dual mechanism of action. To confirm target engagement, we performed CETSA in THP-1 cells. Treatment with **31** (5−40 μM, 1 h) resulted in dose-dependent thermal stabilization of YTHDF2 at 52 °C relative to the DMSO control (Figure 7E,F), demonstrating that **31** is cell-permeable and engages YTHDF2 in intact cells. In contrast, the negative control **31b** did not stabilize YTHDF2 at any concentration tested.

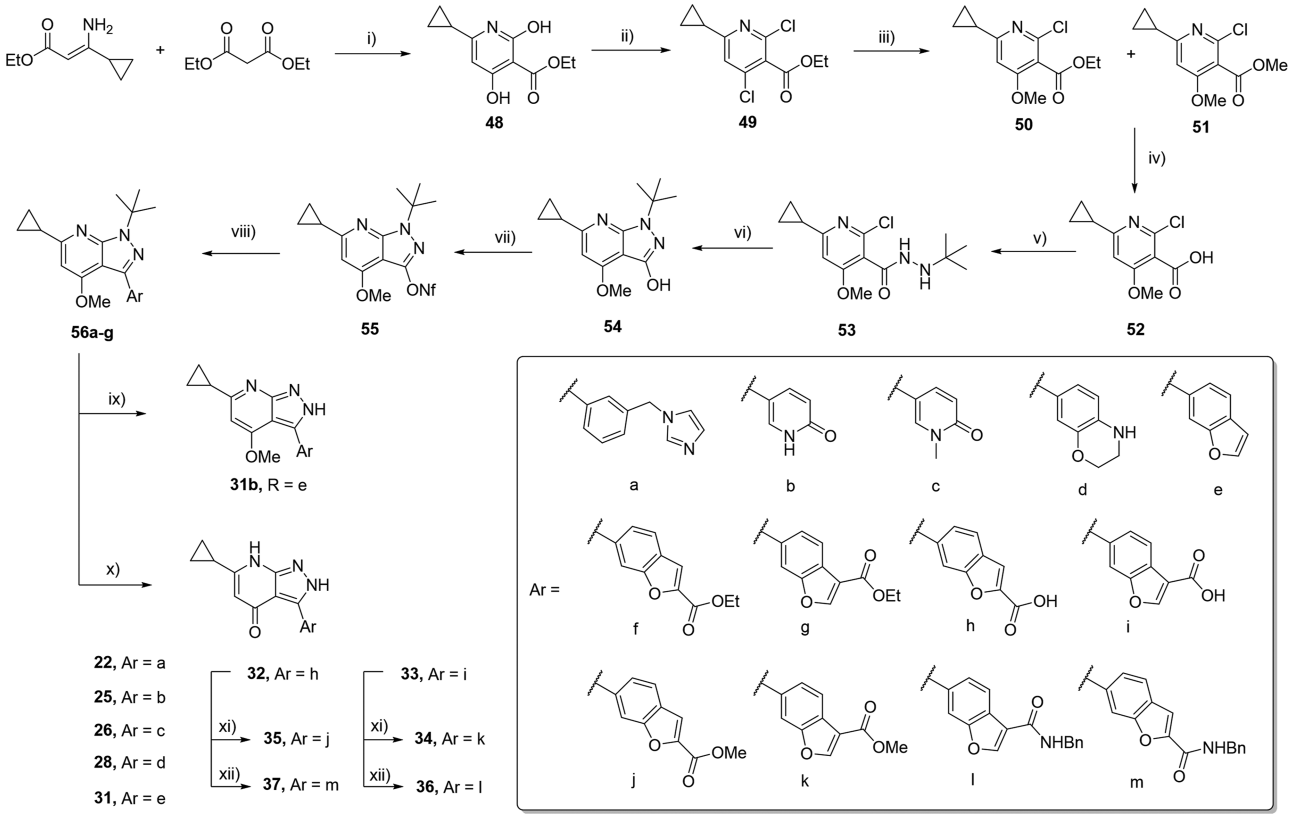
Compound 31 Enhances *TNFRSF1B* mRNA Stability and Expression through m^{6}A-Dependent Mechanisms and Increases the Sensitivity of AML Cells to TNF-α

To evaluate the effects of pharmacological inhibition of the YTHDF readers using compound **31**, we compared it with the reported changes observed after YTHDF2 knockout.[11,40] We investigated the impact on m^{6}A accumulation and found that the m^{6}A fraction in the cytoplasm increased significantly after treatment with 10 μM of compound **31** compared to the DMSO control (Figure 8A). Given the established role of YTHDF2 in the degradation of specific m^{6}A-modified transcripts, we sought to determine whether **31** would increase *TNFRSF1B*[11] mRNA levels and affect its half-life in AML cells. Notably, the *TNFRSF1B* transcript is highly methylated in AML cells and negatively correlates with YTHDF2 expression. RT-qPCR revealed that treatment with compound **31** resulted in approximately 2-fold elevation of *TNFRSF1B* mRNA levels relative to the DMSO control (Figure 8B). Next, we conducted actinomycin D chase experiments to quantify *TNFRSF1B* mRNA decay kinetics. Compound **31** treatment significantly stabilized *TNFRSF1B* mRNA, increasing its half-life to 5.6 h compared to 2.5 h in DMSO control cells (Figure 8C). These findings demonstrate that pharmacological inhibition of the YTHDF readers with our compound effectively prevents the degradation of m^{6}A-modified *TNFRSF1B* transcripts in THP-1 cells, mirroring the effects of genetic knockout of YTHDF2.[11] Serum TNF-α levels are significantly elevated in AML cases compared to healthy controls and show a positive correlation with incomplete remission status.[41] Despite high TNF-α levels, AML-derived cells exhibit increased resistance to TNF-α-induced cell death signals relative to non-cancerous primary human monocytes.[42] We wanted to verify whether the observed increase in the level of TNF receptor 2 transcript (*TNFRSF1B*) following **31** treatment would increase the sensitivity of our AML cell model (THP-1 cells, Figure S9A) to TNF-α. Although TNFR2 lacks the death domain, it has been demonstrated to promote cell death together with TNFR1 in human leukemia.[43,44] First, we performed a co-treatment cytotoxicity experiment where we combined ligand **31** with a single concentration of TNF-α (25 ng/mL) (Figure 8D). THP-1 cells exhibited significantly increased sensitivity to the combination treatment, with an over 6-fold reduction in GI_{50} upon co-treatment with TNF-α (3.1 μM vs 19 μM). The effect was not observed with the negative control compound **31b** (Figure S9B). Notably, the sensitization effect was also not pronounced in the

Downloaded from pubs.acs.org/jmcmar/article-pdf/doi/10.1021/acs.jmedchem.6c02977/6905752/jm6c02977.pdf by guest on 06 November 2026

https://doi.org/10.1021/acs.jmedchem.6c02977
J. Med. Chem. XXXX, XXX, XXX−XXX

Scheme 3. Synthesis Route for Compounds 22, 25, 26, 28, 31b, and 31−37[a]



[a]Reagent and conditions: (i) Na, dry EtOH, 60 °C to 120 °C; (ii) $POCl_3$, 150 °C; (iii) NaOMe 2.5 M in MeOH, dry MeOH, 60 °C; (iv) NaOH, MeOH, 90 °C; (v) $(CH_3)_3NHNH_3Cl$, HATU, DIPEA, dry DMF, 0 °C to rt; (vi) neat, 140 °C; (vii) Nonafluorobutanesulfonic anhydride, pyridine, dry DCM, −78 °C to rt; (viii) $B(OR)_2Ar$ with R = H or Pin, Na_2CO_3, Pd tetrakis, dioxane, 100 °C; (ix) TFA, 120 °C; (x) HCl 37%, dioxane, reflux; (xi) $SOCl_2$, dry MeOH, 0 °C to rt; (xii) $BnNH_2$, EDC, HOBt, DIPEA, dry DMF, 0 °C to rt.

non-cancerous cell line HEK293T, where **31** alone and in combination with TNF-α yielded similar GI_{50} values (24 μM and 16 μM, respectively). In order to evaluate the potential synergistic effect of the combination of **31** and TNF-α, a dose−response inhibition matrix experiment was performed (Figure 8E). The zero interaction potency (ZIP) synergy score measures the effectiveness of drug combinations by comparing the change in potency of the dose−response curves between individual drugs and their combined effect.[45] A ZIP value >10 indicates a synergistic effect, i.e., the combination of two drugs is more effective than the sum of individual effects. A strong synergistic effect was observed, with a ZIP synergy score of approximately 23, confirming positive interactions between YTHDFs inhibition by **31** and TNF-α in THP-1 cells (Figure 8F). The synergy was not observed in a dose−response inhibition matrix with compound **31b** and TNF-α (Figure S9C,D), confirming the specificity of the effect. The results of the biological experiments confirm the proof-of-concept approach of blocking the activity of the YTHDF family of m^6A reader proteins with a small-molecule ligand and open the opportunity for the development of novel treatment strategies for AML.

Chemistry

We initially developed a synthetic strategy to access the DHPP headgroup, as outlined in Scheme 1 for the synthesis of compound **4**. N^1-*para*-methoxybenzyl (PMB)-protected pyrazole was reacted with ethyl propionyl acetate in the presence of catalytic *p*-toluenesulfonic acid to afford the corresponding enamine **39**. This intermediate was used without purification in the subsequent cyclization step, which was performed under solvent-free conditions by heating the crude enamine at 200 °C to form compound **41**.[46] Removal of the PMB protecting group was then achieved by refluxing it in trifluoroacetic acid (TFA), providing compound **4**. The synthesis of compounds **6−10**, **13**, **14**, and **17−20** followed a similar route. First, all pyrazole precursors bearing an aryl substituent at the 3-position had to be prepared in-house, via condensation of the corresponding β-cyanoketones bearing the desired aryl group with PMB-protected hydrazine in the presence of acetic acid, yielding intermediates **38a−h** (Scheme 1).[47] These compounds were then subjected to enamine formation. Notably, under the previously established reaction conditions, compounds **38a−h** proved less reactive toward enamine formation compared to the analogue scaffold without aryl substituents. For this reason, the enamine intermediates **40a−h** were formed from **38a−h** using acetic acid as the solvent and heating the reaction mixture at 70 °C. Formation of the cyclopropyl enamines was particularly challenging and proceeded in very low yield. This limitation represents the main reason why, at this stage of the project, SAR exploration was primarily conducted on the less-potent methyl derivatives, with subsequent translation of the most promising analogues to the cyclopropyl series. Once enamines **40a−h** were obtained, the synthesis remained the same as that used for compound **4**. Cyclization of **40a−h** was conducted under solvent-free conditions at 200 °C, affording compounds **42a−h**. The final TFA-mediated PMB deprotection provided us with compounds **6−10**, **13**, **14**, **17−20**. Compounds **11** and **21** were obtained after the

Downloaded from pubs.acs.org/jmcmar/article-pdf/doi/10.1021/acs.jmedchem.6c02977/6905752/jm6c02977.pdf by guest on 06 November 2026

https://doi.org/10.1021/acs.jmedchem.6c02977
J. Med. Chem. XXXX, XXX, XXX−XXX

deprotection of the methoxy and methyl ester groups from compounds **10** and **19**, respectively.

The synthetic route described in Scheme 1 had a big limitation of not being convergent, requiring the preparation of a differently substituted pyrazole for each target compound. To address this issue, we focused on the optimization of the synthetic route, summarized in Scheme 2. The guiding principle was the generation of an advanced intermediate that could serve as a common precursor for multiple final compounds via cross-coupling reactions. Using the same procedure employed for compound **4**, compound **3** was initially prepared from enamine **43**. All attempts to introduce a halogen at position 3 of the condensed scaffold resulted in the halogenation of position 5 instead. To overcome this regioselectivity issue, the idea was to deactivate position 5 by replacing the oxygen at position 4 with a halogen atom. Treatment of compound **3** with phosphorus oxychloride ($POCl_3$) afforded compound **44** in good yield.[48] Subsequent removal of the PMB protecting group was achieved by refluxing **44** in TFA, providing compound **45** in high yield. Iodination of compound **45** with *N*-iodosuccinimide proceeded at the desired position, affording compound **46** in 65−70% yield.[49] The hydrolysis of the chlorinated position 4 of **46** was performed by refluxing it in a mixture of water and TFA, yielding the advanced intermediate **47**. This compound was subsequently employed as a coupling partner in several Suzuki cross-coupling reactions to access compounds **12**, **15**, **23**, **24**, **27**, **29**, and **30**.

Although the strategy described in Scheme 2 represented a substantial improvement, it still relied on enamine formation as an early synthetic step, which, as discussed above, proved particularly problematic for cyclopropyl derivatives. We therefore moved on with a further optimization of the synthetic strategy, as summarized in Scheme 3. We started with the synthesis of compound **48**, a poly-substituted pyridine bearing a cyclopropyl group at position 6.[50] Chlorination of both hydroxyl groups was then achieved by refluxing compound **48** in $POCl_3$, affording di-chlorinated intermediate **49**.[51] This compound was subjected to a nucleophilic aromatic substitution (S_NAr) reaction to introduce a methoxy group at position 4 of the pyridine ring.[52] This transformation consistently yielded a mixture of **50** and **51**; however, this mixture could be used in the subsequent hydrolysis step, which was carried out using an aqueous solution of sodium hydroxide in methanol at 90 °C, affording compound **52** in quantitative yield.[53] Compound **52** was then reacted with the hydrochloride salt of *tert*-butyl hydrazine to give hydrazide **53**.[54] Cyclization to form the pyrazole ring was performed under neat conditions at 140 °C, providing compound **54**.[55] The oxygen in position 3 of **54** could then be converted into a triflate or nonaflate group, to then undergo a cross-coupling reaction. The nonaflate was preferred to the corresponding triflate due to its higher stability.[56] Accordingly, treatment of compound **54** with nonafluorobutanesulfonic anhydride afforded compound **55**. This intermediate was employed in a series of Suzuki cross-coupling reactions to yield compounds **56a−g**. After the final deprotection of the *tert*-butyl and methoxy groups, the target compounds **22, 25**, **26**, **28**, **31, 32**, and **33** were obtained. Amides **36** and **37** were obtained through an amide coupling reaction between compounds **32** and **33** with benzylamine. Compound **31b** was obtained after the selective deprotection of the *tert*-butyl group from compound **56e**, which was selectively removed with TFA. Methyl esters **34** and **35** were obtained through the methylation of carboxylic acids **32-33**, which was conducted in dry methanol with $SOCl_2$.

CONCLUSIONS

We have presented a protein structure-based medicinal chemistry campaign that has resulted in the pan-YTHDF inhibitor **34** (YTHDF2 K_d = 0.14 μM as measured by ITC and IC_{50} = 0.2 μM by TR-FRET). Compound **34** binds the three YTHDF paralogs with comparable affinity, while it is selective against YTHDC1 and YTHDC2. During the campaign, we solved the high-resolution crystal structures of the complex of YTHDF2 with six analogues of **34**, which provide information on conserved hydrogen bonds with the m^6A recognition pocket of YTHDF2. Compound **34** reduces the proliferation of the AML cell line THP-1 (GI_{50} = 1.9 μM) and shows significantly lower toxicity on the non-cancerous cell line HEK293T (GI_{50} = 35 μM). Evidence of the engagement of the YTHDF2 target in the THP-1 cell line was provided by CETSA for compounds **31** and **34**. Finally, we show that the inhibition of the YTHDF readers by **31** increases the level and stability of the *TNFRSF1B* transcript. This renders THP-1 cells more sensitive to TNF-α-induced cell death. Compound **34** and the pair **31** and **31b** (negative probe) are tool compounds for investigating the role(s) of the cytoplasmic m^6A-RNA readers YTHDF1, YTHDF2, and YTHDF3.

MATERIAL AND METHODS

TR-FRET Assay (IC_{50})

GST-YTHDC1, GST-YTHDF1, GST-YTHDF2, and GST-YTHDF3 were purified as previously reported.[29] The TR-FRET assay was assembled as detailed in ref (Li)[57] with the only difference being that the starting concentration of the dose−response experiments used for the IC_{50} determination was variated dependently from the tested compound. The same protocol was applied to the four proteins. In all cases, the signal was measured using a Spark plate reader (Tecan), with a 320 nm excitation filter and 620 nm (measurement 1) or 665 nm (measurement 2) emission filters, a dichroic 510 nm mirror, 75 flashes, and applying a lag time of 100 μs and an integration time of 400 μs. The dose−response data were analyzed using GraphPad Prism 9.

Fluorescence Polarization Assay (IC_{50})

The FP assay was performed according to the published protocol.[58] In brief, a 5′-fluorescein-labeled 6mA-DNA probe (5′-FAM-AAGAACCGG(6mA)CTAAGCT-3′) at a final concentration of 3 nM was incubated with the protein. For YTHDC2 measurements, the protein concentration was set to 25 nM, whereas for YTHDF2 measurements, it was set to 10 nM. The compound was serially diluted and mixed with the protein−probe complex to generate a dose−response curve. The competition experiments were conducted in a final volume of 20 μL in buffer containing 20 mM Tris−HCl (pH 7.4), 150 mM NaCl, and 0.01% bovine serum albumin (BSA), using a 384-well black, flat-bottom microplate (Corning 3575). After incubation for 1 h, anisotropy values were measured using a Tecan SPARK plate reader with 485/20 nm excitation and 535/25 nm emission polarization filters suitable for fluorescein at 25 °C.

YTHDF2 Protein Crystallography and Soaking

The YTH domain of YTHDF2 was expressed, purified, crystallized, and soaked as described.[1] The structure of YTHDF2 in complex with **20** was exceptionally obtained through co-crystallization. The protein at a concentration of 15 mg/mL was mixed with a large excess of crystalline **20** to create a

Downloaded from pubs.acs.org/jmcmar/article-pdf/doi/10.1021/acs.jmedchem.6c02977/6905752/jm6c02977.pdf by guest on 06 November 2026

https://doi.org/10.1021/acs.jmedchem.6c02977
J. Med. Chem. XXXX, XXX, XXX−XXX

saturated solution. The mix was then sonicated for 30 s, the undissolved powder was resuspended, and the mix was incubated for 5 min on ice. The process was repeated two times. The mix was then centrifuged for 10 min at 14,000 rpm at 4 °C to separate the solution from the remaining undissolved pellet. The supernatant was mixed in a 1:1 ratio with a solution of 0.2 M $(NH_4)2SO_4$, 0.1 M MES pH 6.5, and 30% w/v PEG MME 5K and dispensed (0.2 μL) in an Intelli-Plate 96-3 LVR (sitting drop vapor diffusion). Crystals appeared after approximately one month of incubation at 4 °C. Data were acquired at the P13 (EMBL, DESY, Hamburg), ID30B (ESRF, Grenoble), PXI, and PXIII (Swiss Light Source, Paul Scherrer Institute, Villigen) beamlines. The resulting data were analyzed using AutoPROC, and the structures were solved and refined as described in refs 1,59−63 Data collection and refinement statistics are summarized in Table S1.

Differential Scanning Fluorimetry

The YTH domains of YTHDF1 (residues 361−559), YTHDF2 (residues 383−579), YTHDF3 (residues 387−585), YTHDC1 (residues 345−509), and YTHDC2 (residues 1285−1424) were purified as previously described.[30] YTHDC1, YTHDF1, YTHDF2, YTHDF3, and YTHDC2 were buffered in 50 mM HEPES pH 7.5, 150 mM NaCl, and tested in a white 96-well plate at a final concentration of 2 μM. SYPRO Orange dye was added to the mix with a volume ratio of 1:1000. The ligands were also added to the mix and tested as a set of 2-fold dilutions. Fluorescence monitoring was performed using a LightCycler 480 System. The temperature was set up to increase with a ramp rate of 0.06 °C/s from 20 °C to 85 °C, and 10 acquisitions per °C were taken in dynamic integration time mode and using a red 610 (498−610) filter combination. The melting curves were calculated using the Tm calling analysis of the LightCycler 480 software release 1.5.1.62 SP3, and data were further analyzed using GraphPad Prism 9.

Isothermal Titration Calorimetry

ITC measurements were performed on a MicroCal iTC200 microcalorimeter (GE Healthcare) at 18 °C (compounds **20** and **33**) or 25 °C (compounds **34** and **35**). YTHDF2 (383−579) and the ligands were prepared in 20 mM HEPES pH 7.5 and 150 mM NaCl, with the DMSO concentration (0.05−2%, depending on the compound) matched between the syringe and the sample cell. Titrations were performed in the reverse configuration: protein in the syringe (100 μM for **20**, **34**, and **35**; 200 μM for **33**) was titrated into the sample cell containing the compound (10 or 20 μM). For compounds **20** and **35**, an initial injection of 1 μL was followed by 19 injections of 2 μL; for compound **33**, an initial injection of 0.5 μL was followed by 29 injections of 1.2 μL; and for compound **34**, an initial injection of 0.5 μL was followed by a 2 μL injection and then by 4 μL injections, with ∼3 min between the first and second injections and ∼1.5 min between the subsequent injections. In every experiment, the reduced-volume initial injection was excluded from the fit, as is standard practice, to account for the material lost by diffusion at the syringe tip during equilibration. Thermograms were integrated and fitted with a single-site binding model in the MicroCal Origin software package. Each ligand was measured in a single titration; the reported dissociation constants (K_d) and their errors correspond, respectively, to the best-fit value and to the standard error of the nonlinear least-squares fit. For compound **35**, the limited aqueous solubility of the ligand produced scatter in the binding isotherm and accounted for the larger relative uncertainty of its K_d (633 ± 337 nM).

Cell Culture

THP-1, MOLM-13, and HEK293T cell lines were obtained from DSMZ (German Collection of Microorganisms and Cell Cultures GmbH). THP-1 and MOLM-13 cells were cultured in RPMI 1640 medium supplemented with 10% fetal bovine serum (FBS; Gibco) and 1% penicillin/streptomycin (complete medium). HEK293T cells were maintained in DMEM containing 4.5 g/L glucose and GlutaMAX, supplemented with 10% FBS (Gibco) and 1% penicillin/streptomycin (complete medium). All cell lines were cultured at 37 °C in a humidified incubator with 5% CO_2. All cell lines tested negative for mycoplasma contamination (PCR-based assay; Microsynth, Switzerland).

Cell Viability

THP-1 and MOLM-13 cells were seeded in white clear-bottom 96-well plates at a density of 6×10^3 cells/well or 2×10^4 cells/well, respectively, in 50 μL of complete RPMI medium. HEK293T cells were seeded at a density of 5×10^3 cells/well in 50 μL of complete DMEM. Cells were treated with 50 μL of increasing concentrations of the indicated compounds dissolved in DMSO (final concentration of compounds 0.4−50 μM) or DMSO only (0.5% (v/v)) as a negative control and incubated for 72 h at 37 °C with 5% CO_2. For TNF α treatment, a final concentration of 25 ng/mL TNF α (0291-TA-020, R&D Systems) was used, and data were normalized to the DMSO + TNF α−treated control. For co-treatment experiments, cells were treated with compound 31 and recombinant human TNF-α in a 5 × 5 concentration matrix. Compound **31** was tested at 1.25, 2.5, 5, 10, and 20 μM and TNF-α at 0, 0.17, 0.35, 0.75, and 1.5 μM. Growth inhibition was normalized to the DMSO control. Synergy scores were calculated and visualized using the SynergyFinder web application.[45] Cell viability was determined using a CellTiter-Glo luminescent cell viability assay (G9243, Promega) according to the manufacturer's instructions. 100 μL of the reagent was added to each well and incubated for 10 min at room temperature on an orbital shaker. The luminescence was recorded using a Tecan Infinite 3046 M1000 microplate reader from the top. Cell viability curves were plotted in GraphPad Prism 9 and fitted with nonlinear regression, from which GI_{50} values were determined. The assay was carried out with two technical replicates for each concentration and repeated three to four times on different days.

Cellular Thermal Shift Assay

One million THP-1 cells were suspended in 100 μL of PBS (10010023, Thermo Fisher Scientific) supplemented with a 2× protease inhibitor cocktail (11697498001, Roche) for each experimental condition. The cells were incubated with compounds or DMSO control (1% (v/v)) for 1 h at 37 °C. Samples were then heated up to 52 °C for 3 min, followed by cooling to room temperature. Next, samples were lysed by three freeze−thaw cycles in liquid nitrogen and centrifuged at 16,000*g* for 30 min at 4 °C. Equal volumes of control and tested samples (12 μL) were analyzed by western blot. The protein signal was quantified by densitometry in Image Studio Lite software. The amount of YTHDF2 (#80014, Cell Signaling, 1:1000) protein was first normalized to β-actin (ab8226, Abcam, 1:2000) and then to DMSO control and analyzed in GraphPad Prism 9.

Downloaded from pubs.acs.org/jmcmar/article-pdf/doi/10.1021/acs.jmedchem.6c02977/6905752/jm6c02977.pdf by guest on 06 November 2026

https://doi.org/10.1021/acs.jmedchem.6c02977
J. Med. Chem. XXXX, XXX, XXX−XXX

Quantification of the m^{6}A/A Ratio in the Cytoplasmic Fraction of Polyadenylated RNA Using UPLC-MS/MS

THP-1 cells were seeded in 6-well plates at a density of 5×10^5 cells/mL in 2 mL of complete RPMI medium. Cells were treated with 10 μM of compound **31** in DMSO 0.5% (v/v) or DMSO alone as a negative control. After 72 h, cytoplasmic RNA was isolated using the Cytoplasmic and Nuclear RNA Purification Kit (Norgen Biotek Corp., Thorold, Canada) according to the manufacturer's instructions, with the following modification: after addition of Lysis buffer J and centrifugation-based separation of cellular fractions, the cytoplasmic fraction was further subjected to spin column-based RNA purification, and the nuclear pellet was discarded. Polyadenylated RNA extraction and UPLC-MS/MS were performed as previously described.[64] Briefly, 50 μL of total RNA was subjected to two rounds of purification using 25 μL of Sera-Mag magnetic oligo(dT) particles (Cytiva) per sample. The polyadenylated RNA was eluted with nuclease-free water in a final volume of 25 μL, and its concentration was determined using a NanoDrop. 100 ng of mRNA was digested to nucleosides and dephosphorylated in a one-pot reaction using 0.5 μL of nucleoside digestion mix (M0649S, NEB) in 25 μL of total reaction volume for 4 h at 37 °C. The samples were used for UPLC-MS/MS analysis without further purification steps.

Quantitative Real-Time PCR

THP-1 cells were seeded in 6-well plates at a density of 2.5×10^5 cells/mL in 2 mL of complete RPMI medium. Cells were treated with 10 μM of compound **31** in DMSO 0.5% (v/v) or DMSO alone as a negative control. After 72 h, the cells were collected by centrifugation and washed twice with ice-cold PBS. Total RNA was extracted using the RNeasy Mini Kit (74104, Qiagen, Hilden, Germany) according to the manufacturer's instructions, and RNA concentration and purity were determined using NanoDrop). 1 μg of total RNA was reverse-transcribed into cDNA using the High-Capacity cDNA Reverse Transcription Kit (4368814, Applied Biosystems, Thermo Fisher Scientific) according to the manufacturer's protocol. RT-qPCR was performed on 20 ng of cDNA per reaction using the Fast SYBR Green Master Mix (4385616, Applied Biosystems, Thermo Fisher Scientific) on a LightCycler 480 Real-Time PCR System (Roche, Basel, Switzerland). Thermal cycling conditions were as follows: initial denaturation at 95 °C for 5 min, followed by 40 cycles of denaturation at 95 °C for 15 s, annealing at 56 °C for 30 s, and extension at 72 °C for 30 s. Melt curve analysis was performed at the end of each run to confirm amplicon specificity. The following primers were used: TNF-α forward 5′-TGGGCCAAGTTCCTCTAGTG-3′ and reverse 5′-CAGGTCACAGAGAGTCAGGG-3′; 18S rRNA forward 5′-CTACCACATCCAAGGAAGCA-3′ and reverse 5′-TTTTTC-GTCACTACCTCCCCG-3′. Relative gene expression was normalized to 18S rRNA as the internal reference gene and calculated using the $2^{-\Delta\Delta CT}$ method.

mRNA Stability Assay

THP-1 cells were seeded in 6-well plates at a density of 2.5×10^5 cells/mL in 2 mL of complete RPMI medium. Cells were treated with 10 μM of compound **31** in DMSO 0.5% (v/v) or DMSO alone as a negative control. After 72 h, actinomycin D (A9415, Sigma-Aldrich) was added to a final concentration of 10 μg/mL. Cells were harvested at t = 0, 0.5, 1, 2, 4, and 6 h after actinomycin D addition, and total RNA was extracted and analyzed by RT-qPCR, as described in the previous section. Values were first normalized to 18S rRNA within each sample, then to the DMSO control at each time point, and expressed relative to t = 0 to obtain mRNA decay curves. mRNA half-lives ($t_{1/2}$) were determined by nonlinear regression using a one-phase exponential decay model in GraphPad Prism.

Chemistry

All reagents were purchased from commercial suppliers and used as received. Reactions run at elevated temperatures were carried out in an oil bath, and the temperatures given in the synthetic procedures refer to the oil bath temperature. Unless stated otherwise, reactions carried out according to a general procedure used the reaction time and temperature given in that procedure. Our research group successfully synthesized all the compounds as described, except for compounds **3**, **5**, and **16**, which were obtained from a commercial supplier. All compounds have ≥95% purity (HPLC). Individual purity values for compounds **4**, **6**−**15**, **17**−**37**, **31b**, and **55** are reported in the Characterization section. All reactions were monitored by thin-layer chromatography (aluminum plates coated with silica gel 60 F254). Flash column chromatography was carried out over silica gel (0.040−0.063 mm) or aluminum oxide (0.050−0.200 mm). SiliaMetS TAAcONa (or SiliaMetS Triaminetetraacetate, sodium salt) is a silica-bound metal scavenger for Pd(II), Ni(II), and Cu. It is the supported version of EDTA in its sodium-salt form. 1H and 13C {1H} NMR spectra were recorded on AV2-400 MHz, AV2-500, and AV-600 Bruker spectrometers (400 MHz, 101 MHz, 500 MHz, 126 MHz, and 600 MHz, 150 MHz, respectively) in DMSO-d_6, $CDCl_3$, or MeOD-d_4. Chemical shifts are given in ppm, and their calibration was performed to the residual ^{1}H and ^{13}C signals of the deuterated solvents. Multiplicities are abbreviated as follows: singlet (s), doublet (d), triplet (t), multiplet (m), and broad signal (bs). The purity was acquired by liquid chromatography high-resolution electrospray ionization mass spectrometry (LC-HR-ESI-MS): Acquity UPLC (Waters, Milford, USA) connected to an Acquity eλ diode array detector and a Synapt G2 HR-ESI-QTOF-MS (Waters, Milford, USA); injection of 1 μL sample (c = ca. 10−100 μg/mL in the indicated solvent); Acquity BEH C18 HPLC column (1.7 μm particle size, 2.1 × 50 mm, Waters) kept at 30 °C; elution at a flow rate of 400 μL/min with A: H_2O + 0.02% TFA and B: CH_3CN + 0.02% TFA, linear gradient from 10−95% B within 3 min, then isocratic 95% B for 2 min; UV spectra recorded from 190−300 nm at 1.2 nm resolution and 20 points s-1; ESI: positive ionization mode, capillary voltage 3.0 kV, sampling cone 40 V, extraction cone 4 V, N_2 cone gas 4 L/h, N_2 desolvation gas 800 L/min, source temperature 120 °C; mass analyzer in resolution mode: mass range 100−2′000 m/z with a scan rate of 1 Hz; mass calibration to <2 ppm within 50−2′500 m/z with a 5 mM aq. soln. of HCO_2Na, lockmasses: m/z 195.0882 (caffein, 0.7 ng/mL) and 556.2771 (leucine-enkephalin, 2 ng/mL). The HPLC analyses were performed on a Shimadzu LC − 9A HPLC system equipped with a Shimadzu SPD − 6A VP UV−vis detector; Phenomenex RP-HPLC on a Phenomenex InertClone (5 μm particle size, 4.6 mm × 150 mm i.d.). HPLC purifications were performed on a Shimadzu LC − 8A HPLC system equipped with a Shimadzu SCL −10A VP System control and a Shimadzu SPD −10A VP UV−vis detector on a Phenomenex Gemini C18-110A preparative column (10 μm particle size, 250 mm × 21.2 mm i.d.).

Downloaded from pubs.acs.org/jmcmar/article-pdf/doi/10.1021/acs.jmedchem.6c02977/6905752/jm6c02977.pdf by guest on 06 November 2026

https://doi.org/10.1021/acs.jmedchem.6c02977
J. Med. Chem. XXXX, XXX, XXX−XXX

General Procedure 1 (Synthesis of Compounds 38a−h)

Cyano aryl ketone (1 equiv) was dissolved in EtOH (0.8 M), and (4-methoxybenzyl)hydrazine hydrochloride (1.2 equiv) was added. After the addition of acetic acid (5 equiv), the reaction mixture was stirred at 85 °C for 2 h. After reaction completion (monitored by TLC), the reaction mixture was poured into ice water, and the pH was raised to 7−8 with a 10% NaOH solution. The white precipitate was recovered through filtration on paper and washed with water.

General Procedure 2 (Synthesis of Compounds 42a−h)

Beta-keto ester (1 equiv) bearing alkyl substituents (methyl or cyclopropyl) was dissolved in acetic acid (0.3 M), and the corresponding PMB-protected pyrazole (1.5 equiv) was added. The reaction mixture was stirred at 70 °C for 5 h. After reaction completion (monitored by TLC), the solvent was removed under reduced pressure, and the crude product (**40a−h**) was used in the next step without further purification. The crude mixture was heated without the solvent at 200 °C for 1 h. After reaction completion (monitored by TLC), the crude product was purified using flash column chromatography.

General Procedure 3 (PMB Deprotection)

The corresponding PMB-protected DHPP compound (**41**, **42a−h**) was dissolved in TFA (0.5 M). The reaction mixture was refluxed for 2 h. After reaction completion (monitored by TLC), the solvent was removed under reduced pressure. The product was purified using flash column chromatography.

Preparation of 1-(4-Methoxybenzyl)-3-phenyl-1*H*-pyrazol-5-amine (38a)

Compound **38a** was prepared following general procedure 1 using (4-methoxybenzyl)hydrazine (1.26 g, 8.27 mmol) and Benzoylacetonitrile (1 g, 6.89 mmol). The desired compound was obtained as a white solid (1.54 g, 80%). ^{1}H NMR (400 MHz, $CDCl_3$): δ 7.77 (dd, 2H), 7.42−7.34 (m, 2H), 7.31−7.27 (m, 1H), 7.21−7.14 (m, 2H), 6.86 (dd, 2H), 5.89 (s, 1H), 5.23 (s, 2H), 3.78 (s, 3H), 3.44 (bs, 2H).^{13}C NMR (101 MHz, $CDCl_3$): δ 159.41, 149.95, 145.63, 128.65, 128.56, 128.40, 127.69, 125.60, 114.49, 89.34, 55.45, 51.64. HRMS (ESI) *m/z*: $[M + H]^+$ calcd for $C_{17}H_{18}N_3O^+$, 280.1444; found, 280.1443.

Preparation of 3-(4-Fluorophenyl)-1-(4-methoxybenzyl)-1*H*-pyrazol-5-amine (38b)

Compound **38b** was prepared following general procedure 1 using (4-methoxybenzyl) hydrazine (0.074 g, 0.49 mmol) and 3-(4-fluorophenyl)-3-oxopropionitrile (0.066 g, 0.40 mmol). The desired compound was obtained as a white solid (85 mg, 71%). ^{1}H NMR (400 MHz, $CDCl_3$): δ 7.77−7.69 (m, 2H), 7.21−7.13 (m, 2H), 7.11−7.00 (m, 2H), 6.91−6.83 (m, 2H), 5.83 (s, 1H), 5.21 (s, 2H), 3.78 (s, 3H), 3.43 (bs, 2H). ^{13}C NMR (101 MHz, $CDCl_3$): δ 163.81, 161.37, 159.42, 149.11, 145.70, 128.50, 128.37, 127.24, 127.16, 115.60, 115.38, 114.50, 89.09, 55.44, 51.63. HRMS (ESI) *m/z*: $[M + H]^+$ calcd for $C_{17}H_{17}FN_3O^+$, 298.1350; found, 298.1351.

Preparation of 1-(4-Methoxybenzyl)-3-(4-methoxyphenyl)-1*H*-pyrazol-5-amine (38c)

Compound **38c** was prepared following general procedure 1 using (4-methoxybenzyl)hydrazine (1.04 g, 6.85 mmol) and 3-oxo-3-(4′-methoxyphenyl)propanenitrile (1 g, 5.71 mmol). The desired compound was obtained as a white solid (1.37 g, 78%). ^{1}H NMR (400 MHz, DMSO): δ 7.59−7.56 (m, 2H), 7.18−7.14 (m, 2H), 6.91−6.85 (m, 4H), 5.62 (s, 1H), 5.31 (s, 2H), 5.06 (s, 2H), 3.75 (s, 3H), 3.71 (s, 3H). ^{13}C NMR (101 MHz, DMSO): δ 158.40, 158.37, 148.32, 147.92, 130.12, 128.62, 127.02, 125.94, 113.74, 113.70, 84.74, 55.05, 49.29. HRMS (ESI) *m/z*: $[M + H]^+$ calcd for $C_{18}H_{20}N_3O_2^+$, 310.1550; found, 310.1550.

Preparation of 1-(4-Methoxybenzyl)-3-(4-(trifluoromethyl)phenyl)-1*H*-pyrazol-5-amine (38d)

Compound **38d** was prepared following general procedure 1 using (4-methoxybenzyl) hydrazine (1.71 g, 11.26 mmol) and 3-oxo-3-(4-(trifluoromethyl)phenyl) propanenitrile (2 g, 9.38 mmol). The desired compound was obtained as a white solid (1.37 g, 42%). ^{1}H NMR (400 MHz, DMSO): δ 7.90−7.83 (m, 2H), 7.68−7.66 (m, 2H), 7.19−7.17 (m, 2H), 6.89−6.87 (m, 2H), 5.81 (s, 1H), 5.47 (s, 2H), 5.12 (s, 1H), 3.71 (s, 3H). ^{13}C NMR (101 MHz, DMSO): δ 158.48, 148.40, 147.02, 138.13, 129.71, 128.71, 127.05 (q, J = 31.6 Hz), 125.8, 125.33 (q, J = 3.9 Hz), 125.14, 123.1, 113.77, 85.71, 55.07, 49.56. HRMS (ESI) *m/z*: $[M + H]^+$ calcd for $C_{18}H_{17}F_3N_3O^+$, 348.1318; found, 348.1318.

Preparation of 1-(4-Methoxybenzyl)-3-(3-(trifluoromethyl)phenyl)-1*H*-pyrazol-5-amine (38e)

Compound **38e** was prepared following general procedure 1 using (4-methoxybenzyl)hydrazine (1.08 g, 7.11 mmol) and 3-trifluoromethylbenzoylacetonitrile (1.01 g, 4.74 mmol). The desired compound was obtained as a white solid (0.453 g, 28%). ^{1}H NMR (400 MHz, DMSO): δ 7.96−7.94 (m, 2H), 7.58−7.56 (m, 2H), 7.19−7.15 (m, 2H), 6.90−6.86 (m, 2H), 5.83 (s, 1H), 5.46 (s, 2H), 5.12 (s, 2H), 3.71 (s, 3H). ^{13}C NMR (101 MHz, DMSO): δ 158.45, 148.41, 146.97, 135.22, 129.75, 129.59, 129.27 (q, J = 31.5 Hz), 128.62, 125.67, 123.3 (q, J = 4.0 Hz), 122.96, 120.61 (q, J = 3.9 Hz), 113.77, 85.46, 55.05, 49.50. HRMS (ESI) *m/z*: $[M + H]^+$ calcd for $C_{18}H_{17}F_3N_3O^+$, 348.1318; found, 348.1320.

Preparation of 1-(4-Methoxybenzyl)-3-(pyridin-4-yl)-1*H*-pyrazol-5-amine (38f)

Compound **38f** was prepared following general procedure 1 using (4-methoxybenzyl)hydrazine (2 g, 13.1 mmol) and 3-oxo-3-(pyridin-4-yl)propanenitrile (1.6 g, 10.9 mmol). The desired compound was obtained as a white solid (2.2 g, 72%). ^{1}H NMR (400 MHz, DMSO): δ 8.56−8.48 (m, 2H), 7.69−7.61 (m, 2H), 7.21−7.14 (m, 2H), 6.93−6.82 (m, 2H), 5.88 (s, 1H), 5.13 (s, 2H), 3.71 (s, 3H). ^{13}C NMR (101 MHz, DMSO): δ 158.51, 149.14, 148.56, 145.91, 141.86, 129.52, 128.71, 119.34, 113.79, 86.08, 55.08, 49.66.

Preparation of 3-(4-(Dimethylamino)phenyl)-1-(4-methoxybenzyl)-1*H*-pyrazol-5-amine (38g)

Compound **38g** was prepared following general procedure 1 using (4-methoxybenzyl)hydrazine (0.546 g, 3.59 mmol) and 3-(4-(dimethylamino)phenyl)-3-oxopropanenitrile (0.563 g, 2.99 mmol). The reaction mixture was quenched by the addition of a saturated solution of $NaHCO_3$ and extracted into EtOAc. Combined organic layers were dried over $MgSO_4$, and the volatile were removed under vacuo. The crude product was purified using flash column chromatography (SiO_2; EtOAc/Hept 1:1), and the desired compound was obtained as a white solid (0.16 g, 17%). ^{1}H NMR (400 MHz, DMSO): δ 7.50−7.44 (m, 2H), 7.19−7.12 (m, 2H), 6.91−6.85 (m, 2H), 6.72−6.65 (m, 2H), 5.57 (s, 1H), 5.25 (s, 2H), 5.04 (s, 2H), 3.71 (s, 3H), 2.89 (s, 6H).

Downloaded from pubs.acs.org/jmcmar/article-pdf/doi/10.1021/acs.jmedchem.6c02977/6905752/jm6c02977.pdf by guest on 06 November 2026

https://doi.org/10.1021/acs.jmedchem.6c02977
J. Med. Chem. XXXX, XXX, XXX−XXX

Preparation of Methyl 4-(5-Amino-1-(4-methoxybenzyl)-1*H*-pyrazol-3-yl)benzoate (38h)

Compound **38h** was prepared following general procedure 1 using (4-methoxybenzyl)hydrazine (1.11 g, 5.91 mmol) and methyl-4-(2-cyanoacetyl)benzoate (1 g, 4.92 mmol). The desired compound was obtained as a white solid (1.50 g, 90%). ^{1}H NMR (400 MHz, DMSO): δ 7.96−7.87 (m, 2H), 7.85−7.76 (m, 2H), 7.22−7.14 (m, 2H), 6.92−6.84 (m, 2H), 5.81 (s, 1H), 5.46 (s, 2H), 5.11 (s, 2H), 3.84 (s, 3H), 3.71 (s, 3H). ^{13}C NMR (101 MHz, $CDCl_3$): δ 167.22, 159.49, 148.78, 145.87, 138.23, 130.07, 129.01, 128.43, 128.23, 125.30, 114.54, 89.79, 55.44, 52.18, 51.81. HRMS (ESI) *m/z*: $[M + H]^+$ calcd for $C_{19}H_{20}N_3O_3^+$, 338.1499; found, 338.1506.

Preparation of 6-Ethyl-1-(4-methoxybenzyl)-1,7-dihydro-4*H*-pyrazolo[3,4-*b*]pyridin-4-one (41)

1-(4-Methoxybenzyl)-1*H*-pyrazol-5-amine (0.42 g, 2.08 mmol) was dissolved in DCE (4 mL) followed by the addition of ethyl propanoylacetate (0.15 g, 1.04 mmol) and *para*-toluenesulfonic acid (0.01 g, 0.05 mmol). The reaction was stirred at room temperature for 12 h. After reaction completion (TLC), the solvent was removed under reduced pressure. The crude enamine **39** obtained (0.193 g) was used in the next step without further purification. The crude enamine **39** was heated without a solvent at 200 °C until reaction completion (TLC). The crude product was purified using flash column chromatography (SiO_2; EtOAc/Hept 9:1), and the desired compound was obtained as a light-yellow solid (0.085 g, 29% over 2 steps). ^{1}H NMR (400 MHz, $CDCl_3$): δ 7.91 (s, 1H), 7.21 (d, J = 8.2 Hz, 2H), 6.76 (d, J = 8.1 Hz, 2H), 6.02 (s, 1H), 3.72 (s, 3H), 2.66 (q, J = 7.5 Hz, 2H), 1.24 (t, 3H). HRMS (ESI) *m/z*: $[M + H]^+$ calcd for $C_{16}H_{18}N_3O_2^+$, 284.1394; found, 284.1403.

Preparation of 6-Cyclopropyl-1-(4-methoxybenzyl)-3-phenyl-1,7-dihydro-4*H*-pyrazolo[3,4-*b*]pyridin-4-one (42a)

Compound **42a** was prepared following general procedure 2 using compound **38a** (0.35 g, 1.25 mmol) and ethyl 3-cyclopropyl-3-oxopropionate (0.29 g, 1.88 mmol). The crude product was purified using flash column chromatography (SiO_2; EtOAc/Hept 9:1), and the desired compound was obtained as a light-yellow solid (0.045 g, 19% over 2 steps). ^{1}H NMR (400 MHz, $CDCl_3$): δ 7.94 (d, J = 7.6 Hz, 1H), 7.45 (q, J = 7.7 Hz, 2H), 7.41−7.35 (m, 3H), 6.81 (t, J = 10.3 Hz, 2H), 6.27−6.17 (m, 1H), 5.59 (d, J = 12.7 Hz, 2H), 3.75 (d, J = 9.6 Hz, 3H), 2.13−2.03 (m, 1H), 0.98 (m, 2H), 0.87 (m, 2H). HRMS (ESI) *m/z*: $[M + H]^+$ calcd for $C_{23}H_{22}N_3O_2^+$, 372.1707; found, 372.1697.

Preparation of 3-(4-Fluorophenyl)-1-(4-methoxybenzyl)-6-methyl-1,7-dihydro-4*H*-pyrazolo[3,4-*b*]pyridin-4-one (42b-Me)

Compound **42b-Me** was prepared following general procedure 2 using compound **38b** (0.34 g, 1.15 mmol) and ethyl 3-oxobutanoate (0.1 g, 0.77 mmol). The crude product was purified using flash column chromatography (SiO_2; EtOAc/Hept 9:1), and the desired compound was obtained as a light-yellow solid (0.027 g, 10% over 2 steps). ^{1}H NMR (400 MHz, $CDCl_3$): δ 8.18 (t, J = 7.0 Hz, 2H), 7.29 (d, J = 8.6 Hz, 2H), 7.04 (t, J = 8.6 Hz, 2H), 6.75 (d, 2H), 6.01 (s, 1H), 5.59 (s, 2H), 3.71 (s, 3H), 2.32 (s, 3H). ^{13}C NMR (126 MHz, DMSO): δ 206.48, 170.34, 162.99, 161.04, 158.67, 130.37, 130.31, 129.53, 128.86, 115.00, 114.83, 113.92, 102.76, 59.76, 55.04, 49.50. HRMS (ESI) *m/z*: $[M + H]^+$ calcd for $C_{21}H_{19}FN_3O_2^+$, 364.1456; found, 364.1461.

Preparation of 6-Cyclopropyl-3-(4-fluorophenyl)-1-(4-methoxybenzyl)-1,7-dihydro-4*H*-pyrazolo[3,4-*b*]pyridin-4-one (42b-cPr)

Compound **42b-cPr** was prepared following general procedure 2 using compound **38b** (0.43 g, 1.44 mmol) and ethyl 3-cyclopropyl-3-oxopropionate (0.15 g, 0.96 mmol). The crude product was purified using flash column chromatography (SiO_2; EtOAc/Hept 9:1), and the desired compound was obtained as a light-yellow solid (0.012 g, 3% over 2 steps). ^{1}H NMR (400 MHz, DMSO): δ 11.54 (s, 1H), 8.06 (s, 2H), 7.26 (dt, J = 8.9, 4.6 Hz, 4H), 6.87 (d, 2H), 6.51 (s, 1H), 5.45 (s, 2H), 3.69 (s, 3H), 2.08 (s, 1H), 1.00 (m, 4H). ^{13}C NMR (126 MHz, DMSO): δ 167.78, 164.78, 163.37, 161.43, 159.69, 159.12, 154.25, 149.14, 141.73, 140.05, 130.75, 130.69, 129.72, 115.51, 115.34, 114.35, 114.32, 102.85, 101.35, 55.51, 49.80, 17.43, 10.57. HRMS (ESI) *m/z*: $[M + H]^+$ calcd for $C_{23}H_{21}FN_3O_2^+$, 390.1612; found, 390.1615.

Preparation of 1-(4-Methoxybenzyl)-3-(4-methoxyphenyl)-6-methyl-1,7-dihydro-4*H*-pyrazolo[3,4-*b*]pyridin-4-one (42c-Me)

Compound **42c-Me** was prepared following general procedure 2 using compound **38c** (0.6 g, 1.94 mmol) and ethyl 3-oxobutanoate (0.5 g, 3.88 mmol). The crude product was purified using flash column chromatography (SiO_2 and EtOAc/Hept, from 1:1 to 2:1), and the desired compound was obtained as a light-yellow solid (0.061 g, 8% over 2 steps). ^{1}H NMR (400 MHz, DMSO): δ 11.88−11.63 (bs, 0.3H), 11.58−11.35 (bs, 0.7H), 8.50−8.17 (bs, 0.3H), 8.14−7.95 (bs, 0.9H), 7.27−7.16 (m, 2H), 6.98 (d, J = 8.4 Hz, 2H), 6.87 (d, J = 8.2 Hz, 2 H), 6.46 (s, 1H), 5.49 (s, 2H), 3.79 (s, 3H), 3.69 (s, 3H), 2.47 (s, 3H). HRMS (ESI) *m/z*: $[M + H]^+$ calcd for $C_{22}H_{22}N_3O_3^+$, 376.1656; found, 376.1654.

Preparation of 6-Cyclopropyl-1-(4-methoxybenzyl)-3-(4-methoxyphenyl)-1,7-dihydro-4*H*-pyrazolo[3,4-*b*]pyridin-4-one (42c-cPr)

Compound **42c-cPr** was prepared following general procedure 2 using compound 38c (0.32 g, 1.05 mmol) and ethyl 3-cyclopropyl-3-oxopropionate (0.25 g, 1.57 mmol). The crude product was purified using flash column chromatography (SiO_2; EtOAc/Hept 1:1), and the desired compound was obtained as a light-yellow solid (0.022 g, 5% over 2 steps). ^{1}H NMR (400 MHz, DMSO): δ 11.41 (s, 1H), 7.96 (d, J = 8.3 Hz, 2H), 7.32−7.21 (m, 2H), 7.03−6.95 (m, 2H), 6.90−6.81 (m, 2H), 6.56−6.41 (bs, 1H), 5.43 (s, 2H), 3.79 (s, 3H), 3.69 (s, 3H), 2.13−2.00 (m, 1H), 1.06−0.94 (m, 4H). ^{13}C NMR (101 MHz, DMSO): δ 164.07, 159.36, 159.04, 158.63, 142.14, 129.68, 129.59, 129.22, 125.83, 113.84, 113.50, 102.32, 100.65, 55.14, 16.93, 10.80, 10.03. HRMS (ESI) *m/z*: $[M + H]^+$ calcd for $C_{24}H_{24}N_3O_3^+$, 402.1812; found, 402.1809.

Preparation of 1-(4-Methoxybenzyl)-6-methyl-3-(4-(trifluoromethyl)phenyl)-1,7-dihydro-4*H*-pyrazolo[3,4-*b*]pyridin-4-one (42d)

Compound **42d** was prepared following general procedure 2 using compound **38d** (0.8 g, 2.31 mmol) and ethyl 3-oxobutanoate (0.2 g, 1.54 mmol). The crude product was purified using flash column chromatography (SiO_2; EtOAc/Hept 2:1), and the desired compound was obtained as a light-yellow

Downloaded from pubs.acs.org/jmcmar/article-pdf/doi/10.1021/acs.jmedchem.6c02977/6905752/jm6c02977.pdf by guest on 06 November 2026

https://doi.org/10.1021/acs.jmedchem.6c02977
J. Med. Chem. XXXX, XXX, XXX−XXX

solid (0.35 g, 54% over 2 steps). ^{1}H NMR (400 MHz, MeOD): δ 8.38 (d, J = 6.9 Hz, 2H), 7.69 (d, J = 8.3 Hz, 2H), 7.20 (d, 2H), 6.87 (d, 2H), 6.22 (bs, 1H), 5.54 (s, 2H), 3.74 (s, 3H), 2.47 (s, 3H). HRMS (ESI) m/z: $[M + H]^+$ calcd for $C_{22}H_{19}F_3N_3O_2^+$, 414.1424; found, 414.1417.

Preparation of 1-(4-Methoxybenzyl)-6-methyl-3-(3-(trifluoromethyl)phenyl)-1,7-dihydro-4*H*-pyrazolo[3,4-*b*]pyridin-4-one (42e)

Compound **42e** was prepared following general procedure 2 using compound **38e** (0.42 g, 1.21 mmol) and ethyl 3-oxobutanoate (0.11 g, 0.81 mmol). The crude product was purified using flash column chromatography (SiO_2 and EtOAc/Hept, from 1:1 to 2:1), and the desired compound was obtained as a light-yellow solid (0.053 g, 16% over 2 steps). ^{1}H NMR (500 MHz, DMSO): δ 12.00−11.62 (bs, 1H), 9.08−8.87 (bs, 0.4H), 8.75−8.53 (bs, 0.4H), 8.42 (d, J = 66.7 Hz, 1H), 7.72−7.65 (m, 2H), 7.24−7.23 (m, 2H), 6.88 (d, J = 8.2 Hz, 2H), 6.51 (s, 1H), 5.55 (s, 2H), 3.70 (s, 3H), 2.51−2.37 (bs, 3H). HRMS (ESI) m/z: $[M + H]^+$ calcd for $C_{22}H_{19}F_3N_3O_2^+$, 414.1424; found, 414.1426.

Preparation of 1-(4-Methoxybenzyl)-6-methyl-3-(pyridin-4-yl)-1,7-dihydro-4*H*-pyrazolo[3,4-*b*]pyridin-4-one (42f)

Compound **42f** was prepared following general procedure 2 using compound **38f** (0.32 g, 1.15 mmol) and ethyl 3-oxobutanoate (0.1 g, 0.77 mmol). The crude product was purified using flash column chromatography (SiO_2; EtOAc/MeOH, 95:5), and the desired compound was obtained as a light-yellow solid (0.087 g, 33% over 2 steps). ^{1}H NMR (400 MHz, DMSO): δ 11.86 (bs, 1H), 8.62 (dd, 2H), 8.10 (bs, 2H), 7.24 (dd, 2H), 6.88 (d, 2H), 6.54 (bs, 1H), 5.56 (s, 2H), 3.70 (s, 3H), 2.48 (bs, 3H). HRMS (ESI) m/z: $[M + H]^+$ calcd for $C_{20}H_{19}N_4O_2^+$, 347.1503; found, 347.1501.

Preparation of 3-(4-(Dimethylamino)phenyl)-1-(4-methoxybenzyl)-6-methyl-1,7-dihydro-4*H*-pyrazolo[3,4-*b*]pyridin-4-one (42g)

Compound **42g** was prepared following general procedure 2 using compound 38g (0.143 g, 0.44 mmol) and ethyl 3-oxobutanoate (0.038 g, 0.29 mmol). The crude product was purified using flash column chromatography (SiO_2 and DCM/MeOH, 90:10), and the desired compound was obtained as a light-yellow solid (0.053 g, 46% over 2 steps). HRMS (ESI) m/z: $[M + H]^+$ calcd for $C_{23}H_{25}N_4O_2^+$, 389.1972; found, 389.1967.

Preparation of Methyl 4-(1-(4-Methoxybenzyl)-6-methyl-4-oxo-4,7-dihydro-1H-pyrazolo[3,4-*b*]pyridin-3-yl)benzoate (42h-Me)

Compound **42h-Me** was prepared following general procedure 2 using compound 38h (0.78 g, 2.31 mmol) and ethyl 3-oxobutanoate (0.2 g, 1.54 mmol). The crude product was purified using flash column chromatography (SiO_2; EtOAc/Hept, 2:1), and the desired compound was obtained as a light-yellow solid (0.087 g, 14% over 2 steps). ^{1}H NMR (400 MHz, MeOD): δ 7.92 (d, J = 6.7 Hz, 2H), 7.86 (d, J = 8.2 Hz, 2H), 7.13 (d, 2H), 6.47 (d, 2H), 6.24 (bs, 1H), 5.47 (s, 2H), 3.80 (s, 3H), 2.53 (s, 3H). HRMS (ESI) m/z: $[M + H]^+$ calcd for $C_{23}H_{22}N_3O_4^+$, 404.1605; found, 404.1632.

Preparation of Methyl 4-(6-Cyclopropyl-1-(4-methoxybenzyl)-4-oxo-4,7-dihydro-1*H*-pyrazolo[3,4-*b*]pyridin-3-yl)benzoate (42h-cPr)

Compound **42h-cPr** was prepared following general procedure 2 using compound **38h** (0.54 g, 1.61 mmol) and ethyl 3-cyclopropyl-3-oxopropionate (0.2 g, 1.29 mmol). The crude product was purified using flash column chromatography (SiO_2; DCM/MeOH 95:5), and the desired compound was obtained as a light-yellow solid (0.02 g, 3% over 2 steps). ^{1}H NMR (400 MHz, MeOD): δ 7.94 (d, J = 6.5 Hz, 2H), 7.84 (d, J = 8 Hz, 2H), 7.11 (d, 2H), 6.77 (d, 2H), 6.25 (bs, 1H), 5.43 (s, 2H), 3.83 (s, 3H), 2.32 (tt, 1H), 1.27 (m, 2H), 0.98 (m, 2H).

Preparation of 6-Ethyl-2,7-dihydro-4*H*-pyrazolo[3,4-*b*]pyridin-4-one (4)

Compound **4** was prepared following general procedure 3 using compound **41** (0.028 g, 0.1 mmol). The crude product was purified using flash column chromatography (SiO_2 and DCM/MeOH, 90:10), and the desired compound was obtained as a white solid (0.014 g, 87%). HPLC purity >99%. ^{1}H NMR (500 MHz, MeOD): δ 8.37 (s, 1H), 6.27 (s, 1H), 2.84 (q, J = 7.6 Hz, 2H), 1.37 (t, J = 7.6 Hz, 3H). ^{13}C NMR (126 MHz, MeOD): δ 175.43, 160.91, 151.20, 128.55, 110.85, 104.60, 28.31, 13.77. HRMS (ESI) m/z: $[M + H]^+$ calcd for $C_8H_{10}N_3O^+$, 164.0818; found, 164.0814.

Preparation of 6-Cyclopropyl-3-phenyl-2,7-dihydro-4*H*-pyrazolo[3,4-*b*]pyridin-4-one (6)

Compound **6** was prepared following general procedure 3 using compound **42a** (0.025 g, 0.067 mmol). The crude product was purified using flash column chromatography (SiO_2; EtOAc/Hept, from 80:20 to 100% EtOAc), and the desired compound was obtained as a white solid (0.013 g, 77%). HPLC purity >99%. ^{1}H NMR (400 MHz, MeOD): δ 8.11−8.07 (m, 2H), 7.54−7.37 (m, 3H), 5.75 (s, 1H), 3.69−3.62 (m, 1H), 1.96 (tt, J = 8.4, 5.0 Hz, 1H), 1.12 (dt, 2H), 0.96 (dt, J = 7.2, 4.6 Hz, 2H). ^{13}C NMR (126 MHz, MeOD): δ 179.35, 158.83, 153.43, 130.11, 129.85, 129.40, 108.18, 103.51, 14.75, 9.58. HRMS (ESI) m/z: $[M + H]^+$ calcd for $C_{15}H_{14}N_3O^+$, 252.1131; found, 252.1127.

Preparation of 3-(4-Fluorophenyl)-6-methyl-2,7-dihydro-4*H*-pyrazolo[3,4-*b*]pyridin-4-one (7)

Compound **7** was prepared following general procedure 3 using compound **42b-Me** (0.027 g, 0.074 mmol). The crude product was purified using flash column chromatography (SiO_2; EtOAc/Hept, from 80:20 to 100% EtOAc), and the desired compound was obtained as a white solid (0.013 g, 71%). HPLC purity 98%. ^{1}H NMR (500 MHz, MeOD): δ 7.97 (t, J = 6.6 Hz, 2H), 7.30 (t, J = 8.7 Hz, 2H), 6.66 (s, 1H), 3.76−3.55 (m, 2H), 2.73 (s, 3H). ^{13}C NMR (126 MHz, MeOD): δ 170.62, 166.20, 164.22, 158.39, 151.40, 142.99, 132.59, 132.53, 125.87, 116.83, 116.65, 105.84, 103.86, 20.14. HRMS (ESI) m/z: $[M + H]^+$ calcd for $C_{13}H_{11}FN_3O^+$, 244.0881; found, 244.0880.

Preparation of 6-Cyclopropyl-3-(4-fluorophenyl)-2,7-dihydro-4*H*-pyrazolo[3,4-*b*]pyridin-4-one (8)

Compound **8** was prepared following general procedure 3 using compound **42b-cPr** (0.012 g, 0.074 mmol). The crude product was purified using flash column chromatography (SiO_2 and EtOAc/Hept, from 80:20 to 100% EtOAc), and the desired compound was obtained as a white solid (0.006 g, 64%). HPLC

Downloaded from pubs.acs.org/jmcmar/article-pdf/doi/10.1021/acs.jmedchem.6c02977/69055752/jm6c02977.pdf by guest on 06 November 2026

https://doi.org/10.1021/acs.jmedchem.6c02977
J. Med. Chem. XXXX, XXX, XXX−XXX

purity 95%. ^{1}H NMR (400 MHz, MeOD): δ 8.02−7.92 (m, 2H), 7.35−7.24 (m, 2H), 6.25 (s, 1H), 3.78−3.55 (m, 2H), 2.28 (tt, J = 8.4, 4.9 Hz, 1H), 1.47−1.40 (m, 2H), 1.23−1.17 (m, 2H). ^{13}C NMR (126 MHz, MeOD): δ 170.90, 166.21, 164.23, 132.55, 132.49, 125.73, 116.85, 116.67, 105.89, 98.57, 73.58, 72.46, 62.18, 15.47, 12.17. HRMS (ESI) m/z: $[M + H]^+$ calcd for $C_{15}H_{13}FN_3O^+$, 270.1037; found, 270.1033.

Preparation of 3-(4-Methoxyphenyl)-6-methyl-2,7-dihydro-4*H*-pyrazolo[3,4-*b*]pyridin-4-one (9)

Compound **9** was prepared following general procedure 3 using compound **42c-Me** (0.044 g, 0.12 mmol). The crude product was purified using flash column chromatography (SiO_2 and DCM/MeOH, 95:5), and the desired compound was obtained as a white solid (0.021 g, 70%). HPLC purity >99%. ^{1}H NMR (500 MHz, DMSO): δ 13.66−13.62 (s, 0.5H), 11.79−11.75 (s, 0.5H), 8.27 (d, J = 8.3 Hz, 2H), 7.01 (d, J = 8.6 Hz, 2H), 5.72−5.68 (bs, 1H), 3.81 (s, 3H), 2.28 (s, 3H). ^{13}C NMR (126 MHz, DMSO): δ 159.65, 158.00 (q, J = 31.6 Hz), 152.26, 149.09, 129.69, 117.15 (q, J = 299.0 Hz), 113.71, 107.02, 55.24, 19.40. HRMS (ESI) m/z: $[M + H]^+$ calcd for $C_{14}H_{14}N_3O_2^+$, 256.1081; found, 256.1082.

Preparation of 6-Cyclopropyl-3-(4-methoxyphenyl)-2,7-dihydro-4*H*-pyrazolo[3,4-*b*]pyridin-4-one (10)

Compound **10** was prepared following general procedure 3 using compound **42c-cPr** (0.022 g, 0.055 mmol). The crude product was purified using flash column chromatography (SiO_2 and DCM/MeOH, from 95:5 to 85:15), and the desired compound was obtained as a white solid (0.013 g, 84%). HPLC purity >99%. ^{1}H NMR (600 MHz, DMSO): δ 7.98−7.93 (m, 2H), 7.08 (d, J = 8.5 Hz, 2H), 6.30 (s, 1H), 3.82 (s, 3H), 2.24−2.18 (m, 1H), 1.29−1.19 (m, 2H), 1.10−0.98 (m, 2H). ^{13}C NMR (151 MHz, DMSO): δ 161.65, 160.11, 151.35, 130.21, 128.21, 127.46, 114.00, 104.10, 98.41, 55.34, 14.53, 11.07. HRMS (ESI) m/z: $[M + H]^+$ calcd for $C_{16}H_{16}N_3O_2^+$, 282.1237; found, 282.1235.

Preparation of 6-Methyl-3-(4-(trifluoromethyl)phenyl)-2,7-dihydro-4*H*-pyrazolo[3,4-*b*]pyridin-4-one (13)

Compound **13** was prepared following general procedure 3 using compound **42d** (0.05 g, 0.055 mmol). The crude product was purified using flash column chromatography (SiO_2 and DCM/MeOH, from 90:10), and the desired compound was obtained as a white solid (0.024 g, 60%). HPLC purity >99%. ^{1}H NMR (500 MHz, DMSO): δ 8.29 (d, J = 8.1 Hz, 2H), 7.86 (d, J = 8.2 Hz, 2H), 6.72 (s, 1H), 2.58 (s, 3H). ^{13}C NMR (126 MHz, DMSO): δ 168.76, 154.24, 149.08, 133.83, 129.43, 125.29, 123.13, 105.24, 104.55, 72.16, 70.55, 66.37, 60.11, 19.81. HRMS (ESI) m/z: $[M + H]^+$ calcd for $C_{14}H_{11}F_3N_3O^+$, 294.0849; found, 294.0855.

Preparation of 6-Methyl-3-(3-(trifluoromethyl)phenyl)-2,7-dihydro-4*H*-pyrazolo[3,4-*b*]pyridin-4-one (14)

Compound **14** was prepared following general procedure 3 using compound **42e** (0.035 g, 0.085 mmol). The crude product was purified using flash column chromatography (SiO_2 and DCM/MeOH, from 90:10 to 75:25), and the desired compound was obtained as a white solid (0.012 g, 48%). HPLC purity >99%. ^{1}H NMR (400 MHz, MeOD): δ 8.67 (s, 1H), 8.43 (s, 1H), 7.70−7.60 (m, 2H), 5.99−5.95 (s, 1H), 2.42 (s, 3H). ^{13}C NMR (126 MHz, MeOD): δ 152.14, 133.01, 131.80 (q, J = 33.2Hz), 130.17, 129.81, 129.65, 128.92, 126.81 (q, J = 4.0 Hz), 126.38, 124.60, 122.44, 115.11, 108.98, 108.59, 19.74. HRMS (ESI) m/z: $[M + H]^+$ calcd for $C_{14}H_{11}F_3N_3O^+$, 294.0849; found, 294.0849.

Preparation of 6-Methyl-3-(pyridin-4-yl)-2,7-dihydro-4*H*-pyrazolo[3,4-*b*]pyridin-4-one (17)

Compound **17** was prepared following general procedure 3 using compound **42f** (0.05 g, 0.14 mmol). The crude product was purified using flash column chromatography (SiO_2 and DCM/MeOH, from 90:10 to 85:15), and the desired compound was obtained as a white solid (0.028 g, 86%). HPLC purity >99%. ^{1}H NMR (400 MHz, MeOD): δ 8.98 (s, 4H), 6.81 (s, 1H), 2.75 (s, 3H). ^{13}C NMR (126 MHz, MeOD): δ 169.52, 156.35, 149.96, 148.58, 142.94, 142.34, 126.98, 107.97, 107.26, 107.20, 19.95. HRMS (ESI) m/z: $[M + H]^+$ calcd for $C_{12}H_{11}N_4O^+$, 227.0927; found, 227.0924.

Preparation of 3-(4-(Dimethylamino)phenyl)-6-methyl-2,7-dihydro-4*H*-pyrazolo[3,4-*b*]pyridin-4-one (18)

Compound **18** was prepared following general procedure 3 using compound **42g** (0.062 g, 0.14 mmol). The crude product was purified using flash column chromatography (SiO_2 and DCM/MeOH, from 90:10 to 85:15), and the desired compound was obtained as a white solid (0.032 g, 58%). HPLC purity >99%. ^{1}H NMR (400 MHz, DMSO): δ 13.33 (s, 0.5H), 11.46 (s, 0.5H), 8.24 (d, J = 8.4 Hz, 2H), 6.77 (d, J = 8.6 Hz, 2H), 5.52 (s, 1H), 5.52 (s, 1H), 2.97 (s, 6H), 2.22 (s, 3H). ^{13}C NMR (126 MHz, DMSO): δ 176.57, 157.39, 152.66, 150.53, 148.26, 140.26, 129.07, 116.11, 113.70, 111.54, 107.27, 107.05, 54.93, 18.99. HRMS (ESI) m/z: $[M + H]^+$ calcd for $C_{15}H_{17}N_4O^+$, 269.1397; found, 269.1395.

Preparation of Methyl 4-(6-Methyl-4-oxo-4,7-dihydro-2*H*-pyrazolo[3,4-*b*]pyridin-3-yl)benzoate (19)

Compound **19** was prepared following general procedure 3 using compound **42h-Me** (0.020 g, 0.05 mmol). The crude product was purified using flash column chromatography (SiO_2 and DCM/MeOH, from 90:10), and the desired compound was obtained as a white solid (0.013 g, 82%). HPLC purity >99%. ^{1}H NMR (400 MHz, DMSO): δ 8.34 (d, J = 8.3 Hz, 2H), 8.06 (d, J = 8.3 Hz, 2H), 6.22 (s, 1H), 3.89 (s, 3H), 3.56 (s, 3H), 2.45 (s, 3H). ^{13}C NMR (126 MHz, MeOD): δ 171.22, 167.88, 157.79, 132.33, 130.73, 130.31, 106.48, 104.67, 73.58, 72.46, 68.14, 52.87, 20.07. HRMS (ESI) m/z: $[M + H]^+$ calcd for $C_{15}H_{14}N_3O_3^+$, 284.1030; found, 284.1031.

Preparation of Methyl 4-(6-Cyclopropyl-4-oxo-4,7-dihydro-2*H*-pyrazolo[3,4-*b*]pyridin-3-yl)benzoate (20)

Compound **20** was prepared following general procedure 3 using compound **42h-cPr** (0.015 g, 0.05 mmol). The crude product was purified using flash column chromatography (SiO_2 and DCM/MeOH, from 95:5 to 90:10), and the desired compound was obtained as a white solid (0.008 g, 74%). HPLC purity >99%. ^{1}H NMR (600 MHz, DMSO): δ 8.23−8.22 (m, 2H), 8.06−8.05 (m, 2H), 6.37 (s, 1H), 3.88 (s, 3H), 2.18−2.15 (m, 1H), 1.14−1.13 (m, 2H), 1.02−1.01 (m, 2H). ^{13}C NMR (151 MHz, DMSO): δ 166.01, 161.87, 152.51, 129.16, 128.64, 104.23, 100.41, 66.36, 52.27, 15.25, 10.56. HRMS (ESI) m/z: $[M + H]^+$ calcd for $C_{17}H_{16}N_3O_3^+$, 310.1186; found, 310.1184.

Downloaded from pubs.acs.org/jmcmar/article-pdf/doi/10.1021/acs.jmedchem.6c02977/6905752/jm6c02977.pdf by guest on 06 November 2026

https://doi.org/10.1021/acs.jmedchem.6c02977
J. Med. Chem. XXXX, XXX, XXX−XXX

Preparation of 6-Cyclopropyl-3-(4-hydroxyphenyl)-2,7-dihydro-4*H*-pyrazolo[3,4-*b*]pyridin-4-one (11)

Compound **10** (0.024 g, 0.085 mmol) was dissolved in dry DMF (1.5 mL), followed by the addition of ethanethiolate (0.036 mg, 0.425 mmol). The reaction was stirred at 150 °C for 15 h. After the reaction completion (Monitored by TLC), the volatiles were removed under vacuo. The crude product was purified using flash column chromatography (SiO_2 and DCM/MeOH, from 90:10 to 80:20), and the desired compound was obtained as a white solid (0.009 g, 39%). HPLC purity >99%. ^{1}H NMR (400 MHz, DMSO): δ 13.37−13.07 (bs, 0.5H), 11.72−11.37 (bs, 0.5H), 9.77−9.46 (bs, 1H), 8.23−7.80 (bs, 2H), 6.83−6.77 (m, 2H), 5.53−5.23 (bs, 1H), 2.06−1.80 (bs, 1H), 1.05−0.86 (m, 4H). ^{13}C NMR (126 MHz, DMSO): δ 129.68, 114.92, 101.84, 69.82, 8.97. HRMS (ESI) *m/z*: $[M + H]^+$ calcd for $C_{15}H_{14}N_3O_2^+$, 268.1081; found, 268.1084.

Preparation of 4-(6-Methyl-4-oxo-4,7-dihydro-2*H*-pyrazolo[3,4-*b*]pyridin-3-yl)benzoic Acid (21)

Compound **19** (0.032 g, 0.11 mmol) was dissolved in HCl 6 M (1 mL). The reaction was stirred at 120 °C for 3 h. After the reaction completion (Monitored by TLC), the volatiles were removed under vacuo. The desired compound was obtained as a white solid (0.031 g, 90%). HPLC purity >99%. ^{1}H NMR (400 MHz, DMSO): δ 8.26 (d, J = 8.2 Hz, 2H), 8.05 (d, J = 8.3 Hz, 2H), 6.37 (s, 1H). ^{13}C NMR (126 MHz, MeOD): δ 170.80, 169.01, 158.23, 151.43, 143.02, 133.72, 133.10, 130.97, 130.25, 106.27, 104.30, 20.12. HRMS (ESI) *m/z*: $[M + H]^+$ calcd for $C_{14}H_{12}N_3O_3^+$, 270.0873; found, 270.0877.

Preparation of 4-Chloro-1-(4-methoxybenzyl)-6-methyl-1*H*-pyrazolo[3,4-*b*]pyridine (44)

Compound **3** (0.196 g, 0.728 mmol) was dissolved in MeCN (1.96 mL), followed by the addition of $POCl_3$ (0.2 mL, 2.18 mmol). The reaction was refluxed for 2 h. After reaction completion (TLC), the solvent was removed under reduced pressure. The crude mixture was quenched with a saturated aqueous solution of Na_2CO_3 and extracted with EtOAc (3×). Combined organic layers were dried over $MgSO_4$, and the volatiles were removed in vacuo. The desired compound was obtained as a light-brown oil (0.184 g, 88%). ^{1}H NMR (400 MHz, DMSO): δ 8.18 (s, 1H), 7.32 (s, 1H), 7.18 (d, J = 2.4 Hz, 2H), 6.86 (d, J = 8.7 Hz, 2H), 5.57 (s, 2H), 2.62 (s, 3H). HRMS (ESI) *m/z*: $[M + H]^+$ calcd for $C_{15}H_{15}ClN_3O^+$, 288.0898; found, 288.0900.

Preparation of 4-Chloro-6-methyl-1*H*-pyrazolo[3,4-*b*]pyridine (45)

PMB deprotection was performed using general procedure 3 using compound **44** (0.209 g, 0.73 mmol). The crude product was purified using flash column chromatography (SiO_2; EtOAc/Hept = 1:4), and the desired compound was obtained as a white solid (0.091 g, 44%). ^{1}H NMR (500 MHz, DMSO): δ 13.79 (s, 1H), 8.14 (s, 1H), 7.26 (s, 1H), 2.58 (s, 3H). ^{13}C NMR (126 MHz, DMSO): δ 159.21, 152.48, 135.73, 131.11, 116.77, 111.96, 24.17. HRMS (ESI) *m/z*: $[M + H]^+$ calcd for $C_7H_7ClN_3^+$, 168.0323; found, 168.0327.

Preparation of 4-Chloro-3-iodo-6-methyl-1*H*-pyrazolo[3,4-*b*]pyridine (46)

Compound **45** (0.34 g, 2 mmol) was dissolved in DMF (5 mL), followed by the addition of *N*-Iodosuccinimide (1.4 g, 8.1 mmol). The reaction was stirred at 50 °C for 5 h. After reaction completion (TLC), the solvent was removed under reduced pressure. The crude mixture was diluted in EtOAc and washed with an aqueous solution of $Na_2S_2O_3$ (3×). The organic layer was dried over $MgSO_4$, and then, the volatiles were removed under vacuo. The compound was obtained as a gray solid (0.58 g, 97%). ^{1}H NMR (400 MHz, DMSO): δ 14.16 (s, 1H), 7.26 (s, 1H), 2.56 (s, 3H). HRMS (ESI) *m/z*: $[M + H]^+$ calcd for $C_7H_6ClIN_3^+$, 293.9289; found, 293.9289.

Preparation of 3-Iodo-6-methyl-1*H*-pyrazolo[3,4-*b*]pyridin-4-ol (47)

Compound **46** (0.1 g, 0.35 mmol) was dissolved in TFA (3 mL), followed by the addition of water (0.4 mL). The reaction mixture was refluxed for 12 h. After reaction completion (TLC), the volatiles were removed in vacuo. The crude product was purified using flash column chromatography (SiO_2 and DCM/MeOH, from 10 to 20%), and the desired compound was obtained as a gray solid (0.035 g, 26%). ^{1}H NMR (400 MHz, DMSO): δ 12.75 (s, 1H), 6.32 (s, 1H), 2.47 (s, 3H). HRMS (ESI) *m/z*: $[M + H]^+$ calcd for $C_7H_7IN_3O^+$, 275.9628; found, 275.9643.

General Procedure 4 (Suzuki−Miyaura Cross Coupling 1)

Compound **47** (1 equiv) was dissolved in dioxane (0.2 M), and the corresponding boronic acid or ester (1.5 equiv) was added together with a 2 M aqueous solution of Na_2CO_3 (3 equiv). The reaction mixture was degassed for 20 min, and then, Pd(dppf)Cl_2 (0.1 equiv) was added. The reaction was stirred at 120 °C for 10 h. After reaction completion (monitored by TLC), the reaction mixture was filtered over celite, and the volatiles were removed under reduced pressure. The crude product was purified using flash column chromatography.

Preparation of 3-(3-Methoxyphenyl)-6-methyl-2,7-dihydro-4*H*-pyrazolo[3,4-*b*]pyridin-4-one (12)

Compound **12** was prepared following general procedure 4 using compound **47** (0.007 g, 0.025 mmol) and 3-methoxyphenylboronic acid (0.006 g, 0.038 mmol). The crude product was purified using flash column chromatography (SiO_2 and DCM/MeOH, from 95:5 to 90:10), and the desired compound was obtained as a white solid (0.002 g, 31%). HPLC purity 98%. ^{1}H NMR (400 MHz, MeOD): δ 7.98 (s, 1H), 7.66−7.57 (m, 1H), 7.40−7.32 (m, 1H), 7.03−6.93 (s, 1H), 5.86 (s, 1H), 3.88 (s, 3H), 2.39 (s, 3H). ^{13}C NMR (126 MHz, MeOD): δ 151.63, 121.01, 111.97, 107.09, 105.72, 46.42. HRMS (ESI) *m/z*: $[M + H]^+$ calcd for $C_{14}H_{14}N_3O_2^+$, 256.1081; found, 256.1087.

Preparation of *N*-(3-(6-Methyl-4-oxo-4,7-dihydro-2*H*-pyrazolo[3,4-*b*]pyridin-3-yl)phenyl)methanesulfonamide (15)

Compound **15** was prepared following general procedure 4 using compound **47** (0.015 g, 0.038 mmol) and *N*-(3-(4,4,5,5-tetramethyl-1,3,2-dioxaborolan-2-yl)phenyl) methane-sulfonamide (0.017 g, 0.058 mmol). The crude product was purified using flash column chromatography (SiO_2 and DCM/MeOH, from 95:5 to 90:10), and the desired compound was obtained as a white solid (0.005 g, 41%). HPLC purity >99%. ^{1}H NMR (400 MHz, MeOD): δ 8.08 (t, J = 2.0 Hz, 1H), 7.78 (bs, 1H), 7.44 (t, J = 8.0 Hz, 1H), 7.33−7.27 (m, 1H), 5.91 (s, 1H), 3.10 (s, 3H), 2.40 (s, 3H). ^{13}C NMR (126 MHz, MeOD): δ 139.38, 130.88, 130.43, 129.55, 126.86, 125.43, 122.24, 122.04, 71.53, 64.32, 39.51, 39.02.

Downloaded from pubs.acs.org/jmcmar/article-pdf/doi/10.1021/acs.jmedchem.6c02977/6905752/jm6c02977.pdf by guest on 06 November 2026

https://doi.org/10.1021/acs.jmedchem.6c02977
J. Med. Chem. XXXX, XXX, XXX−XXX

HRMS (ESI) *m/z*: $[M + H]^+$ calcd for $C_{14}H_{15}N_4O_3S^+$, 319.0859; found, 319.0855.

Preparation of 3-(4-(Benzyloxy)phenyl)-6-methyl-2,7-dihydro-4*H*-pyrazolo[3,4-*b*]pyridin-4-one (23)

Compound **23** was prepared following general procedure 4 using compound **47** (0.015 g, 0.038 mmol) and 2-(4-(benzyloxy)phenyl)-4,4,5,5-tetramethyl-1,3,2-dioxaborolane (0.018 g, 0.058 mmol). The crude product was purified using flash column chromatography (SiO_2 and DCM/MeOH, from 95:5 to 90:10), and the desired compound was obtained as a white solid (0.002 g, 16%). HPLC purity >99%. ^{1}H NMR (400 MHz, MeOD): δ 6.54−6.51 (m, 2H), 5.93−5.90 (m, 2H), 5.85−5.81 (m, 2H), 5.78−5.75 (m, 1H), 5.58−5.52 (m, 1H), 4.31 (s, 1H), 3.62 (s, 2H), 0.83 (s, 3H). HRMS (ESI) *m/z*: $[M + H]^+$ calcd for $C_{20}H_{18}N_3O_2^+$, 332.1394; found, 332.1394.

Preparation of 6-Methyl-3-(6-oxo-1,6-dihydropyridin-3-yl)-2,7-dihydro-4*H*-pyrazolo[3,4-*b*]pyridin-4-one (24)

Compound **24** was prepared following general procedure 4 using compound **47** (0.015 g, 0.038 mmol) and 5-(4,4,5,5-tetramethyl-1,3,2-dioxaborolan-2-yl)pyridin-2(1*H*)-one (0.018 g, 0.058 mmol). The crude product was purified using flash column chromatography (SiO_2 and DCM/MeOH, from 95:5 to 90:10), and the desired compound was obtained as a white solid (0.005 g, 53%). HPLC purity was >99%. ^{1}H NMR (500 MHz, DMSO): δ 13.35 (bs, 1H), 11.83 (s, 1H), 9.29 (s, 1H), 8.17 (dd, J = 9.7, 2.7 Hz, 1H), 6.41 (d, J = 9.6 Hz, 1H), 5.62 (s, 1H), 2.25 (s, 3H). ^{13}C NMR (126 MHz, DMSO): δ 161.69, 158.24, 158.00, 157.75, 157.51, 138.96, 120.92, 119.69, 118.53, 116.14, 113.75. HRMS (ESI) *m/z*: $[M + H]^+$ calcd for $C_{12}H_{11}N_4O_2^+$, 243.0877; found, 243.0870.

Preparation of 3-(1*H*-Indol-6-yl)-6-methyl-2,7-dihydro-4*H*-pyrazolo[3,4-*b*]pyridin-4-one (27)

Compound **27** was prepared following general procedure 4 using compound **47** (0.015 g, 0.038 mmol) and 6-(4,4,5,5-tetramethyl-1,3,2-dioxaborolan-2-yl)-1*H*-indole (0.014 g, 0.058 mmol). The crude product was purified using flash column chromatography (SiO_2 and DCM/MeOH, from 95:5 to 90:10), and the desired compound was obtained as a white solid (0.006 g, 59%). HPLC purity >99%. ^{1}H NMR (400 MHz, MeOD): δ 8.40 (s, 1H), 7.63 (s, 2H), 7.34 (d, J = 3.1 Hz, 1H), 6.50 (dd, J = 3.1, 1.0 Hz, 1H), 5.86 (s, 1H), 2.40 (s, 3H). ^{13}C NMR (126 MHz, DMSO): δ 148.81, 135.69, 135.38, 129.65, 127.89, 126.90, 123.26, 119.58, 118.56, 112.58, 107.73, 107.31, 101.15, 69.79. HRMS (ESI) *m/z*: $[M + H]^+$ calcd for $C_{15}H_{13}N_4O^+$, 265.1084; found, 265.1083.

Preparation of 3-(Benzofuran-6-yl)-6-methyl-2,7-dihydro-4*H*-pyrazolo[3,4-*b*]pyridin-4-one (29)

Compound **29** was prepared following general procedure 4 using compound **47** (0.015 g, 0.038 mmol) and 2-(benzofuran-6-yl)-4,4,5,5-tetramethyl-1,3,2-dioxaborolane (0.014 g, 0.058 mmol). The crude product was purified using flash column chromatography (SiO_2 and DCM/MeOH, from 95:5 to 90:10), and the desired compound was obtained as a white solid (0.007 g, 68%). HPLC purity 96%. ^{1}H NMR (500 MHz, MeOD): δ 8.52 (s, 1H), 7.96 (d, J = 8.2 Hz, 1H), 7.84 (d, J = 2.2 Hz, 1H), 7.70 (d, J = 8.1 Hz, 1H), 6.90 (s, 1H), 5.91 (s, 1H), 2.40 (s, 3H). ^{13}C NMR (126 MHz, MeOD): δ 156.35, 148.00, 144.18, 133.23, 129.77, 127.98, 127.63, 125.21, 124.17, 123.43, 122.00, 113.27, 108.84, 107.65, 45.10. HRMS (ESI) *m/z*: $[M + H]^+$ calcd for $C_{15}H_{12}N_3O_2^+$, 266.0924; found, 266.0933.

Preparation of 3-(Benzofuran-5-yl)-6-methyl-2,7-dihydro-4*H*-pyrazolo[3,4-*b*]pyridin-4-one (30)

Compound **30** was prepared following general procedure 4 using compound **47** (0.025 g, 0.091 mmol) and 2-(benzofuran-5-yl)-4,4,5,5-tetramethyl-1,3,2-dioxaborolane (0.033 g, 0.136 mmol). The crude product was purified using flash column chromatography (SiO_2 and DCM/MeOH, from 95:5 to 90:10), and the desired compound was obtained as a white solid (0.011 g, 46%). HPLC purity 98%. ^{1}H NMR (400 MHz, MeOD): δ 8.43 (s, 1H), 8.01 (dd, J = 8.6, 1.8 Hz, 1H), 7.82 (d, J = 2.3 Hz, 1H), 7.60 (d, J = 8.6 Hz, 1H), 6.93 (dd, J = 2.2, 1.0 Hz, 1H), 5.89 (s, 1H), 2.40 (s, 3H). HRMS (ESI) *m/z*: $[M + H]^+$ calcd for $C_{15}H_{12}N_3O_2^+$, 266.0924; found, 266.0930.

Preparation of Ethyl 6-Cyclopropyl-2,4-dihydroxynicotinate (48)

Sodium (0.44 g, 19.3 mmol) was slowly added to dry ethanol (20 mL) at room temperature, and then the temperature was increased to 60 °C. After sodium completely dissolved, diethyl malonate (3.1 g, 19.3 mmol) was added, and the reaction mixture was stirred for 1 h at 60 °C, after which 3-amino-3-cyclopropyl-acrylic acid ethyl ester (1 g, 6.44 mmol) was added dropwise as a 4 M solution in dry ethanol (0.8 mL). The reaction was stirred at 120 °C for 12 h. After reaction completion (Monitored by TLC), a white precipitate was formed. The reaction mixture was filtered, and the solid was recovered. The filtrate was concentrated in vacuo to provide more solid. The combined solid parts were washed with EtOAc (2×). The aqueous part was collected, and the pH was lowered to pH = 2 with concentrated HCl. The formation of a white precipitate was observed, which was recovered through filtration on paper and combined with the other solid. The desired compound was obtained as a light-yellow solid (1.2 g, 83%). ^{1}H NMR (600 MHz, DMSO): δ 12.75 (bs, 1H), 11.50 (bs, 1H), 5.51 (s, 1H), 4.25 (q, J = 7.1 Hz, 2H), 1.82 (tt, J = 8.3, 5.0 Hz, 1H), 1.26 (t, J = 7.1 Hz, 3H), 1.05−1.01 (m, 2H), 0.90−0.86 (m, 2H). ^{13}C NMR (151 MHz, DMSO): δ 173.45, 170.76, 160.41, 158.87, 96.55, 91.69, 60.65, 14.17, 12.92, 9.84. HRMS (ESI) *m/z*: $[M + H]^+$ calcd for $C_{11}H_{14}NO_4^+$, 224.0917; found, 224.0918.

Preparation of Ethyl 2,4-Dichloro-6-cyclopropylnicotinate (49)

Compound **48** (0.454 g, 2.03 mmol) was dissolved in $POCl_3$ (4 mL) at room temperature. The reaction was stirred at 150 °C for 3 h. After reaction completion (Monitored by TLC), the volatiles were removed under vacuo. The crude product was diluted with ice water and extracted in EtOAc (3×). The combined organic layers were washed with a saturated solution of sodium carbonate (2×) and then dried over $MgSO_4$, and the volatiles were removed under vacuo. The desired compound was obtained as a brown oil (0.459 g, 87%). ^{1}H NMR (400 MHz, DMSO): δ 7.72 (s, 1H), 4.39 (q, J = 7.0 Hz, 2H), 2.20 (tt, J = 8.3, 4.7 Hz, 1H), 1.31 (t, J = 7.0 Hz, 3H), 1.11−1.05 (m, 2H), 1.01−0.95 (m, 2H). HRMS (ESI) *m/z*: $[M + H]+$ calcd for $C_{11}H_{12}Cl_2NO_2$, 260.024; found, 260.0240.

Preparation of 2-Chloro-6-cyclopropyl-4-methoxynicotinic Acid (52)

Compound **49** (0.359 g, 1.38 mmol) was dissolved in dry methanol (1.5 mL), followed by the addition of a 2.5 M solution

Downloaded from pubs.acs.org/jmcmar/article-pdf/doi/10.1021/acs.jmedchem.6c02977/6905752/jm6c02977.pdf by guest on 06 November 2026

https://doi.org/10.1021/acs.jmedchem.6c02977
J. Med. Chem. XXXX, XXX, XXX−XXX

of sodium methoxide (0.23 mL, 0.57 mmol). The reaction mixture was stirred at 60 °C for 3 h. After reaction completion (monitored by TLC), the reaction mixture was filtered through Celite, and the volatiles were removed under vacuo. A mixture of compounds **50** and **51** (0.281 g) was obtained and used in the next step without further purification. The mixture of **50** and **51** was dissolved in MeOH (2 mL), followed by the addition of a 1.5 M solution of NaOH (3.66 mL). The reaction mixture was stirred at 90 °C for 90 min. After reaction completion (TLC), the reaction mixture was quenched with an aqueous solution of HCl (3 M). The formation of a white precipitate was observed. The solid was recovered through filtration on paper, and it was washed with ice water (2×). The desired compound was obtained as a white solid (0.21 g, 67% over two steps). ^{1}H NMR (600 MHz, DMSO): δ 7.12 (s, 1H), 3.89 (s, 3H), 2.10 (tt, J = 8.1, 4.7 Hz, 1H), 1.00−0.97 (m, 2H), 0.94−0.90 (m, 2H). ^{13}C NMR (151 MHz, DMSO): δ 165.40, 165.15, 163.55, 145.67, 117.64, 104.63, 56.66, 17.01, 10.32. HRMS (ESI) m/z: $[M + H]^+$ calcd for $C_{10}H_{11}ClNO_3^+$, 228.0422; found, 228.0428.

Preparation of *N*′-(*tert*-Butyl)-2-chloro-6-cyclopropyl-4-methoxynicotinohydrazide (53)

Compound **52** (2 g, 8.79 mmol) was dissolved in DMF (40 mL), followed by the addition of DIPEA (5.36 mL, 30.8 mmol). The temperature was lowered to 0 °C, and HATU (4.01 g, 10.5 mmol) was added. After 20 min, tertbutylhydrazine hydrochloride (2.74 g, 22 mmol) was added. The reaction was stirred at room temperature for 4 h. After reaction completion (monitored by TLC), the reaction was quenched with water and extracted with EtOAc (3×). The combined organic layers were washed with a 10% aqueous solution of LiCl (3×) and dried over $MgSO_4$. The volatiles were removed under vacuo, and the crude product was purified using flash column chromatography (SiO_2; EtOAc/Hept, from 70:30 to 100% EtOAc). The desired product was obtained as a white solid (1.26 g, 48%). ^{1}H NMR (400 MHz, DMSO): δ 9.63 (d, J = 7.9 Hz, 1H), 7.11 (s, 1H), 4.77 (d, J = 8.0 Hz, 1H), 3.85 (s, 3H), 2.11 (tt, J = 8.1, 4.8 Hz, 1H), 1.05 (s, 9H), 1.03−0.94 (m, 2H), 0.92 (dt, J = 4.6, 2.9 Hz, 2H). HRMS (ESI) m/z: $[M + H]^+$ calcd for $C_{14}H_{21}ClN_3O_2^+$, 298.1317; found, 298.1322.

Preparation of 1-(*tert*-Butyl)-6-cyclopropyl-4-methoxy-1*H*-pyrazolo[3,4-*b*]pyridin-3-ol (54)

Compound **53** (0.35 g, 1.18 mmol) was heated to 140 °C in an open vessel for 1 h. After reaction completion (monitored by TLC), the crude product was purified using flash column chromatography (SiO_2; EtOAc/Hept, from 20:80). The desired product was obtained as a white solid (0.13 g, 42%). ^{1}H NMR (400 MHz, DMSO): δ 10.39 (s, 1H), 6.54 (s, 1H), 3.90 (s, 3H), 2.15−2.04 (m, 1H), 1.59 (s, 9H), 0.99−0.92 (m, 4H). HRMS (ESI) m/z: $[M + H]^+$ calcd for $C_{14}H_{20}N_3O_2^+$, 262.1550; found, 262.1501.

Preparation of 1-(*tert*-Butyl)-6-cyclopropyl-4-methoxy-1*H*-pyrazolo[3,4-*b*]pyridin-3-yl 1,1,2,2,3,3,4,4,4-nonafluorobutane-1-sulfonate (55)

Compound **54** (0.4 g, 1.5 mmol) was dissolved in dry DCM (7 mL), followed by the addition of pyridine (0.24 mL, 3.03 mmol). The temperature was lowered to −78 °C, and nonaflyl anhydride (0.6 mL, 1.97 mmol) was added. The reaction was stirred at −78 °C for 30 min, and then it was stirred at room temperature for 90 min. After reaction completion (monitored by TLC), the reaction was quenched with water and extracted in DCM (3×). The combined organic layers were dried over $MgSO_4$, and volatiles were removed under vacuo. The crude product was purified using flash column chromatography (SiO_2 and EtOAc/Hept, from 20:80). The desired product was obtained as a colorless oil (0.621 g, 75%). HPLC purity >99%. ^{1}H NMR (400 MHz, $CDCl_3$): δ 6.48 (s, 1H), 3.99 (s, 3H), 2.04 (tt, J = 8.0, 4.7 Hz, 1H), 1.72 (s, 9H), 1.18−1.11 (m, 2H), 1.03 (dt, J = 8.2, 3.2 Hz, 2H). ^{13}C NMR (101 MHz, $CDCl_3$): δ 166.36, 159.53, 152.55, 140.67, 97.98, 97.81, 60.85, 55.80, 29.11, 18.17, 11.19. HRMS (ESI) m/z: $[M + H]^+$ calcd for $C_{18}H_{19}F_9N_3O_4S^+$, 544.0947; found, 544.0947.

General Procedure 5 (Suzuki−Miyaura Cross Coupling 2)

Compound **55** (1 equiv) was dissolved in dioxane (0.2 M), and the corresponding boronic acid or ester (1.3 equiv) was added together with a 2 M aqueous solution of Na_2CO_3 (5.5 equiv). The reaction mixture was degassed for 20 min with nitrogen, and then Pd tetrakis (0.1 equiv) was added. The reaction was stirred at 100 °C for 3 h. After reaction completion (monitored by TLC), the reaction was quenched with water and extracted with EtOAc (3×). The combined organic layers were dried over $MgSO_4$, and the volatiles were removed under vacuo. The crude product was purified using flash column chromatography.

General Procedure 6 (*tert*-Butyl and Methoxy Group Final Deprotection)

Compounds **56a−g** (1 equiv) were dissolved in dioxane (0.2 M), followed by the addition of a 37% solution of HCl (5 equiv). The reaction mixture was refluxed for 8 h. After reaction completion (monitored by TLC), the solvent was removed under reduced pressure. The crude product was purified using flash column chromatography.

General Procedure 7 (Synthesis of Compounds 36 and 37)

Carboxylic acids **32** or **33** (1 equiv) were dissolved in DMF (0.2 M), followed by the addition of DIPEA (5 equiv). The temperature was lowered to 0 °C, and EDC hydrochloride (1.5 equiv) and HOBt (1.5 equiv) were added. After 20 min, benzylamine (1.2 equiv) was added. The reaction was stirred at room temperature for 12 h. After reaction completion (monitored by TLC), the volatiles were removed in vacuo, and the crude product was purified using flash column chromatography.

General Procedure 8 (Synthesis of Compounds 34 and 35)

Carboxylic acids **32** or **33** (1 equiv) were dissolved in MeOH (0.25 M), followed by the addition of thionyl chloride (1.5 equiv) at 0 °C. The reaction was stirred at room temperature for 12 h. After reaction completion (monitored by TLC), the volatiles were removed under vacuo, and the desired product was obtained. No further purification was needed.

Preparation of 3-(3-((1*H*-Imidazole-1-yl)methyl)phenyl)-1-(*tert*-butyl)-6-cyclopropyl-4-methoxy-1*H*-pyrazolo[3,4-*b*]pyridine (56a)

Compound **56a** was prepared following general procedure 5 using compound **55** (0.07 g, 0.13 mmol) and 1-(3-(4,4,5,5-tetramethyl-1,3,2-dioxaborolan-2-yl)benzyl)-1*H*-imidazole (0.048 g, 0.17 mmol). The crude product was purified using flash column chromatography (SiO_2 and EtOAc/Hept, from 50:50 to 60:40), and the desired compound was obtained as a white solid (0.048 g, 92%). ^{1}H NMR (400 MHz, MeOD): δ 7.91 (s, 1H), 7.88 (s, 1H), 7.77 (d, J = 7.8 Hz, 1H), 7.61 (t, J = 7.2 Hz, 1H), 7.52 (d, J = 8.2 Hz, 1H), 7.15 (s, 1H), 6.93 (s, 1H),

Downloaded from pubs.acs.org/jmcmar/article-pdf/doi/10.1021/acs.jmedchem.6c02977/6905752/jm6c02977.pdf by guest on 06 November 2026

https://doi.org/10.1021/acs.jmedchem.6c02977
J. Med. Chem. XXXX, XXX, XXX−XXX

5.92 (bs, 1H), 5.37 (s, 2H), 2.15 (m, 1H), 1.74 (s, 9H), 1.15 (m, 2H), 1.03 (m, 2H). HRMS (ESI) *m/z*: $[M + H]^+$ calcd for $C_{24}H_{28}N_5O^+$, 402.2288; found, 402.2294.

Preparation of 5-(1-(*tert*-Butyl)-6-cyclopropyl-4-methoxy-1*H*-pyrazolo[3,4-*b*]pyridin-3-yl)pyridin-2(1*H*)-one (56b)

Compound **56b** was prepared following general procedure 5 using compound **55** (0.06 g, 0.11 mmol) and 5-(4,4,5,5-tetramethyl-1,3,2-dioxaborolan-2-yl)pyridin-2(1*H*)-one (0.032 g, 0.14 mmol). The crude product was purified using flash column chromatography (SiO_2 and DCM/MeOH, from 95:5 to 90:10), and the desired compound was obtained as a white solid (0.036 g, 96%). ^{1}H NMR (400 MHz, DMSO): δ 11.67 (s, 1H), 7.98 (dd, J = 9.5, 2.6 Hz, 1H), 7.94 (d, J = 2.6 Hz, 1H), 6.77 (s, 1H), 6.42 (dd, J = 9.5, 0.7 Hz, 1H), 3.98 (s, 3H), 2.20 (p, J = 6.3 Hz, 1H), 1.72 (s, 9H), 1.03 (s, 2H), 1.02 (s, 1H). HRMS (ESI) *m/z*: $[M + H]^+$ calcd for $C_{19}H_{23}N_4O_2^+$, 339.1816; found, 339.1809.

Preparation of 5-(1-(*tert*-Butyl)-6-cyclopropyl-4-methoxy-1*H*-pyrazolo[3,4-*b*]pyridin-3-yl)-1-methylpyridin-2(1*H*)-one (56c)

Compound **56c** was prepared following general procedure 5 using compound **55** (0.058 g, 0.107 mmol) and 1-methyl-5-(4,4,5,5-tetramethyl-[1,3,2]dioxaborolan-2-yl)-1*H*-pyridin-2-one (0.033 g, 0.14 mmol). The crude product was purified using flash column chromatography (SiO_2 and DCM/MeOH, from 98:2 to 95:5), and the desired compound was obtained as a white solid (0.033 g, 88%). ^{1}H NMR (400 MHz, DMSO): δ 8.19 (d, J = 2.5 Hz, 1H), 7.91 (dd, J = 9.4, 2.6 Hz, 1H), 6.77 (s, 1H), 6.47 (dd, J = 9.5, 0.6 Hz, 1H), 4.00 (s, 3H), 3.53 (s, 3H), 2.20 (p, J = 6.3 Hz, 1H), 1.72 (s, 9H), 1.04 (s, 2H), 1.02 (s, 2H).

Preparation of 7-(1-(*tert*-Butyl)-6-cyclopropyl-4-methoxy-1*H*-pyrazolo[3,4-*b*]pyridin-3-yl)-3,4-dihydro-2*H*-benzo[*b*][1,4]oxazine (56d)

Compound **56d** was prepared following general procedure 5 using compound **55** (0.06 g, 0.11 mmol) and 7-(4,4,5,5-tetramethyl-1,3,2-dioxaborolan-2-yl)-3,4-dihydro-2*H*-benzo[*b*][1,4]oxazine (0.037 g, 0.14 mmol). The crude product was purified using flash column chromatography (SiO_2 and EtOAc/Hept, from 50:50 to 60:40), and the desired compound was obtained as a white solid (0.028 g, 67%). ^{1}H NMR (400 MHz, DMSO): δ 7.24 (dd, J = 8.2, 2.0 Hz, 1H), 7.20 (d, J = 1.9 Hz, 1H), 6.72 (s, 1H), 6.58 (d, J = 8.2 Hz, 1H), 5.89 (s, 1H), 4.14 (t, 2H), 3.94 (s, 3H), 3.31−3.29 (m, 2H), 2.18 (tt, J = 7.4, 5.4 Hz, 1H), 1.71 (s, 9H), 1.04−0.99 (m, 4H). HRMS (ESI) *m/z*: $[M + H]^+$ calcd for $C_{22}H_{27}N_4O_2^+$, 379.2129; found, 379.2127.

Preparation of 3-(Benzofuran-6-yl)-1-(*tert*-butyl)-6-cyclopropyl-4-methoxy-1*H*-pyrazolo[3,4-*b*]pyridine (56e)

Compound **56e** was prepared following general procedure 5 using compound **55** (0.143 g, 0.263 mmol) and 2-(benzofuran-6-yl)-4,4,5,5-tetramethyl-1,3,2-dioxaborolane (0.084 g, 0.34 mmol). The crude product was purified using flash column chromatography (SiO_2 and EtOAc/Hept, from 10:90 to 30:70), and the desired compound was obtained as a white solid (0.07 g, 74%). ^{1}H NMR (400 MHz, DMSO): δ 8.07 (s, 1H), 8.03 (d, J = 2.2 Hz, 1H), 7.82 (dd, J = 8.1, 1.4 Hz, 1H), 7.69 (d, J = 8.1 Hz, 1H), 7.00 (dd, J = 2.1, 1.0 Hz, 1H), 6.81 (s, 1H), 3.99 (s, 3H), 2.22 (tt, J = 7.4, 5.3 Hz, 1H), 1.76 (s, 9H), 1.09−1.01 (m, 4H). HRMS (ESI) *m/z*: $[M + H]^+$ calcd for $C_{22}H_{24}N_3O_2^+$, 362.1863; found, 362.1859.

Preparation of Ethyl 6-(1-(*tert*-Butyl)-6-cyclopropyl-4-methoxy-1*H*-pyrazolo[3,4-*b*]pyridin-3-yl)benzofuran-2-carboxylate (56f)

Compound **56f** was prepared following general procedure 5 using compound **55** (0.120 g, 0.22 mmol) and ethyl 6-(4,4,5,5-tetramethyl-1,3,2-dioxaborolan-2-yl)-1-benzofuran-2-carboxylate (0.091 g, 0.29 mmol). The crude product was purified using flash column chromatography (SiO_2 and EtOAc/Hept, from 20:80), and the desired compound was obtained as a white solid (0.094 g, 98%). ^{1}H NMR (400 MHz, DMSO): δ 8.21−8.15 (m, 1H), 7.94 (dd, J = 8.3, 1.4 Hz, 1H), 7.84 (dd, J = 8.3, 0.7 Hz, 1H), 7.80 (d, J = 1.0 Hz, 1H), 6.84 (s, 1H), 4.38 (q, J = 7.1 Hz, 2H), 4.01 (s, 3H), 2.24 (p, J = 6.6 Hz, 1H), 1.77 (s, 9H), 1.36 (t, J = 7.1 Hz, 3H), 1.08−1.02 (m, 4H). HRMS (ESI) *m/z*: $[M + H]^+$ calcd for $C_{25}H_{28}N_3O_4^+$, 434.2075; found, 434.2076.

Preparation of Ethyl 6-(1-(*tert*-Butyl)-6-cyclopropyl-4-methoxy-1*H*-pyrazolo[3,4-*b*]pyridin-3-yl)benzofuran-3-carboxylate (56g)

Compound **56g** was prepared following general procedure 5 using compound **55** (0.25 g, 0.46 mmol) and ethyl 6-(4,4,5,5-tetramethyl-1,3,2-dioxaborolan-2-yl)benzofuran-3-carboxylate (0.189 g, 0.59 mmol). The crude product was purified using flash column chromatography (SiO_2 and EtOAc/Hept, from 40:60), and the desired compound was obtained as a white solid (0.173 g, 87%). ^{1}H NMR (400 MHz, $CDCl_3$): δ 8.28 (s, 1H), 8.17 (s, 1H), 8.10−7.99 (m, 2H), 6.49 (s, 1H), 4.43 (q, J = 7.1 Hz, 2H), 3.99 (s, 3H), 2.07 (tt, 1H), 1.83 (s, 9H), 1.45 (t, J = 7.1 Hz, 3H), 1.21−1.15 (m, 2H), 1.06−0.99 (m, 2H). HRMS (ESI) *m/z*: $[M + H]^+$ calcd for $C_{25}H_{28}N_3O_4^+$, 434.2074; found, 434.2077.

Preparation of 3-(Benzofuran-6-yl)-6-cyclopropyl-4-methoxy-2*H*-pyrazolo[3,4-*b*]pyridine (31b)

Compound **56e** was dissolved in TFA (2.5 mL), and the reaction was stirred at 120 °C for 1 h. After reaction completion (monitored by TLC), the volatiles were removed under vacuo, and the desired product was obtained as a white powder (0.059 g, 94%). HPLC purity >99%. ^{1}H NMR (400 MHz, DMSO): δ 13.42 (s, 1H), 8.11 (s, 1H), 8.04 (d, J = 2.2 Hz, 1H), 7.85 (d, J = 8.1, 1.4 Hz, 1H), 7.70 (d, J = 8.1 Hz, 1H), 7.00 (d, J = 2.2 Hz, 1H), 6.77 (s, 1H), 4.00 (s, 3H), 2.26−2.17 (m, 1H), 1.06−0.99 (m, 4H). ^{13}C NMR (126 MHz, DMSO): δ 165.09, 160.31, 155.45, 154.33, 146.60, 143.15, 130.23, 126.70, 123.50, 120.60, 111.20, 106.74, 101.96, 97.38, 55.83, 17.36, 10.24. HRMS (ESI) *m/z*: $[M + H]^+$ calcd for $C_{18}H_{16}N_3O_2^+$, 306.1237; found, 306.1235.

Preparation of 3-(3-((1*H*-Imidazole-1-yl)methyl)phenyl)-6-cyclopropyl-2,7-dihydro-4*H*-pyrazolo[3,4-*b*]pyridin-4-one (22)

Compound **22** was prepared following general procedure 6 using compound **56a** (0.05 g, 0.086 mmol). The crude product was purified using flash column chromatography (SiO_2 and DCM/MeOH, from 90:10 to 85:15), and the desired compound was obtained as a white solid (0.028 g, 68%). HPLC purity >99%. ^{1}H NMR (400 MHz, MeOD): δ 8.13 (s, 1H), 8.02 (d, J = 7.8 Hz, 1H), 7.82 (s, 1H), 7.46 (t, J = 7.7 Hz, 1H), 7.30 (d, J = 7.7 Hz, 1H), 7.20 (s, 1H), 7.00 (s, 1H), 5.79 (s, 1H), 5.29 (s, 2H), 1.97 (tt, J = 8.5, 4.9 Hz, 1H), 1.12 (dt, J = 8.4, 3.4 Hz, 2H), 0.97 (dt, J = 7.1, 4.6 Hz, 2H). ^{13}C NMR (126 MHz, MeOD): δ 163.56, 163.29, 138.55, 138.29, 130.04, 129.72,

Downloaded from pubs.acs.org/jmcmar/article-pdf/doi/10.1021/acs.jmedchem.6c02977/6905752/jm6c02977.pdf by guest on 06 November 2026

https://doi.org/10.1021/acs.jmedchem.6c02977
J. Med. Chem. XXXX, XXX, XXX−XXX

129.39, 129.24, 129.03, 121.55, 121.08, 119.23, 116.91, 114.59, 103.73, 51.70, 14.86, 9.60. HRMS (ESI) m/z: $[M + H]^+$ calcd for $C_{19}H_{18}N_5O^+$, 332.1506; found, 332.1505.

Preparation of 6-Cyclopropyl-3-(6-oxo-1,6-dihydropyridin-3-yl)-2,7-dihydro-4*H*-pyrazolo[3,4-*b*]pyridin-4-one (25)

Compound **25** was prepared following general procedure 6 using compound **56b** (0.029 g, 0.086 mmol). The crude product was purified using flash column chromatography (SiO_2 and DCM/MeOH, from 90:10 to 85:15), and the desired compound was obtained as a white solid (0.012 g, 52%). HPLC purity 99%. ^{1}H NMR (400 MHz, DMSO): δ 13.10 (bs, 1H), 11.77 (bs, 1H), 9.17 (bs, 1H), 8.40 (bs, 1H), 8.13 (dd, J = 9.6, 2.6 Hz, 1H), 6.42 (d, J = 9.6 Hz, 1H), 5.43 (bs, 1H), 2.04−1.89 (m, 1H), 1.03−0.94 (m, 2H), 0.94−0.88 (m, 2H). ^{13}C NMR (126 MHz, DMSO): δ 161.70, 152.89, 139.65, 135.91, 119.69, 111.52, 101.70, 14.10, 9.41. HRMS (ESI) m/z: $[M + H]^+$ calcd for $C_{14}H_{13}N_4O_2^+$, 269.1034; found, 269.1029.

Preparation of 6-Cyclopropyl-3-(1-methyl-6-oxo-1,6-dihydropyridin-3-yl)-2,7-dihydro-4*H*-pyrazolo[3,4-*b*]pyridin-4-one (26)

Compound **26** was prepared following general procedure 6 using compound **56c** (0.016 g, 0.045 mmol). The crude product was purified using flash column chromatography (SiO_2 and DCM/MeOH, 90:10), and the desired compound was obtained as a white solid (0.006 g, 47%). HPLC purity >99%. ^{1}H NMR (500 MHz, MeOD): δ 9.18 (s, 1H), 8.21 (d, J = 9.5 Hz, 1H), 6.62 (d, J = 9.5 Hz, 1H), 5.80 (s, 1H), 3.66 (s, 3H), 1.96 (tt, J = 8.4, 5.0 Hz, 1H), 1.17−1.05 (m, 2H), 0.96 (dt, J = 7.1, 4.6 Hz, 2H). ^{13}C NMR (126 MHz, MeOD): δ 164.59, 142.25, 140.85, 119.72, 38.60, 14.76, 9.51. HRMS (ESI) m/z: $[M + H]^+$ calcd for $C_{15}H_{15}N_4O_2^+$, 283.1190; found, 283.1188.

Preparation of 6-Cyclopropyl-3-(3,4-dihydro-2*H*-benzo[*b*][1,4]oxazin-7-yl)-2,7-dihydro-4*H*-pyrazolo[3,4-*b*]pyridin-4-one (28)

Compound **28** was prepared following general procedure 6 using compound **56d** (0.022 g, 0.058 mmol). The crude product was purified using flash column chromatography (SiO_2 and DCM/MeOH, from 95:5 to 90:10), and the desired compound was obtained as a white solid (0.009 g, 50%). HPLC purity >99%. ^{1}H NMR (400 MHz, MeOD): δ 7.60−7.51 (m, 2H), 6.66 (d, J = 8.3 Hz, 1H), 5.60 (s, 1H), 4.21 (t, 2H), 3.40 (t, J = 4.4 Hz, 2H), 1.98−1.89 (m, 1H), 1.17−1.05 (m, 2H), 0.94 (dt, J = 7.4, 4.8 Hz, 2H). ^{13}C NMR (126 MHz, MeOD): δ 164.87, 158.16, 153.57, 144.67, 137.45, 123.22, 117.75, 115.72, 108.11, 103.26, 66.12, 41.68, 14.45, 9.44. HRMS (ESI) m/z: $[M + H]^+$ calcd for $C_{17}H_{17}N_4O_2^+$, 309.1346; found, 309.1349.

Preparation of 3-(Benzofuran-6-yl)-6-cyclopropyl-2,7-dihydro-4*H*-pyrazolo[3,4-*b*]pyridin-4-one (31)

Compound **31** was prepared following general procedure 6 using compound **56e** (0.028 g, 0.077 mmol). The crude product was purified using flash column chromatography (SiO_2 and DCM/MeOH, 95:5), and the desired compound was obtained as a white solid (0.019 g, 84%). HPLC purity >99%. ^{1}H NMR (400 MHz, MeOD): δ 8.49 (s, 1H), 7.95 (d, J = 8.2 Hz, 1H), 7.83 (d, J = 2.2 Hz, 1H), 7.69 (d, J = 8.2 Hz, 1H), 6.89 (dd, J = 2.2, 1.0 Hz, 1H), 5.74 (s, 1H), 2.01−1.93 (m, 1H), 1.16−1.10 (m, 2H), 0.97 (dt, J = 7.2, 4.6 Hz, 2H). ^{13}C NMR (126 MHz, DMSO): δ 164.02, 158.97, 156.19, 154.40, 146.54, 143.20, 130.28, 126.56, 123.19, 122.38, 120.58, 111.19, 106.75, 101.96, 100.84, 16.94, 9.83. HRMS (ESI) m/z: $[M + H]^+$ calcd for $C_{17}H_{14}N_3O_2^+$, 292.1081; found, 292.1086.

Preparation of 6-(6-Cyclopropyl-4-oxo-4,7-dihydro-2*H*-pyrazolo[3,4-*b*]pyridin-3-yl)benzofuran-2-carboxylic acid (32)

Compound **32** was prepared following general procedure 6 using compound **56f** (0.095 g, 0.22 mmol). After solvent evaporation, the desired compound was obtained as a white solid (0.077 g, 94%); no further purification was needed. HPLC purity 95%. ^{1}H NMR (500 MHz, DMSO): δ 8.41 (s, 1H), 8.01 (dd, J = 8.3, 1.5 Hz, 1H), 7.90 (d, J = 8.3 Hz, 1H), 7.72 (s, 1H), 6.46 (s, 1H), 2.27 (tt, J = 8.5, 4.8 Hz, 1H), 1.28−1.19 (m, 2H), 1.10−1.01 (m, 2H). ^{13}C NMR (126 MHz, DMSO): δ 161.74, 159.92, 159.88, 154.80, 151.04, 147.34, 141.49, 127.41, 124.33, 122.99, 113.45, 112.40, 104.44, 99.02, 14.63, 11.11. HRMS (ESI) m/z: $[M + H]^+$ calcd for $C_{18}H_{14}N_3O_4^+$, 336.0979; found, 336.0985.

Preparation of 6-(6-Cyclopropyl-4-oxo-4,7-dihydro-2*H*-pyrazolo[3,4-*b*]pyridin-3-yl)benzofuran-3-carboxylic Acid (33)

Compound **33** was prepared following general procedure 6 using compound **56g** (0.09 g, 0.21 mmol). After solvent evaporation, the desired compound was obtained as a white solid (0.049 g, 70%); no further purification was needed. HPLC purity 97%. ^{1}H NMR (400 MHz, DMSO): δ 8.77 (s, 1H), 8.43 (s, 1H), 8.09−8.02 (m, 2H), 6.40 (s, 1H), 2.25 (tt, J = 8.2, 4.9 Hz, 1H), 1.26−1.19 (m, 2H), 1.11−1.01 (m, 2H). ^{13}C NMR (126 MHz, DMSO): δ 163.94, 161.67, 154.85, 153.33, 151.26, 125.15, 124.72, 121.29, 114.67, 112.31, 104.36, 99.09, 14.68, 11.01. HRMS (ESI) m/z: $[M + H]^+$ calcd for $C_{18}H_{14}N_3O_4^+$, 336.0979; found, 336.0996.

Preparation of Methyl 6-(6-Cyclopropyl-4-oxo-4,7-dihydro-2*H*-pyrazolo[3,4-*b*]pyridin-3-yl)benzofuran-3-carboxylate (34)

Compound **34** was prepared following general procedure 8 using compound **33** (0.005 g, 0.013 mmol) and MeOH (0.5 mL). The desired compound was obtained as a white powder (0.004 g, 85%). HPLC purity >99%. ^{1}H NMR (400 MHz, MeOD): δ 8.59 (s, 1H), 8.21 (d, J = 1.4 Hz, 1H), 8.17 (d, J = 8.2 Hz, 1H), 7.92 (d, J = 8.3, 1.5 Hz, 1H), 6.29 (s, 1H), 3.96 (s, 3H), 2.30 (tt, J = 8.5, 4.8 Hz, 1H), 1.46 (td, J = 7.5, 4.9 Hz, 2H), 1.25−1.19 (m, 2H). ^{13}C NMR (126 MHz, MeOD): δ 170.56, 164.87, 164.75, 156.74, 154.57, 151.75, 143.12, 127.31, 126.60, 126.18, 123.05, 115.62, 113.85, 105.88, 98.48, 52.30, 15.51, 12.37. HRMS (ESI) m/z: $[M + H]^+$ calcd for $C_{19}H_{16}N_3O_4^+$, 350.1135; found, 350.1131.

Preparation of *N*-Benzyl-6-(6-cyclopropyl-4-oxo-4,7-dihydro-2*H*-pyrazolo[3,4-*b*]pyridin-3-yl)benzofuran-3-carboxamide (36)

Compound **36** was prepared following general procedure 7 using compound **33** (0.041 g, 0.11 mmol) and benzylamine (0.014 mL, 0.13 mmol). The crude product was purified by flash column chromatography (SiO_2 and DCM/MeOH, 95:5), and the desired compound was obtained as a white solid (0.015 g, 32%). HPLC purity >99%. ^{1}H NMR (400 MHz, DMSO): δ 13.34 (s, 1H), 8.91 (t, J = 6.0 Hz, 1H), 8.63 (s, 1H), 8.15 (s, 1H), 8.12−8.05 (m, 1H), 7.41−7.32 (m, 4H), 7.30−7.23 (m, 1H), 4.52 (d, J = 5.9 Hz, 2H), 1.99 (s, 1H), 1.02−0.89 (m, 4H). ^{13}C NMR (126 MHz, DMSO): δ 161.99, 154.80, 148.09, 139.51, 131.00, 128.37, 127.36, 126.86, 124.63, 123.90, 123.25, 121.31, 116.95, 112.23, 111.51, 107.91, 102.12, 101.01, 42.13,

Downloaded from pubs.acs.org/jmcmar/article-pdf/doi/10.1021/acs.jmedchem.6c02977/6905752/jm6c02977.pdf by guest on 06 November 2026

https://doi.org/10.1021/acs.jmedchem.6c02977
J. Med. Chem. XXXX, XXX, XXX−XXX

16.92, 9.73. HRMS (ESI) *m/z*: $[M + H]^+$ calcd for $C_{25}H_{21}N_4O_3^+$, 425.1608; found, 425.1606.

Preparation of Methyl 6-(6-Cyclopropyl-4-oxo-4,7-dihydro-2*H*-pyrazolo[3,4-*b*]pyridin-3-yl)benzofuran-2-carboxylate (35)

Compound **35** was prepared following general procedure 8 using compound **32** (0.01 g, 0.03 mmol) and MeOH (0.5 mL). The desired compound was obtained as a white powder (0.008 g, 76%). HPLC purity was >99%. ^{1}H NMR (400 MHz, MeOD) δ 8.27 (s, 1H), 7.92 (s, 2H), 7.71 (s, 1H), 6.27 (s, 1H), 3.98 (s, 3H), 2.28 (tt, J = 8.4, 4.4 Hz, 1H), 1.44 (td, J = 7.5, 4.8 Hz, 2H), 1.24−1.18 (m, 2H). ^{13}C NMR (126 MHz, MeOD): δ 170.38, 164.92, 161.00, 156.74, 151.61, 148.41, 143.11, 129.73, 128.71, 125.80, 124.45, 114.74, 114.07, 105.92, 98.55, 52.98, 15.52, 12.42. HRMS (ESI) *m/z*: $[M + H]^+$ calcd for $C_{19}H_{16}N_3O_4^+$, 350.1135; found, 350.1138.

Preparation of *N*-Benzyl-6-(6-cyclopropyl-4-oxo-4,7-dihydro-2*H*-pyrazolo[3,4-*b*]pyridin-3-yl)benzofuran-2-carboxamide (37)

Compound **37** was prepared following general procedure 7 using compound **32** (0.033 g, 0.098 mmol) and benzylamine (0.012 mL, 0.12 mmol). The crude product was purified using flash column chromatography (SiO_2 and DCM/MeOH, 95:5), and the desired compound was obtained as a white solid. HPLC purity >99%. ^{1}H NMR (400 MHz, MeOD): δ 8.67 (s, 1H), 8.02 (s, 1H), 7.79 (d, J = 8.3 Hz, 1H), 7.54 (s, 1H), 7.41−7.31 (m, 4H), 7.29−7.23 (m, 1H), 5.70 (s, 1H), 4.63−4.59 (m, 2H), 1.98 (s, 1H), 1.20−1.08 (m, 2H), 1.03−0.94 (m, 2H). ^{13}C NMR (126 MHz, MeOD): δ 160.99, 156.46, 151.21, 139.88, 130.85, 129.58, 128.64, 128.31, 124.42, 123.66, 113.91, 111.36, 103.55, 43.97, 14.43, 9.22. HRMS (ESI) *m/z*: $[M + H]^+$ calcd for $C_{25}H_{21}N_4O_3^+$, 425.1609; found, 425.1611.

■ ASSOCIATED CONTENT

Supporting Information

The Supporting Information is available free of charge at https://pubs.acs.org/doi/10.1021/acs.jmedchem.6c02977.

Molecular formula strings and the associated biochemical and biological data (CSV)

Materials, characterization data, ^{1}H and ^{13}C NMR spectra, and HPLC traces for compounds **4**, **6**−**15**, **17**−**37**, **31b**, and **55** (PDF)

Accession Codes

Atomic coordinates and structure factors have been deposited in the Protein Data Bank under the accession codes 32RD (compound **3**), 32SH (compound **4**), 32SA (compound **5**), 32TH (compound **20**), 32SJ (compound **22**), and 32QY (compound **24**), and will be released upon publication of the article.

■ AUTHOR INFORMATION

Corresponding Authors

František Zálešák − *Department of Biochemistry, University of Zürich, Zurich CH-8057, Switzerland;* Email: f.zalesak@bioc.uzh.ch

Amedeo Caflisch − *Department of Biochemistry, University of Zürich, Zurich CH-8057, Switzerland;* orcid.org/0000-0002-2317-6792; Email: caflisch@bioc.uzh.ch

Authors

Francesco Errani − *Department of Biochemistry, University of Zürich, Zurich CH-8057, Switzerland;* orcid.org/0009-0004-4658-9022

Francesco Nai − *Department of Biochemistry, University of Zürich, Zurich CH-8057, Switzerland;* orcid.org/0000-0002-4258-3174

Elena Bochenkova − *Department of Biochemistry, University of Zürich, Zurich CH-8057, Switzerland*

Marcin Herok − *Department of Biochemistry, University of Zürich, Zurich CH-8057, Switzerland*

Annalisa Invernizzi − *Department of Biochemistry, University of Zürich, Zurich CH-8057, Switzerland;* orcid.org/0009-0000-3380-8602

Rajiv Kumar Bedi − *Department of Biochemistry, University of Zürich, Zurich CH-8057, Switzerland;* orcid.org/0000-0002-8193-9006

Yaozong Li − *Department of Biochemistry, University of Zürich, Zurich CH-8057, Switzerland;* orcid.org/0000-0002-5796-2644

Complete contact information is available at: https://pubs.acs.org/doi/10.1021/acs.jmedchem.6c02977

Author Contributions

[†]F.E. and F.N. contributed equally to this work. F.E., F.N., and A.C. wrote the manuscript with contributions from other authors. All authors have approved the final version of the manuscript.

Funding

This work was supported by grants of the Lotte and Adolf Hotz-Sprenger Stiftung, Swiss Cancer Research Foundation (KFS-5748-02−2023) and the Hartmann-Müller Stiftung to AC.

Notes

The authors declare no competing financial interest.

■ ACKNOWLEDGMENTS

We thank Anezka Lykova for the help in the synthesis of compounds **32** and **37**, and Dr. Ivan Corbeski for technical assistance with the calorimetry. We thank Beat Blattmann and Görkem Kurtuldu at the Protein Crystallization Center of the University of Zurich for assistance with crystallization, and the beamline scientists at P13 (EMBL Hamburg, DESY), ID30B (ESRF, Grenoble) and the Swiss Light Source (Paul Scherrer Institute, Villigen) for their help with the X-ray diffraction experiments.

■ ABBREVIATIONS:

ACTB, actin beta; CETSA, cellular thermal shift assay; CI, confidence interval; DD, death domain; DHPP, dihydropyrazolopyridinone; DIPEA, *N*,*N*-diisopropylethylamine; DMEM, Dulbecco's modified Eagle's medium; DSF, differential scanning fluorimetry; EDC, 1-ethyl-3-(3-dimethylaminopropyl)carbodiimide; FBS, fetal bovine serum; FP, fluorescence polarization;

Downloaded from pubs.acs.org/jmcmar/article-pdf/doi/10.1021/acs.jmedchem.6c02977/6905752/jm6c02977.pdf by guest on 06 November 2026

GI_{50}, half-maximal growth inhibitory concentration; HATU, 1-[bis(dimethylamino)methylene]-1H-1,2,3-triazolo[4,5-b]pyridinium 3-oxide hexafluorophosphate; HEPES, 4-(2-hydroxyethyl)piperazine-1-ethanesulfonic acid; HOBt, 1-hydroxybenzotriazole; ITC, isothermal titration calorimetry; K_d, equilibrium dissociation constant; m6A, N^6-methyladenosine; MES, 2-(*N*-morpholino)ethanesulfonic acid; NIS, *N*-iodosuccinimide; pTSA, p-toluenesulfonic acid; RPMI, Roswell Park Memorial Institute medium; RT-qPCR, reverse transcription quantitative real-time polymerase chain reaction; SD, standard deviation; SNAr, nucleophilic aromatic substitution; TNFR1, tumor necrosis factor receptor 1; TNFR2, tumor necrosis factor receptor 2; TNFRSF1B, tumor necrosis factor receptor superfamily member 1B; tPSA, topological polar surface area; TR-FRET, time-resolved fluorescence resonance energy transfer; UPLC, ultra-performance liquid chromatography; YTH, YT521-B homology; YTHDC1, YTH domain-containing protein 1; YTHDC2, YTH domain-containing protein 2; YTHDF1, YTH domain-containing family protein 1; YTHDF2, YTH domain-containing family protein 2; YTHDF3, YTH domain-containing family protein 3; ZIP, zero interaction potency.

REFERENCES

(1) Nai, F.; Nachawati, R.; Zálešák, F.; Wang, X.; Li, Y.; Caflisch, A. Fragment Ligands of the m^6 A-RNA Reader YTHDF2. *ACS Med. Chem. Lett.* **2022**, *13* (9), 1500−1509.

(2) Liao, S.; Sun, H.; Xu, C. YTH Domain: A Family of N6-Methyladenosine (m6A) Readers. *Genomics, Proteomics Bioinf.* **2018**, *16* (2), 99−107.

(3) Roundtree, I. A.; Luo, G.-Z.; Zhang, Z.; Wang, X.; Zhou, T.; Cui, Y.; Sha, J.; Huang, X.; Guerrero, L.; Xie, P.; He, E.; Shen, B.; He, C. YTHDC1 Mediates Nuclear Export of N6-Methyladenosine Methylated mRNAs. *eLife* **2017**, *6*, e31311.

(4) Zou, Z.; He, C. The YTHDF Proteins Display Distinct Cellular Functions on m6A-Modified RNA. *Trends Biochem. Sci.* **2024**, *49* (7), 611−621.

(5) Du, H.; Zhao, Y.; He, J.; Zhang, Y.; Xi, H.; Liu, M.; Ma, J.; Wu, L. YTHDF2 Destabilizes m6A-Containing RNA through Direct Recruitment of the CCR4−NOT Deadenylase Complex. *Nat. Commun.* **2016**, *7* (1), 12626.

(6) Zaccara, S.; Jaffrey, S. R. A Unified Model for the Function of YTHDF Proteins in Regulating m6A-Modified mRNA. *Cell* **2020**, *181* (7), 1582−1595.e18.

(7) Lasman, L.; Krupalnik, V.; Viukov, S.; Mor, N.; Aguilera-Castrejon, A.; Schneir, D.; Bayerl, J.; Mizrahi, O.; Peles, S.; Tawil, S.; Sathe, S.; Nachshon, A.; Shani, T.; Zerbib, M.; Kilimnik, I.; Aigner, S.; Shankar, A.; Mueller, J. R.; Schwartz, S.; Stern-Ginossar, N.; Yeo, G. W.; Geula, S.; Novershtern, N.; Hanna, J. H. Context-Dependent Functional Compensation between Ythdf m6A Reader Proteins. *Genes Dev.* **2020**, *34* (19−20), 1373−1391.

(8) Kontur, C.; Jeong, M.; Cifuentes, D.; Giraldez, A. J. Ythdf m6A Readers Function Redundantly during Zebrafish Development. *Cell Rep.* **2020**, *33* (13), 108598.

(9) Zou, Z.; Sepich-Poore, C.; Zhou, X.; Wei, J.; He, C. The Mechanism Underlying Redundant Functions of the YTHDF Proteins. *Genome Biol.* **2023**, *24* (1), 17.

(10) Ren, W.; Yuan, Y.; Li, Y.; Mutti, L.; Peng, J.; Jiang, X. The Function and Clinical Implication of YTHDF1 in the Human System Development and Cancer. *Biomark. Res.* **2023**, *11* (1), 5.

(11) Paris, J.; Morgan, M.; Campos, J.; Spencer, G. J.; Shmakova, A.; Ivanova, I.; Mapperley, C.; Lawson, H.; Wotherspoon, D. A.; Sepulveda, C.; Vukovic, M.; Allen, L.; Sarapuu, A.; Tavosanis, A.; Guitart, A. V.; Villacreces, A.; Much, C.; Choe, J.; Azar, A.; van de Lagemaat, L. N.; Vernimmen, D.; Nehme, A.; Mazurier, F.; Somervaille, T. C. P.; Gregory, R. I.; O'Carroll, D.; Kranc, K. R. Targeting the RNA m6A Reader YTHDF2 Selectively Compromises Cancer Stem Cells in Acute Myeloid Leukemia. *Cell Stem Cell* **2019**, *25* (1), 137−148.e6.

(12) Einstein, J. M.; Perelis, M.; Chaim, I. A.; Meena, J. K.; Nussbacher, J. K.; Tankka, A. T.; Yee, B. A.; Li, H.; Madrigal, A. A.; Neill, N. J.; Shankar, A.; Tyagi, S.; Westbrook, T. F.; Yeo, G. W. Inhibition of YTHDF2 Triggers Proteotoxic Cell Death in MYC-Driven Breast Cancer. *Mol. Cell* **2021**, *81* (15), 3048−3064.e9.

(13) Wang, J.; Lu, A. The Biological Function of m6A Reader YTHDF2 and Its Role in Human Disease. *Cancer Cell Int.* **2021**, *21* (1), 109.

(14) Chang, G.; Shi, L.; Ye, Y.; Shi, H.; Zeng, L.; Tiwary, S.; Huse, J. T.; Huo, L.; Ma, L.; Ma, Y.; Zhang, S.; Zhu, J.; Xie, V.; Li, P.; Han, L.; He, C.; Huang, S. YTHDF3 Induces the Translation of m6A-Enriched Gene Transcripts to Promote Breast Cancer Brain Metastasis. *Cancer Cell* **2020**, *38* (6), 857−871.e7.

(15) Xu, Y.; He, X.; Wang, S.; Sun, B.; Jia, R.; Chai, P.; Li, F.; Yang, Y.; Ge, S.; Jia, R.; Yang, Y.-G.; Fan, X. The m6A Reading Protein YTHDF3 Potentiates Tumorigenicity of Cancer Stem-like Cells in Ocular Melanoma through Facilitating CTNNB1 Translation. *Oncogene* **2022**, *41* (9), 1281−1297.

(16) Shi, H.; Wang, X.; Lu, Z.; Zhao, B. S.; Ma, H.; Hsu, P. J.; Liu, C.; He, C. YTHDF3 Facilitates Translation and Decay of N6-Methyladenosine-Modified RNA. *Cell Res.* **2017**, *27* (3), 315−328.

(17) Wang, X.; Zhao, B. S.; Roundtree, I. A.; Lu, Z.; Han, D.; Ma, H.; Weng, X.; Chen, K.; Shi, H.; He, C. *N6*-Methyladenosine Modulates Messenger RNA Translation Efficiency. *Cell* **2015**, *161* (6), 1388−1399.

(18) Zaccara, S.; Jaffrey, S. R. Understanding the Redundant Functions of the m6A-Binding YTHDF Proteins. *RNA* **2024**, *30* (5), 468−481.

(19) Li, Y.; Bedi, R. K.; Moroz-Omori, E. V.; Caflisch, A. Structural and Dynamic Insights into Redundant Function of YTHDF Proteins. *J. Chem. Inf. Model.* **2020**, *60* (12), 5932−5935.

(20) Zhu, T.; Roundtree, I. A.; Wang, P.; Wang, X.; Wang, L.; Sun, C.; Tian, Y.; Li, J.; He, C.; Xu, Y. Crystal Structure of the YTH Domain of YTHDF2 Reveals Mechanism for Recognition of N6-Methyladenosine. *Cell Res.* **2014**, *24* (12), 1493−1496.

(21) Micaelli, M.; Dalle Vedove, A.; Cerofolini, L.; Vigna, J.; Sighel, D.; Zaccara, S.; Bonomo, I.; Poulentzas, G.; Rosatti, E. F.; Cazzanelli, G.; Alunno, L.; Belli, R.; Peroni, D.; Dassi, E.; Murakami, S.; Jaffrey, S. R.; Fragai, M.; Mancini, I.; Lolli, G.; Quattrone, A.; Provenzani, A. Small-Molecule Ebselen Binds to YTHDF Proteins Interfering with the Recognition of N6-Methyladenosine-Modified RNAs. *ACS Pharmacol. Transl. Sci.* **2022**, *5* (10), 872−891.

(22) Hong, Y.-G.; Yang, Z.; Chen, Y.; Liu, T.; Zheng, Y.; Zhou, C.; Wu, G.-C.; Chen, Y.; Xia, J.; Wen, R.; Liu, W.; Zhao, Y.; Chen, J.; Gao, X.; Chen, Z. The RNA m6A Reader YTHDF1 Is Required for Acute Myeloid Leukemia Progression. *Cancer Res.* **2023**, *83* (6), 845−860.

(23) Zou, Z.; Wei, J.; Chen, Y.; Kang, Y.; Shi, H.; Yang, F.; Shi, Z.; Chen, S.; Zhou, Y.; Sepich-Poore, C.; Zhuang, X.; Zhou, X.; Jiang, H.; Wen, Z.; Jin, P.; Luo, C.; He, C. FMRP Phosphorylation Modulates Neuronal Translation through YTHDF1. *Mol. Cell* **2023**, *83* (23), 4304−4317.e8.

(24) Wang, C.-H.; Zhou, H. Discovery of a New Inhibitor for YTH Domain-Containing m6A RNA Readers. *RSC Chem. Biol.* **2024**, *5* (9), 914−923.

(25) Wang, L.; Dou, X.; Chen, S.; Yu, X.; Huang, X.; Zhang, L.; Chen, Y.; Wang, J.; Yang, K.; Bugno, J.; Pitroda, S.; Ding, X.; Piffko, A.; Si, W.; Chen, C.; Jiang, H.; Zhou, B.; Chmura, S. J.; Luo, C.; Liang, H. L.; He, C.; Weichselbaum, R. R. YTHDF2 Inhibition Potentiates Radiotherapy Antitumor Efficacy. *Cancer Cell* **2023**, *41* (7), 1294−1308.e8.

(26) Qiu, X.; Kemker, C.; Goebel, G. L.; Lampe, P.; Wallis, N.; Schiller, D.; Bigler, K.; Jiang, M.; Sievers, S.; Yeo, G. W.; Wu, P. Phenylpyrazoles as Inhibitors of the m6A RNA-Binding Protein YTHDF2. *JACS Au* **2025**, *5* (2), 618−630.

(27) Wu, Y.; Feng, G.; Shuai, W.; Yang, X.; Pan, X.; Zhu, C.; Wang, A.; Sun, Q.; Wang, G.; Ouyang, L. Identification of a Selective

Downloaded from pubs.acs.org/jmcmar/article-pdf/doi/10.1021/acs.jmedchem.6c02977/6905752/jm6c02977.pdf by guest on 06 November 2026

https://doi.org/10.1021/acs.jmedchem.6c02977
J. Med. Chem. XXXX, XXX, XXX−XXX

YTHDF1 Inhibitor Targeting the m6A Recognition Domain for Breast Cancer. *Angew. Chem., Int. Ed.* **2025**, *64* (41), e202509316.
(28) Invernizzi, A.; Nai, F.; Bedi, R. K.; Vargas-Rosales, P. A.; Li, Y.; Bochenkova, E.; Herok, M.; Zálešák, F.; Caflisch, A. Discovery of YTHDF2 Ligands by Fragment-Based Design. *ACS Bio Med Chem Au* **2025**, *5* (4), 753−765.
(29) Wiedmer, L.; Eberle, S. A.; Bedi, R. K.; Śledź, P.; Caflisch, A. A Reader-Based Assay for m^6 A Writers and Erasers. *Anal. Chem.* **2019**, *91* (4), 3078−3084.
(30) Zálešák, F.; Nai, F.; Herok, M.; Bochenkova, E.; Bedi, R. K.; Li, Y.; Errani, F.; Caflisch, A. Structure-Based Design of a Potent and Selective YTHDC1 Ligand. *J. Med. Chem.* **2024**, *67* (11), 9516−9535.
(31) Daina, A.; Michielin, O.; Zoete, V. SwissADME: A Free Web Tool to Evaluate Pharmacokinetics, Drug-Likeness and Medicinal Chemistry Friendliness of Small Molecules. *Sci. Rep.* **2017**, *7* (1), 42717.
(32) Daina, A.; Michielin, O.; Zoete, V. iLOGP: A Simple, Robust, and Efficient Description of n-Octanol/Water Partition Coefficient for Drug Design Using the GB/SA Approach. *J. Chem. Inf. Model.* **2014**, *54* (12), 3284−3301.
(33) Ertl, P.; Rohde, B.; Selzer, P. Fast Calculation of Molecular Polar Surface Area as a Sum of Fragment-Based Contributions and Its Application to the Prediction of Drug Transport Properties. *J. Med. Chem.* **2000**, *43* (20), 3714−3717.
(34) Lassalas, P.; Gay, B.; Lasfargeas, C.; James, M. J.; Tran, V.; Vijayendran, K. G.; Brunden, K. R.; Kozlowski, M. C.; Thomas, C. J.; Smith, A. B. I.; Huryn, D. M.; Ballatore, C. Structure Property Relationships of Carboxylic Acid Isosteres. *J. Med. Chem.* **2016**, *59* (7), 3183−3203.
(35) Rautio, J.; Meanwell, N. A.; Di, L.; Hageman, M. J. The Expanding Role of Prodrugs in Contemporary Drug Design and Development. *Nat. Rev. Drug Discovery* **2018**, *17* (8), 559−587.
(36) Zhang, Z.; Zhou, K.; Han, L.; Small, A.; Xue, J.; Huang, H.; Weng, H.; Su, R.; Tan, B.; Shen, C.; Li, W.; Zhao, Z.; Qing, Y.; Qin, X.; Wang, K.; Leung, K.; Boldin, M.; Chen, C.-W.; Ann, D.; Qian, Z.; Deng, X.; Chen, J.; Chen, Z. RNA m6A Reader YTHDF2 Facilitates Precursor miR-126 Maturation to Promote Acute Myeloid Leukemia Progression. *Genes Dis.* **2024**, *11* (1), 382−396.
(37) Chen, Z.; Shao, Y.-L.; Wang, L.-L.; Lin, J.; Zhang, J.-B.; Ding, Y.; Gao, B.; Liu, D.-H.; Gao, X.-N. YTHDF2 Is a Potential Target of AML1/ETO-HIF1α Loop-Mediated Cell Proliferation in t(8;21) AML. *Oncogene* **2021**, *40* (22), 3786−3798.
(38) Zhong, F.; Wang, Z.; Huang, J.; Yao, F. Integrated m6A Reader Network in Acute Myeloid Leukemia: Prognostic Modeling, Immune Modulation, and Functional Validation of YTHDF3. *Int. Immunopharmacol.* **2026**, *169*, 115976.
(39) Jafari, R.; Almqvist, H.; Axelsson, H.; Ignatushchenko, M.; Lundbäck, T.; Nordlund, P.; Molina, D. M. The Cellular Thermal Shift Assay for Evaluating Drug Target Interactions in Cells. *Nat. Protoc.* **2014**, *9* (9), 2100−2122.
(40) Wang, X.; Lu, Z.; Gomez, A.; Hon, G. C.; Yue, Y.; Han, D.; Fu, Y.; Parisien, M.; Dai, Q.; Jia, G.; Ren, B.; Pan, T.; He, C. N6-Methyladenosine-Dependent Regulation of Messenger RNA Stability. *Nature* **2014**, *505* (7481), 117−120.
(41) Verma, S.; Singh, A.; Yadav, G.; Kushwaha, R.; Ali, W.; Verma, S. P.; Singh, U. S. Serum Tumor Necrosis Factor-Alpha Levels in Acute Leukemia and Its Prognostic Significance. *Cureus* **2022**, *14* (5), e24835.
(42) Rushworth, S. A.; MacEwan, D. J. HO-1 Underlies Resistance of AML Cells to TNF-Induced Apoptosis. *Blood* **2008**, *111* (7), 3793−3801.
(43) Höckendorf, U.; Yabal, M.; Herold, T.; Munkhbaatar, E.; Rott, S.; Jilg, S.; Kauschinger, J.; Magnani, G.; Reisinger, F.; Heuser, M.; Kreipe, H.; Sotlar, K.; Engleitner, T.; Rad, R.; Weichert, W.; Peschel, C.; Ruland, J.; Heikenwalder, M.; Spiekermann, K.; Slotta-Huspenina, J.; Groß, O.; Jost, P. J. RIPK3 Restricts Myeloid Leukemogenesis by Promoting Cell Death and Differentiation of Leukemia Initiating Cells. *Cancer Cell* **2016**, *30* (1), 75−91.
(44) Aguadé-Gorgorió, J.; McComb, S.; Eckert, C.; Guinot, A.; Marovca, B.; Mezzatesta, C.; Jenni, S.; Abduli, L.; Schrappe, M.; Dobay, M. P.; Stanulla, M.; Von Stackelberg, A.; Cario, G.; Bourquin, J.-P.; Bornhauser, B. C. TNFR2 Is Required for RIP1-Dependent Cell Death in Human Leukemia. *Blood Adv.* **2020**, *4* (19), 4823−4833.
(45) Ianevski, A.; Giri, A. K.; Aittokallio, T. SynergyFinder 3.0: An Interactive Analysis and Consensus Interpretation of Multi-Drug Synergies across Multiple Samples. *Nucleic Acids Res.* **2022**, *50* (W1), W739−W743.
(46) Dorn, H.; Zubek, A. Pyrazolo[3,4-b]Pyridine. *Angew. Chem.* **1967**, *79* (22), 981.
(47) Konteatis, Z.; Travins, J.; Gross, S.; Marjon, K.; Barnett, A.; Mandley, E.; Nicolay, B.; Nagaraja, R.; Chen, Y.; Sun, Y.; Liu, Z.; Yu, J.; Ye, Z.; Jiang, F.; Wei, W.; Fang, C.; Gao, Y.; Kalev, P.; Hyer, M. L.; DeLaBarre, B.; Jin, L.; Padyana, A. K.; Dang, L.; Murtie, J.; Biller, S. A.; Sui, Z.; Marks, K. M. Discovery of AG-270, a First-in-Class Oral MAT2A Inhibitor for the Treatment of Tumors with Homozygous *MTAP* Deletion. *J. Med. Chem.* **2021**, *64* (8), 4430−4449.
(48) Gross, R. S.; Guo, Z.; Dyck, B.; Coon, T.; Huang, C. Q.; Lowe, R. F.; Marinkovic, D.; Moorjani, M.; Nelson, J.; Zamani-Kord, S.; Grigoriadis, D. E.; Hoare, S. R. J.; Crowe, P. D.; Bu, J. H.; Haddach, M.; McCarthy, J.; Saunders, J.; Sullivan, R.; Chen, ; Williams, J. P. Design and Synthesis of Tricyclic Corticotropin-Releasing Factor-1 Antagonists. *J. Med. Chem.* **2005**, *48* (18), 5780−5793.
(49) Zhu, X.; Liu, B.; Li, B.; Mondal, S.; Debnath, S. An Expedient Approach for the Synthesis of TAM and MET Receptor Kinase Inhibitor's Core (R)-2-((4-(4-Amino-2-Fluorophenoxy)-1-(4-Methoxybenzyl)-1H-Pyrazolo[3,4-b]Pyridin-3-Yl)Amino)Propan-1-Ol. *Org. Process Res. Dev.* **2025**, *29* (8), 2116−2123.
(50) Jones, P.; Pryde, D. C.; Tran, T. D. 3 -Deazapurine Derivatives as Tlr7 Modulators. WO 2007093901 A1, August 23, 2007.
(51) Mittelbach, M. An Easy and Convenient Synthesis of 6-Methyl-4(1H)-Pyridone-3-Carboxylic Acid. *Synthesis* **1988**, *1988* (06), 479−480.
(52) Luzzio, M. J.; Autry, C. L.; Bhattacharya, S. K.; Freeman-Cook, K. D.; Hayward, M. M.; Hulford, C. A.; Nelson, K. L.; Xiao, J.; Zhao, X. Sulfonyl Amide Derivatives for the Treatment of Abnormal Cell Growth. WO 2008129380 A1, October 30, 2008.
(53) Anderson, R. J.; Hill, J. B.; Morris, J. C. Concise Total Syntheses of Variolin B and Deoxyvariolin B. *J. Org. Chem.* **2005**, *70* (16), 6204−6212.
(54) Qju, L.; Zhang, Y.; Kang, X.; Liu, Y.; Zhu, W.; Zhao, Y.; Yu, Y.; Hu, A.; Ye, J.; Yan, Z. Synthesis, Antifungal Activity, Structure-Activity Relationship and Mechanism of Action of Nicotinohydrazide Derivatives. *Bioorg. Chem.* **2025**, *164*, 108868.
(55) Taniguchi, T.; Kunitomo, J.; Yoshikawa, M.; Hasui, T.; Honda, E.; Imamura, K.; Kamisaki, H.; Suzuki, S.; Miura, K. Condensed Heterocyclic Compound. WO 2012124782 A1, September 20, 2012.
(56) Joy, M. N.; Bakulev, V. A. Is Nonaflate a Better Leaving Group than Corresponding Triflate? A Case Study in the Palladium Catalyzed Cross-Coupling Reaction of 7-Substituted Coumarins. *AIP Conf. Proc.* **2019**, *2059* (1), 030015.
(57) Li, Y.; Bedi, R. K.; Nai, F.; von Roten, V.; Dolbois, A.; Zálešák, F.; Nachawati, R.; Huang, D.; Caflisch, A. Structure-Based Design of Ligands of the m6A-RNA Reader YTHDC1. *Eur. J. Med. Chem. Rep.* **2022**, *5*, 100057.
(58) Bedi, R. K.; Caflisch, A. A DNA-Based Binding Assay for the m6A-RNA Reader Proteins. *ChemBioChem* **2026**, *27* (6), e202500897.
(59) Emsley, P.; Cowtan, K. *Coot* : Model-Building Tools for Molecular Graphics. *Acta Crystallogr., Sect. D:Biol. Crystallogr.* **2004**, *60* (12), 2126−2132.
(60) Liebschner, D.; Afonine, P. V.; Baker, M. L.; Bunkóczi, G.; Chen, V. B.; Croll, T. I.; Hintze, B.; Hung, L.-W.; Jain, S.; McCoy, A. J.; Moriarty, N. W.; Oeffner, R. D.; Poon, B. K.; Prisant, M. G.; Read, R. J.; Richardson, J. S.; Richardson, D. C.; Sammito, M. D.; Sobolev, O. V.; Stockwell, D. H.; Terwilliger, T. C.; Urzhumtsev, A. G.; Videau, L. L.; Williams, C. J.; Adams, P. D. Macromolecular Structure Determination Using X-Rays, Neutrons and Electrons: Recent Developments in *Phenix*. *Acta Crystallogr., Sect. D:Struct. Biol.* **2019**, *75* (10), 861−877.
(61) Afonine, P. V.; Grosse-Kunstleve, R. W.; Echols, N.; Headd, J. J.; Moriarty, N. W.; Mustyakimov, M.; Terwilliger, T. C.; Urzhumtsev, A.;

Downloaded from pubs.acs.org/jmcmar/article-pdf/doi/10.1021/acs.jmedchem.6c02977/6905752/jm6c02977.pdf by guest on 06 November 2026

Zwart, P. H.; Adams, P. D. Towards Automated Crystallographic Structure Refinement with Phenix.Refine. *Acta Crystallogr., Sect. D:Biol. Crystallogr.* **2012**, *68* (4), 352−367.
(62) McCoy, A. J.; Grosse-Kunstleve, R. W.; Adams, P. D.; Winn, M. D.; Storoni, L. C.; Read, R. J. Phaser Crystallographic Software. *J. Appl. Crystallogr.* **2007**, *40* (4), 658−674.
(63) Kabsch, W. XDS. *Acta Crystallogr., Sect. D:Biol. Crystallogr.* **2010**, *66* (2), 125−132.
(64) Moroz-Omori, E. V.; Huang, D.; Kumar Bedi, R.; Cheriyamkunnel, S. J.; Bochenkova, E.; Dolbois, A.; Rzeczkowski, M. D.; Li, Y.; Wiedmer, L.; Caflisch, A. METTL3 Inhibitors for Epitranscriptomic Modulation of Cellular Processes. *ChemMedChem* **2021**, *16* (19), 3035−3043.

Downloaded from pubs.acs.org/jmcmar/article-pdf/doi/10.1021/acs.jmedchem.6c02977/6905752/jm6c02977.pdf by guest on 06 November 2026

https://doi.org/10.1021/acs.jmedchem.6c02977
J. Med. Chem. XXXX, XXX, XXX−XXX